ABSTRACT

The Gas Chromatographic Separation Properties of Azulene and the Synthesis and Characterization of Bulky Bis-pyrazolylpyridine Metal-Ligand Complexes

Matthew T. Jackson, Ph.D.

Mentor: Charles M. Garner, Ph.D.

The separation of complex mixtures of molecules is vital to the conduct and understanding of modern chemical research. In this work, new materials for gas chromatographic separations are developed, evaluated, and discussed. Also discussed are the synthesis and characterization of bulky tridentate ligand-metal complexes.

Azulene is an aromatic molecule with interesting properties, most notably a permanent dipole moment of 1.08 D. This degree of polarity in the absence of heteroatoms is quite rare and offers potential for use in unique gas chromatographic stationary phases. Here, we report the first examples of azulene-derivatized stationary phases for gas chromatographic separations. Poly(dimethyl/azulenylmethyl) siloxane polymers containing 15% and 35% of an azulene derivative were synthesized, coated onto capillary columns, and evaluated. To compare the effects of increased polarity vs the effects of polarizability, isomeric naphthalene analogues were also prepared, coated, and evaluated. The coated phases displayed efficiencies up to 2700 plates/m. For both azulene and naphthalene columns, retention increased as substitution level increased. The more

polarizable naphthalene columns tended to retain analytes more strongly. Columns were also evaluated for the separation of several different mixtures of isomers against a commercial HP-5 column. All azulene and naphthalene columns exhibited separations comparable to the commercial column. The solvation thermodynamic parameters phases were measured, showing an excellent linear relationship and no change in the mechanism of interaction over the temperature range measured.

Crystal structures of transition metal complexes of a recently-available bis-pyrazolylpyridine (bpp) ligand, 2,6-bis(3',5'-diphenylpyrazolyl)pyridine (bdppp), prepared by reaction with transition metal chlorides, are reported. The ligand forms two types of structures: a 2:1 complex with Fe (II) chloride, and 1:1 complexes with Mn(II), Ni(II), Co(II), Zn(II), Ru(III), Pd(II), and Rh(III) chlorides, resulting in two different geometries. In all cases the ligand is tridentate, but in contrast to reported bpp structures, the plane of the pyridine ring coordinating with the metal is significantly distorted from the plane of the pyrazoles and metal. The Ru, Cu, and Fe complexes show quasi-reversible redox couples.

The Gas Chromatographic Separation Properties of Azulene and the Synthesis and Characterization of Bulky Bis-pyrazolylpyridine Metal-Ligand Complexes

by

Matthew Todd Jackson, B.S.

A Dissertation

Approved by the Department of Chemistry and Biochemistry

_____

Patrick J. Farmer, Ph.D., Chairperson

Submitted to the Graduate Faculty of
Baylor University in Partial Fulfillment of the
Requirements for the Degree
of

Doctor of Philosophy

Approved by the Dissertation Committee

_____

Charles M. Garner, Ph.D., Chairperson

_____

Kevin G. Pinney, Ph.D.

_____

Robert R. Kane, Ph.D.

_____

Kevin K. Klausmeyer, Ph.D.

_____

Stephen I. Dworkin, Ph.D.

Accepted by the Graduate School

May 2018

_____

J. Larry Lyon, Ph.D., Dean

Page bearing signatures is kept on file in the Graduate School.

TABLE OF CONTENTS

LIST OF FIGURES

LIST OF TABLES

LIST OF SCHEMES

LIST OF ABBREVIATIONS

GC	Gas chromatography
°C	Degrees Celsius
s	Seconds
m	Meters
mm	Millimeters
μm	Micrometers
FID	Flame ionization detector
TCD	Thermal conductivity detector
MS	Mass spectrometry
EI	Electron impact
GC-MS	Gas chromatography-mass spectrometry
PDMS	Poly(dimethyl)siloxane
PEG	Polyethylene glycol
IL	Ionic liquid
D	Debye
EAS	Electrophilic aromatic substitution
TMA	4,6,8-trimethylazulene
TLC	Thin layer chromatography
R_f	Retention factor
terpy	2,2';6',2"-terpyridine
bpp	2,6-bis(pyrazol-1-yl)pyridine
BHP	2,6-bis(hydrazino)pyridine
Me	Methyl
pTSA	Para-toluenesulfonic acid
cat.	Catalytic
bpy	2,2’-bipyridine
DNA	Deoxyribonucleic acid

HPLC	High performance liquid chromatography
nBuLi	*n*-butyllithium
THF	Tetrahydrofuran
MeI	Iodomethane
DDQ	2,3-Dichloro-5,6-dicyano-1,4-benzoquinone
^{i}PrMgBr	Isopropylmagnesium bromide
min	Minutes
naphth	Naphthalene
^{t}Bu	*Tert*-butyl
NMR	Nuclear magnetic resonance
mL	Milliliters
cm	Centimeters
h	Hours
calc	Calculated
bdppp	2,6-bis(3,5-diphenylpyrazolyl)pyridine
ESI	Electrospray ionization
UV-Vis	Ultraviolet-visible light
UV	Ultraviolet light
$TBAPF_6$	Tetrabutylammonium hexafluorophosphate
V	Volts
mV	Millivolts
ACN	Acetonitrile
M	Molarity
EPR	Electron paramagnetic resonance
TMS	Tetramethylsilane
ppm	Parts per million
Anal. Calcd.	Calculated elemental analysis

ACKNOWLEDGMENTS

First and foremost, I would like to thank my advisor, Dr. Charles Garner. It was his guidance, expertise, and creativity that made this dissertation possible. I learned more chemistry from him than I would have thought possible when I first started this program. His ability to devise new methods in the lab always amazed me. Additionally, I appreciated the conversations we shared, both on chemistry and other topics.

I would also like to thank the rest of my committee members, Drs. Kevin Pinney, Bob Kane, Kevin Klausmeyer and Steve Dworkin for their time and support during this endeavor.

I would like to thank the many people that acted as collaborators on various projects. Without them, none of the work presented here would have been possible. Thank you to Dr. Kevin Klausmeyer and his student for their work in obtaining X-ray crystal structures reported here. Thank you to Dr. Kim Brien and her students for electronic spectra. Thanks to Dr. Patrick Farmer, Dr. Murugaeson Kumar, and Michael Spiegel for their assistance with electrochemistry and EPR spectroscopy. Many thanks to Dr. Daniel Armstrong, Lillian Frink, and Dr. Joe Harland for their crucial instruction in the art of capillary column coating.

Thank you to the many friends and colleagues that I have found over the years at Baylor. Particularly, my lab mates Dana Horgen, Nelson van der Velde, and Jessica Almond were always encouraging, helpful, and a pleasure to be around. I would also like

to thank the undergraduates I have mentored: Jason Schaffer, Lauren Freeman, Rick Betori, and Steven Nadakal. Their enthusiasm made mentoring a joy.

And finally, I would like to thank my family members, because without their love and support I would never have been able to accomplish this. Thank you to my lovely wife Jasmine for putting up with the demands of my graduate work. Thank you to my parents, Michael and Patricia, for first inspiring me to pursue a Ph.D. in chemistry, and for teaching me that whatever you do, you should do it to the best of your ability. Thank you as well to the rest of my family, including my brother Nate who first encouraged me to think about attending Baylor. Without their loving encouragement I would never have been able to reach where I am today. I will always be grateful for all the encouragement I have received from them throughout my life.

CHAPTER ONE

Introduction

Background—Gas Chromatography

The separation of complex mixtures is crucial to the conduct of chemical research. Chromatography is the separation of molecules through their partition between two phases, one stationary and one mobile. In gas chromatography (GC) the mobile phase is a gas, and the stationary phase is typically a liquid. While various stationary phases have been used since the invention of GC, modern GC is most often conducted using polysiloxane-based stationary phases. Polysiloxanes are polymers of oxygen and silicon, with two organic side group substituents attached to the silicon. By changing the side groups, it is possible to change the properties of the stationary phase and affect the separation.

The setup for gas chromatography consists of several components.[1] Samples are introduced at the injection port, which is heated to high temperatures (~ 275 °C) in order to vaporize the sample. From the injection port, the sample moves to the column, which is where separation occurs. The column consists of a long, narrow tube with a coating of the stationary phase on its interior wall. The column is in an oven, which allows the temperature to be controlled. After passing through the column, analytes travel to a detector, which reports the retention time and the response. Many different detectors are used in GC. While other modifications can be added, these are the most basic components of GC.

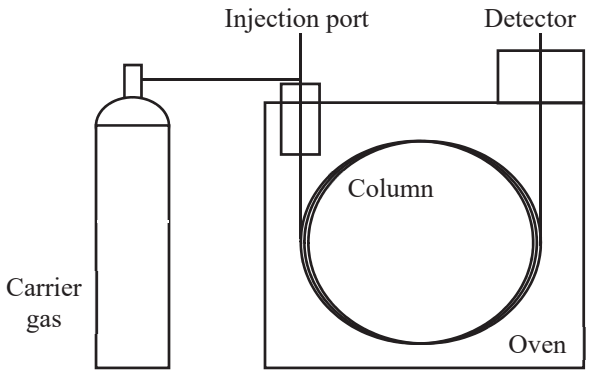

Figure 1.1 Simplified diagram of a gas chromatograph.

Most GC analysis conducted today is performed using split injection.[1-2] These allow the majority of the sample to be vented out of the instrument without being applied to the column. In order to apply the mixture to the column as a narrow (~ 2 s) band, only a small portion of the sample is applied to the column.

Most GC columns are fused silica capillary columns.[1] A cross sectional diagram is shown in Figure 1.2. These are very long thin glass tubes, anywhere from 5-100 m long and with an internal diameter from 0.10 to 0.53 mm. The outside of the column is usually coated with a polyimide protective coating. Without the coating, the capillaries are brittle and tend to break easily.

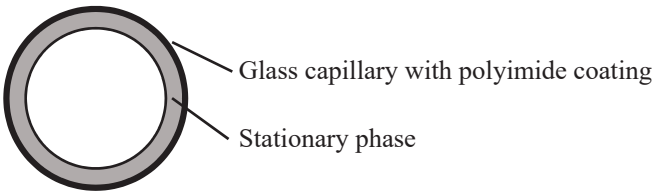

Figure 1.2. Cross-sectional diagram of a wall-coated gas chromatography column.

The polyimide fills in the microscopic fissure in the glass surface, making the capillaries flexible. The stationary phase coats the interior wall of the capillary in a thin layer, ranging from 0.1-5 μm.

Many different detectors are used in GC.[1] One of the most common is the flame ionization detector (FID).[3] The FID measures the ions generated from the combustion of organic molecules. It is easy to operate and maintain, and has a wide linear response range. However, FID's have a few disadvantages. Compounds containing heteroatoms have lower levels of detection compared to hydrocarbons, and some highly oxygenated compounds are not detected. Several other detectors are also common. The thermal conductivity detector (TCD) measures differences in the thermal conductivity of the gas flowing off the column in comparison to a reference flow of the carrier gas.[3] TCD's are useful because they can detect any compound, but are less sensitive than FID's. They are also nondestructive, so they can be used in preparative GC applications. Mass spectrometers (MS) are also frequently used as GC detectors.[3-4] The most common type of MS used with GC is electron impact (EI) ionization. Because EI is a hard ionization technique, analyte molecules will often fragment extensively when ionized, which gives structural information about the analytes. This makes database comparisons possible, and GC-MS a very powerful technique for both separating complex mixtures and identifying the components.

Gas Chromatography Theory

The separation in gas chromatography, or any other form of chromatography for that matter, arises from differences in interaction that analytes have with the mobile and

stationary phases.[3] The more an analyte favors the mobile phase, the more time it will spend there. Three factors influence the separation of analytes from each other: retention, efficiency, and selectivity. Retention measures the time spent in the stationary phase vs. the time spent in the mobile phase. The more time it is in the mobile phase, the more it is moving, and the faster it elutes. This is represented by the distribution constant, given in the equation,

$$K_c = \frac{[A]_S}{[A]_M}$$

where K_c is the distribution constant, $[A]_S$ is the concentration of analyte in the stationary phase, and $[A]_M$ is the concentration of analyte in the mobile phase. This is a highly-simplified model of the distribution of analytes. Chromatography is clearly a dynamic process. However, the general operation of chromatography is usually not far from equilibrium. The distribution constant should rightfully use activities rather than concentrations as well. It is also assumed that the analytes do not change form or interact with each other. The distribution constant can be broken down into two parts: the phase ratio β and the retention factor k. The phase ratio is defined as the ratio between the volume of the mobile phase and the volume of the stationary phase.

$$\beta = \frac{V_M}{V_S}$$

V_M is the volume of the mobile phase and V_S is the volume of the stationary phase. The phase ratio for gas chromatography columns are generally very high due to the extremely thin layer of stationary phase. The retention factor is the ratio between the mass of the analyte in the stationary phase and the mass of analyte in the mobile phase.

$$k = \frac{(mass)_S}{(mass)_A}$$

The retention factor can also be expressed in terms of time:

$$k = \frac{(t_R - t_0)}{t_0}$$

Where t_R is the retention time of an analyte and t_0 is the dead volume, i.e., the retention time of a completely unretained peak. The retention factor is most often measured by the retention time of an analyte.

The selectivity, α, of an analyte is a measurement of the separation of one analyte peak to another. It is defined as the ratio of the retention factors between two peaks:

$$\alpha = \frac{k_2}{k_1}$$

The retention factor of the more retained peak, k_2, is divided by the retention factor of the less retained peak, k_1. While selectivity is a good indicator of a stationary phase's ability to separate analytes, it is not a perfect measurement. It is only a measurement of the separation of the apices of the peaks.

To most accurately measure the degree of separation, resolution, *R*, is used. Resolution measures how well peaks can be differentiated. It is defined by the equation

$$R = 1.18\frac{[(t_R)_B - (t_R)_A]}{w_A + w_B}$$

where t_R *A* and *B* are the retention times of two peaks, and *w A* and *B* are the peak widths at half height. Widths at half-height are more easily measured than baseline values. As a general rule, a resolution of about 1.5 is considered complete ("baseline") separation.

Stationary Phases in Gas Chromatography

The two major factors driving separation in GC are the temperature of the column and analyte interaction with the stationary phase. A wide variety of stationary phases

have been used since the original invention of gas chromatography. Several important properties must be considered when developing materials for use as stationary phases. The temperature stability should be high to allow high-temperature separations, required in the analysis of higher-boiling molecules. The viscosity should also be high, so that the stationary phase does not bead in spots on the column, but forms a smooth and even coating on the interior wall of the column. Since the beginning of GC development, polysiloxanes have been recognized as useful stationary phase materials. Polysiloxanes, or silicones, are alternating polymers of silicon and oxygen, with two substituent groups attached to the silicon. It is possible to tune the properties of the polysiloxane by chemically altering its structure in different ways.

The viscosity and temperature stability can be improved by ensuring chain lengths are long and introducing a small amount of crosslinking. However, too much crosslinking can render the polysiloxane insoluble and therefore unusable. The ideal consistency is that of a thick gum.

Varying the side groups can affect both the stability and the separatory properties of the polymer. The most basic side groups employed are methyl groups. This polymer is referred to as a poly(dimethylsiloxane), abbreviated PDMS. This gives a nicely stable (T_{max} ~ 300 °C) nonpolar stationary phase that does not retain any particular analyte strongly. More commonly, a slightly more polar phenyl-/methylpolysiloxane is used. The phenyl rings provide a small amount of dipole interaction, which increases the polarity. The most commonly used commercial stationary phase is a 5% phenyl, 95% methyl polysiloxane. While higher levels of substitution are available, the increased phenyl composition has deleterious effects on the temperature stability and film-forming

properties of the polymer. For more polar applications, cyanopropyl or trifluoropropyl groups can be used, which feature strong dipole interactions. The cyanopropyl groups also can interact with analytes using hydrogen bonding. Many other side groups are also used, but these are the most common.

Polysiloxanes are the most common stationary types. Several other materials are also used frequently. These include polyethylene glycol (PEG), which is much more polar than polysiloxane but less temperature stable.[3] Ionic liquids (IL's) have recently been developed as stationary phases, and show good temperature stability, as well as an interesting dual selectivity, retaining both polar and nonpolar analytes.[5]

While these are the commonly available commercial stationary phases, many other substituents are used and countless others have been characterized. In the 1980's, Lee and colleagues began researching polysiloxane stationary phases with highly polarizable substituents, such as large aromatic groups, that were very effective at separating polar mixtures, particularly isomers with very slight differences.[6-9] A similar line of investigation was conducted by Wu and colleagues around 2015.[10-12] They found that polyphenyl substituents—multiple phenyl rings connected together—could be used instead of a higher percentage of phenyl substitution. This has multiple benefits. A lower overall degree of substitution means that the polymer has higher temperature stability without sacrificing performance. Additionally, the very large, very polarizable groups provided excellent separatory properties for different groups of isomers. While a great deal of research, particularly that of Lee and Wu, shows the utility of these types of substituents, several possibilities are still yet to be explored.

Characterization of Stationary Phases

The term polarity is used frequently when describing stationary phase separation behavior, but it is poorly defined in this case, and does not provide an extensive enough description for how analytes are retained. Multiple types of intermolecular interactions with the stationary phase exist and methods of characterizing these have been developed. One of the earliest and simplest is the Rohrschneider-McReynolds index. First developed by Rohrschneider[13] and later modified by McReynolds,[14] this method uses a series of probe molecules to measure different types of interaction with the stationary phase. McReynolds originally chose five probes, but McReynolds increased the number to ten and changed some of the molecules used. Rohrschneider's original probe molecules, McReynolds' modified list, and the molecules normally used today are shown in Table 1.1.

Table 1.1. Rohrschneider-McReynolds probes.

Rohrschneider	McReynolds	Modern
benzene	benzene	benzene
ethanol	*n*-butanol	*n*-butanol
2-butanone	2-pentanone	2-pentanone
nitromethane	nitropropane	nitropropane
pyridine	pyridine	pyridine
	2-methyl-2-propanol	
	iodobutane	
	2-octyne	
	1,4-dioxane	
	cis-hydrindane	

The Rohrschneider-McReynolds is calculated using the Kovats retention index (*I*) of the analyte. The Kovats retention index is a method of standardizing analyte retention

between instruments. First developed by Kovats in 1958, the index uses n-alkanes as relative standards. Each alkane is assigned a reference value of 100 times the number of carbons it contains, so n-hexane has a value of 600, n-heptane has a value of 700, and so on.[15] When performing an isothermal separation of n-alkanes, the retention time of each alkane increases logarithmically. To calculate the Kovats retention index of a particular analyte, the formula is used:

$$I = 100 \times \left[n + \frac{\left(\log t_{r(u)}\right) - \left(\log t_{r(x)}\right)}{\left(\log t_{r(N)}\right) - \left(\log t_{r(n)}\right)} \right]$$

n is the number of carbons in the alkane preceding the analyte, $t_{r(u)}$ is the retention time of the analyte, $t_{r(x)}$ is the retention time of the n-alkane preceding the analyte, and $t_{r(N)}$ is the retention time of the succeeding n-alkane.[3]

The Rohrschneider-McReynolds numbers are calculated by subtracting the Kovats index of the probe molecules on a squalene-coated column from those on the column being investigated. Squalane is a thirty-carbon alkane that has been defined as a zero-polarity stationary phase for this purpose. The sum of all the probes' Rohrschneider-McReynolds numbers is the general polarity of the column. This provides a quick way to gauge the overall polarity of different stationary phases. In general, phases with a general polarity between zero and 100 are considered low polarity, between 100 and 400 are considered moderate polarity, those with general polarities greater than 400 are considered polar stationary phases.

The thermodynamic properties of the interaction between analyte and stationary phase can also be analyzed.[1] This is because the retention factor, *k'*, is related to the equilibrium constant *K* by the equation

$$K = k' \times \beta$$

where β is the phase ratio. K can also be represented as the distribution constant, as stated earlier. Chromatography is not an equilibrium process, but acts close enough to it that thermodynamic equations can be used for analysis. Since the equilibrium constant can also be expressed by the equation

$$\Delta G = -RT\ln(K)$$

where ΔG is the Gibbs free energy, R is the gas constant, and T is the temperature. Using this equation and the equation

$$\Delta G = \Delta H - T\Delta S$$

where ΔH is the enthalpy of the transition between mobile and stationary phases, and ΔS is the entropy, the equation can be substituted to

$$\ln k = \frac{\Delta H}{RT} - \frac{\Delta S}{R} + \ln \beta$$

To relate the retention factor to the enthalpy and entropy of phase transition, the Gibbs free energy can then be calculated using the previous equation. This is important because information about the nature of interaction between stationary phase and analyte can be gained by examining how the different terms change. This concept is expanded on more thoroughly in Chapter Two.

Introduction to Azulene

Azulene is an aromatic molecule consisting of a seven-membered ring fused to a five-membered ring. It features ten pi electrons, making it isoelectronic with naphthalene. The structures of azulene and naphthalene are shown in Figure 1.3. However, while naphthalene is colorless, azulene is a deep, brilliant blue. Azulene also features a permanent dipole moment of 1.08 D (approximately equal to that of an H-Cl bond) while

naphthalene's dipole moment is zero.[16] This arises from the uneven ring structure of azulene. It is possible to resonate a negative charge onto the five-membered ring and a positive charge onto the seven-membered ring while still maintaining aromaticity. Azulene compounds have been known since the middle ages, but the first synthesis of an azulene compound was not reported until 1939.[17] A variety of applications have been investigated including anti-inflammatory activity,[18] antiulcer activity,[19] and tumor cytotoxicity.[20] They are also used as chromophores in metal-ligand complexes, and are found as defects in graphene sheets.[21] Because of its ring structure, azulene tends to react in predictable ways. The 1- and 3-positions on the five-membered ring have a partial negative charge, so electrophilic aromatic substitution (EAS) occurs readily at these positions.[22]

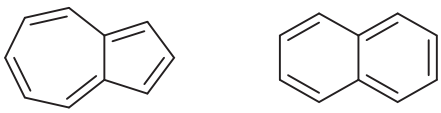

azulene naphthalene

Figure 1.3. Chemical structures of azulene and naphthalene.

Unmodified azulene is expensive to purchase, with one gram costing $300 from Sigma-Aldrich as of October 2017. While several syntheses of azulene was have been described, they are all time-consuming and relatively low-yielding. Its derivative 4,6,8-trimethylazulene (TMA), on the other hand, is easily synthesized.[23] In fact, Baylor University has used its synthesis, shown in Scheme 1.1, as an undergraduate level experiment in the advanced organic laboratory course for many years. Over several lab periods, students first synthesize 2,4,6-trimethylpyrilium tetrafluoroborate from *tert*-butanol, acetic anhydride, and tetrafluoroboric acid. This is then reacted with sodium

cyclopentadienide to form TMA. TMA is easily purified using flash chromatography. By using perchlorate salts instead of tetrafluoroborate salts the yield can be increased, but these salts are shock sensitive and not suited for use in a teaching setting. The methyl groups on TMA are more acidic than those on a benzene ring, due to azulene's structure. When deprotonated, the negative charge can resonate into the five-membered ring, preserving partial aromaticity of the molecule.

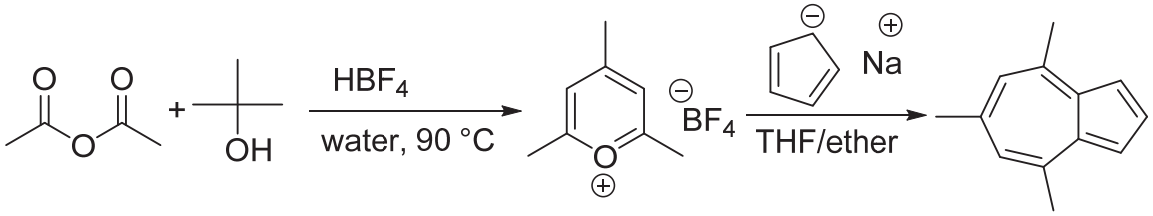

Scheme 1.1. Synthesis of 4,6,8-trimethylazulene.

Separation Properties of Azulene

While azulene has never been used as part of a gas chromatography stationary phase, some of its separation properties have been previously investigated. Previously, our lab synthesized azulene 1,5-diol diastereomers by trifluoroacetylating azulene and TMA in the 1- and 3- positions, then reducing the resulting ketones to alcohols.[24] This is shown in Figure 1.5. The diastereomers produced tended to be much more highly separated by TLC than comparable non-azulene alcohol diastereomers. Retention factor (R_f) differences between diastereomers ranged from 0.10 to 0.46. Additionally, the chiral separation of diol enantiomers appeared to benefit from the presence of the azulene ring.[24] In comparison, non-azulene diols had no R_f difference between diastereomers on TLC. This unexpected property gave us further insight to the unusual separation properties of azulene.

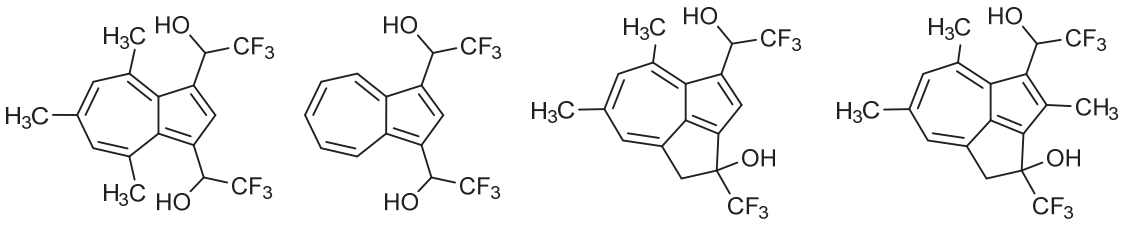

Figure 1.5. Azulene diols showing large R_f differences on TLC.

Because of the previous studies performed, and because of azulenes unusual combination of polarity without heteroatoms, we believed that azulene may provide interesting separation characteristics that would expand the power of gas chromatography in new and useful directions. This topic will be further discussed in Chapter Two.

Metal Complexes with the Sterically Hindered Ligand 2,6-bis(3',5'-diphenylpyrazolyl)pyridine

Tridentate ligands, or ligands that bind to metals from three atoms, are commonly used in inorganic chemistry for a variety of applications. One of the most commonly used is 2,2':6',2"-terpyridine (terpy).[25] Terpy is composed of three linked pyridine rings that bind to the metal from the three nitrogen heteroatoms. Terpy is a popular ligand because of its ability to bind to a wide variety of metals in different oxidation states, its interesting reactive and catalytic activity, and its synthetic accessibility. 2,6-Bis-pyrazolylpyridine (bpp) ligands are superficially like terpy.[26] The two ligands are shown in Figure 1.6.

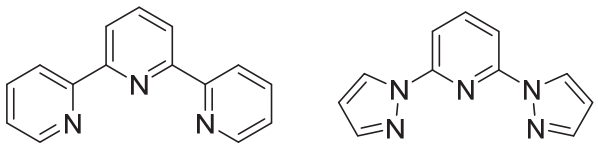

2,2':6',2"-terpyridine 2,6-bis-pyrazolylpyridine

Figure 1.6. Structures of terpy and bpp ligands.

Both are tridentate ligands binding to metals with three aromatic nitrogens. However, the incorporation of different aromatic rings into the ligand change several properties, such as the electronics and lability of the ligands in their metal complexes. The synthesis of bpp also lends itself to different substitution patterns than terpy. Changing the substitution on the pyrazole rings is straightforward. Bpp has typically been synthesized by the nucleophilic aromatic substitution of 2,6-dihalopyridine with the potassium salt of pyrazoles. This method is effective up to a point; while substituted pyrazoles can be used, substituents larger than methyl groups cannot be placed in the 5'-position. Our lab has developed an alternative synthetic pathway that is able to place larger substituents, including tert-butyl and phenyl groups, at the 5'-position.[22, 27-29] This is done by first synthesizing 2,6-bis-hydrazinopyridine followed by reaction with a 1,3-diketone to form the pyrazole ring. Metal-ligand complexes with bpp ligands have been synthesized with many different metals in many different oxidation states. Bpp ligands and their metal complexes have a variety of uses, including medicinal chemistry, catalysis, solar cells, and others. While the properties of bpp ligands and their metal complexes have been studied thoroughly, the effects of bulky substituents have not been investigated to any great extent.

Synthesis of bpp and bpp Complexes

Bis-pyrazolylpyridine is usually synthesize via the nucleophilic aromatic substitution of 2,6-dihalopyridine with potassium salts of pyrazole rings.[26] The general synthesis is shown in Scheme 1.2.

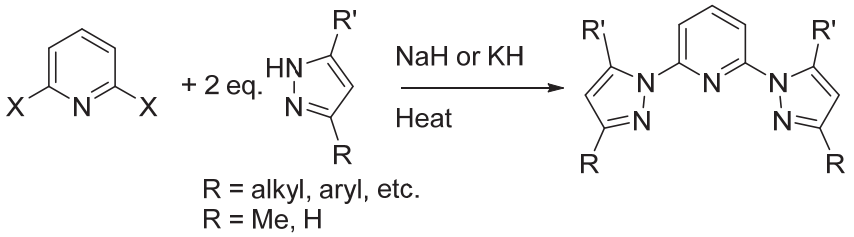

Scheme 1.2. Synthesis of 2,6-bispyrazolylpyridines through the nucleophilic aromatic substitution of a pyrazole anion with a 2,6-dihalopyridine.

If the two R-groups are different, the bulkier group will be placed in the 3-position of the pyrazole ring. This is because of the sterics of the nucleophilic aromatic substitution reaction used to couple the pyrazole and pyridine rings. As the size of the substituents increases, the efficiency of the reaction decreases. It is difficult to place any R-group larger than a methyl in the 5-position.

Our lab developed a synthesis of bpp ligands using an alternative route that circumvents this limitation. By first forming 2,6-bis-hydrazinopyridine (BHP) via the nucleophilic aromatic substitution of 2,6-difluoropyridine with hydrazine, followed by reaction with a 1,3-diketone, bpp ligands can be formed with larger substituents in the 5-position of the pyrazoles.[22] The general synthesis is shown in Scheme. 1.6. If the R groups are not equivalent, the larger of the two will go to the 5-position.[29] This is due to the mechanism of the ring formation, which proceeds via the Knorr pyrazole synthesis.

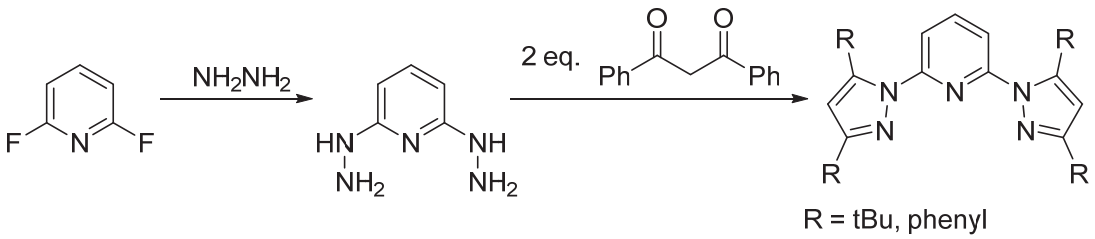

Scheme 1.6. Synthesis of bpp ligands from bis-hydrazinopyridine.

This reaction consists of two consecutive imine formations and a tautomerization to form the aromatic pyrazole ring. The less hindered imine forms first, between the distal hydrazine nitrogen and the less hindered ketone. This leaves the bulkier ketone to react with the proximal hydrazine. The effects of electron donating and withdrawing groups on the regiochemistry of pyrazole ring formation have also been investigated.[28] In short, the electron withdrawing group is placed in the 3-position because it activates the ketone closer to it.

BHP can also be used to synthesize other ligands, such as 2,6-indazolylpyridines.[27] While bis-indazolylpyridines are not widely reported, they are usually synthesized in the same way as the traditional bpp synthesis. The anion of indazole is reacted with 2,6-dihalopyridine. This leads to the formation of several regioisomers as products. This is shown in Scheme 1.6

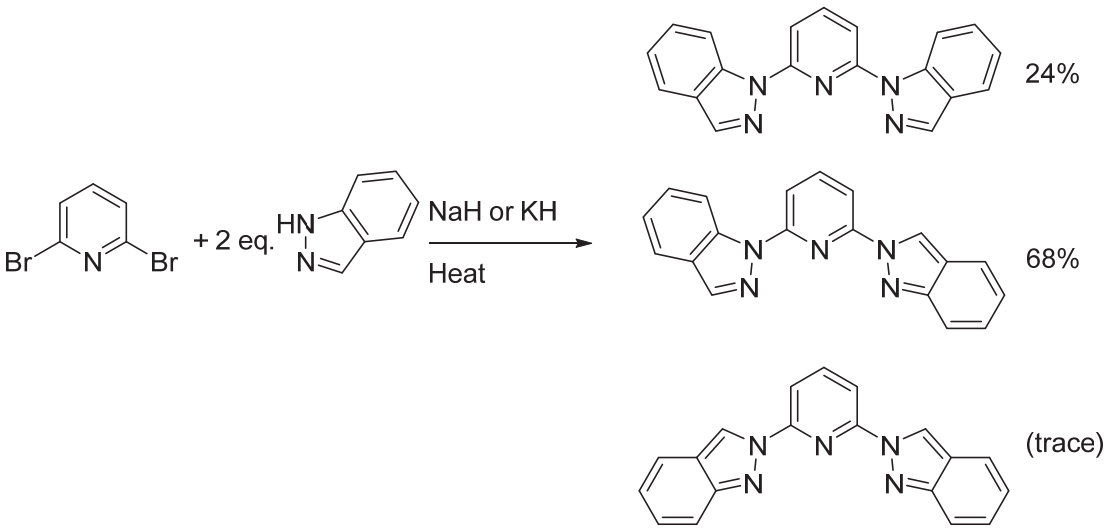

Scheme1.6. Product distribution from the nuclelphilic aromatic substitution of the indazoyl anion with 2,6-dibromopyridine.

By reacting bpp with 2-bromoacetophenone, the regioselectivity can be controlled. The ketone and distal hydrazine nitrogen first react to form an imine, then the proximal

hydrazine nitrogen substitutes the bromine using a copper catalyst to form the ring. This is shown in in Scheme 1.7.

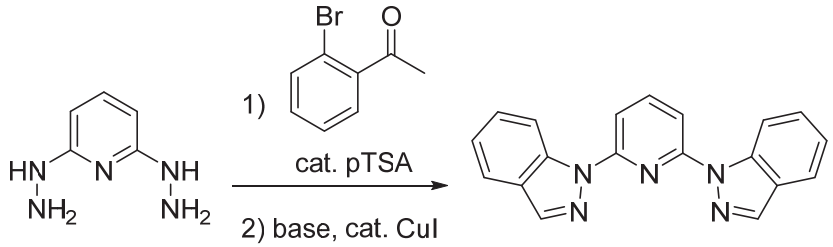

Scheme 1.7. Synthesis of 2,6-bis-indazolylpyridine from BHP.

Use of Bpp-Metal Complexes

Catalytic applications have been found for bpp-metal complexes, including several asymmetric examples. They have also been evaluated for use in solar cells, as spin-crossover materials, and had their biological activity investigated. A wide range of transition metals have been complexed with bpp ligands.

The use of bpp-metal complexes in a variety of catalytic applications have been evaluated. While several different reactions have been studied as catalytic applications for bpp complexes, one of the most widely studied is transfer hydrogenation. Ru complexes are generally used,[30-32] and turnover frequencies of up to 29400 h^{-1} have been achieved for the hydrogenation of acetophenone derivatives. Ni and Fe complexes have also been evaluated, with Fe showing more activity than Ni.[33]

Various polymerization reactions have also been catalyzed with bpp complexes. Butadiene polymerization has been accomplished using Cr,[34] Fe,[35] and Co[35] complexes. Ethylene has been polymerized using Fe and Co complexes.[36] The ring-opening polymerization catalysis of Cu an Zn complexes has also been evaluated.[37]

Several chiral reactions have also been shown to be catalyzed by bpp complexes. The asymmetric cyclopropanation of alkenes has been accomplished using chiral Cu and Rh complexes.[38-39] Enantiomeric excesses of up to 85% can be achieved. Chiral epoxidation has been catalyzed by Ru complexes, with enantiomeric excesses of up to 36%.[32]

Several other reactions have also been shown to be catalyzed by bpp complexes. The alkane photooxidation using Ru-bpp complexes has also been shown, with the conversion of adamantane to adamantanol (67%) and adamantane-1,3-diol (24%) with turnover numbers of up to 230.[40] Zn complexes have been used to catalyze the cycloaddition of CO_2 to epoxides.[41]

Bpp complexes have also found use in dye-sensitized solar cells.[35, 42-48] Complexes with aromatic nitrogen ligands have long been investigated for this use, because of their generally high absorption of visible light, appropriate electrochemical properties, and high stability. 2,2'-bipyridine (bpy) has been the standard ligand for several decades.[49] Generally Ru-bpp complexes are used, but some other metals have been investigated. These complexes tend to have high efficiencies and absorption spectra that allow for the maximum aborbance of solar radiation.

Metal-bpp complexes have shown biological activity as well. Ni, Co, and Cu complexes have been shown to cleave DNA.[50] Additionally, the Cd complex has shown activity against certain cancer cell lines.[50]

Conclusion

Bis(pyrazolyl)pyridine ligands have shown many useful properties and applications in the literature. However, the previous limits to their synthesis have imposed limits on the investigation of those properties. Through the development of a new synthetic pathway, and the initial characterization of the metal-ligand complexes formed by the bulkier ligand synthesized, we have advanced the field and opened new pathways for investigation of various applications.

CHAPTER TWO

Azulene-modified Polysiloxanes as Gas Chromatographic Stationary Phases

Introduction

Azulene is a highly colored aromatic molecule consisting of a five-membered ring fused to a seven-membered ring. It is isoelectronic with naphthalene. However, while naphthalene is nonpolar, azulene has a dipole moment of 1.08 D—approximately equal to that of HCl.[51] As shown in Figure 2.1, it is possible to resonate a negative charge onto the five-membered ring and a positive charge onto the seven-membered ring while maintaining the aromaticity of both ring subunits, which is impossible with naphthalene. 4,6,8-Trimethylazulene is more easily prepared and features the same combination of aromaticity and polarity.[52]

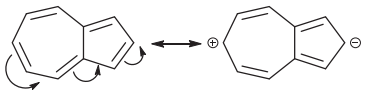

Figure 2.1. Resonance structure of azulene that contributes to its dipole moment.

The properties of azulene offer the intriguing possibility of polarity without heteroatoms, which might be of advantage in certain chromatographic applications. Consistent with this expectation, the Kovats retention indices for azulene (1296) [53] and 4,6,8-trimethylazulene (1638) [54] are significantly higher than those of naphthalene (1184)[54] or trimethylnaphthalene (1501, 1522, and 1533 for 1,3,7-, 2,3,6- and 2,3,5-trimethylnaphthalene, respectively) on poly(dimethyl)siloxane columns. [54] This implies that incorporating azulene into a stationary phase could lead to significant interactions

with analytes, possibly allowing for new or enhanced separations. Horgen[24] and colleagues showed that diastereomeric azulene 1,5-diols have significantly greater separation on TLC than analogous benzene derivatives and that the enantioseparation of azulene 1,5-diols using HPLC is much easier than that of the corresponding benzene 1,5-diols; this indicates that the azulene ring has unusual interactions with the stationary phase that may be beneficial for separations.

Capillary gas chromatography (GC) columns are typically coated with polysiloxane stationary phases. By varying the composition of the side groups of the polysiloxane, it is possible to change the separation properties of the column. Polysiloxane containing other aromatic groups including biphenyl and its derivatives,[6-7] naphthyl,[7] phenoxyphenyl,[7] and methoxyphenyl[8] have been investigated. The enhanced polarizability of these side groups over phenyl was found to be key. Additionally, polycyclic phenyl phases with a variety of functional groups have been prepared, showing good temperature stability and excellent selectivity for polycyclic aromatic hydrocarbons.[10-12]

This chapter describes the synthesis of a new polysiloxane material containing trimethylazulene-based side chains. To our knowledge, this is the first report of azulenes being incorporated into gas chromatographic stationary phases. Closely related naphthalene analogues were also synthesized for comparison purposes. These materials were prepared by the hydrosilylation of alkene-functionalized trimethylazulene or naphthalene onto poly(hydromethyl/dimethyl)siloxane.[9] These polymers were coated onto capillary columns and an evaluation of their properties was performed. All columns were also compared with a commercial HP-5 column—5% phenyl polydimethylsiloxane,

the most common commercially available stationary phase. These results show the azulene-derivatized phases' potential utility in gas chromatographic separations.

Synthesis and Modification of Azulene

4,6,8-trimethylazulene (TMA) was used instead of azulene due to the ease of its synthesis and the expense of azulene and the ease with which TMA may be derivatized. The TMA used was synthesized by the Baylor University undergraduate students in CHE 4237, advanced organic chemistry lab. TMA is synthesized from 2,4,6-trimethylpyrilium tetrafluoroborate and cyclopentadiene. TMA is then modified via the reaction with allyl bromide to form 4-butenyl-6,8-dimethylazulene (Scheme 2.1).

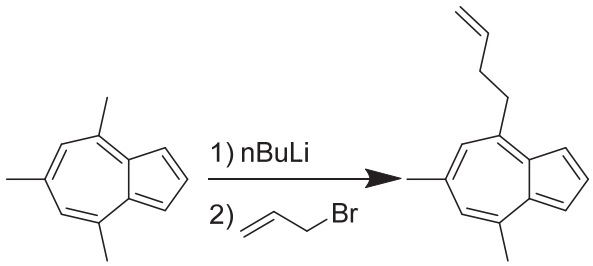

Scheme 2.1. Allylation of trimethylazulene.

TMA is first reacted with n-butyllithium to form an anion. The protons on the TMA methyl groups are more acidic than might be expected because the negative charge can be resonated onto the five-membered ring, preserving partial aromaticity of the molecule. The allyl bromide initially alkylates the ring-fusion carbon, then undergoes a slow Cope rearrangement to form the desired product. At room temperature, this rearrangement takes several hours. With heat, it is complete considerably faster. It is possible to add multiple allyl groups to one TMA molecule, which when reacted with the polymer acts as a cross linker. While some degree of cross linking can impart beneficial properties to the

polymer in terms of temperature stability and film formation, too much crosslinking leads to an insoluble material. Fortunately, if substantial amounts of the multiply allylated product was present, the product could be purified using silver nitrate doped silica gel chromatography.

Other Methods

Several other approaches were also attempted, though none had the level of success we had with TMA. A synthesis of 6-butenylazulene was attempted, from 4-butenylpyridine and cyclopentadiene, in a modification of a standard preparation of azulene.[55] This is shown in Scheme 2.2. Ultimately, no product was isolated. 6-Methylazulene was synthesized from 3-methylthiophene-1,1-dioxide and 6-(dimethylamino)fulvene, shown in Scheme 2.2. While this synthesis was successful, allylation in the same manner described above led to no product. We believe that this is because the initial addition of the allyl group occurs at the ring-fusion carbon.

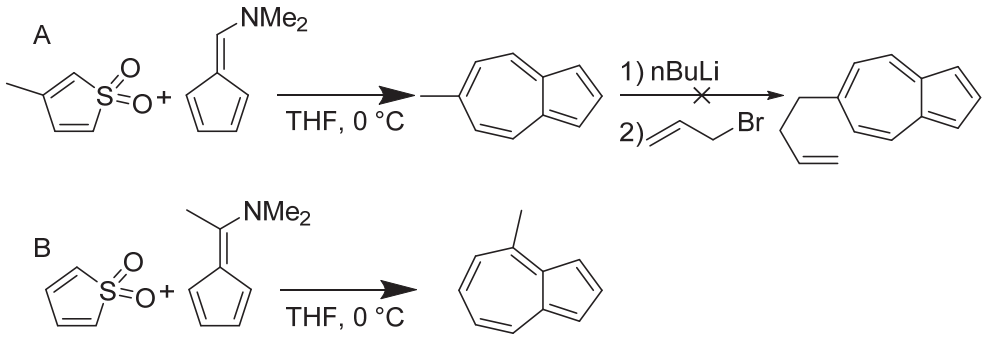

Scheme 2.2. Synthetis of methylazulenes. A. 6-methylazulene and attempted allylation. B. 4-methylazulene.

This puts it too far away to undergo the Cope rearrangement required to complete the reaction. To circumvent this, 4-methylazulene was synthesized from thiophene-1,1-

dioxide and 6-(dimethaylamino)-6-methylfulvene. While product was isolated, the yield was too low (~2%) to be useful.

Guaiazulene (1,4-dimethyl-7-isopropylazulene) was also allylated in the same manner, but produced a large number of multiply-allylated products that could not be separated.

In another approach, azulene was reacted first with Eschenmoser's salt followed by N-methylation to form an azulenylaminium salt. This was then reacted with allylmagnesium chloride to form 1-butenylazulene (Scheme 2.3). While it was possible to generate this material in moderate yields (30-50%), it was found to be unstable and would decompose upon standing. To prevent this, the material was trifluoroacetylated using trifluoroacetic anhydride. This material was stable both neat and in solution. The trifluoroacetyl-butenylazulene underwent hydrosilylation with no problems to form the modified polymer. However, because of the extra steps needed, and the possible effects of the trifluoroacetyl group on the separation properties, the polymer was not investigated any further.

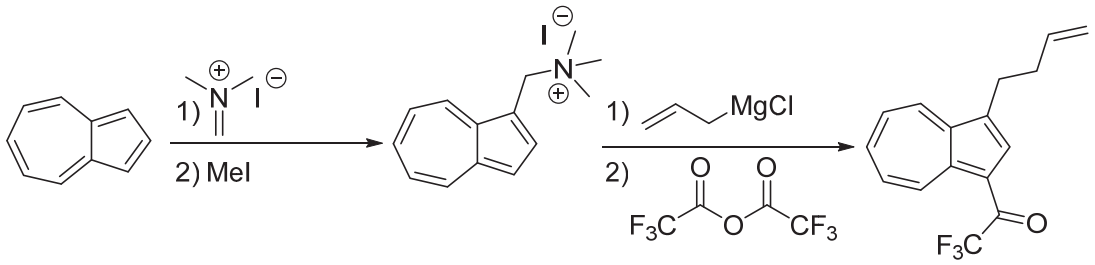

Scheme 2.3. Synthesis of 1-trifluoroacetyl-3-butenylazulene.

We thought azulenyl Grignard reagents might be used either to directly attach the azulene to the polysiloxane backbone, or to react with allyl bromide to form allyl azulene. 1-chloro- and 1-iodoazulene were synthesized from N-chlorosuccinimide and N-

iodosuccinimide and reacted with magnesium metal. Unfortunately, the azulenyl Grignard reagent does not form from either, even under sonication. Reaction of azulene with N-bromosuccinimide leads exclusively to 1,3-dibromoazulene.

While ruthenium, rhodium, and palladium catalysis have been applied to form silicon-carbon bonds on aromatic rings,[56-58] application of these reactions to azulene was not successful.

In another attempt, azulene was reacted with allylmagnesium chloride (Scheme 2.4). Taking advantage of the resonance of the rings, the allyl group would add to either the 4- or 6-position. The ring would then be re-aromatized using DDQ. While this method did result in small amounts of product, they were inseparable from the azulene starting material and yields were very low (<2%).

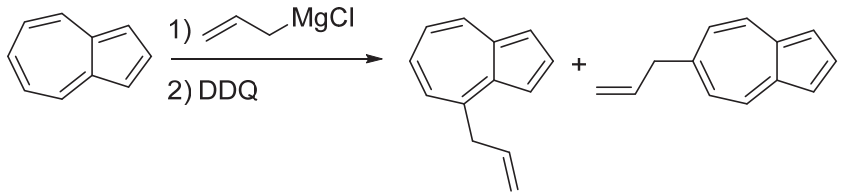

Scheme 2.4. Allylation and rearomatization of azulene using allyl Grignard and DDQ.

Synthesis of Allylnaphthalene

1-allylnapthalene could be synthesized by generating naphthyl Grignard reagents starting with 1-iodonaphthalene and reacting it with ally bromide (Scheme 2.5). 2-Allylnaphthalene can be synthesized using the same process, but results in lower yields.

Polymers were synthesized using an acid-catalyzed “scrambling” of cyclic tetramers octamethylcyclotetrasiloxane and tetramethylcyclotetrasiloxane (Scheme 2.6). A small amount of triflic acid is used as a catalyst.

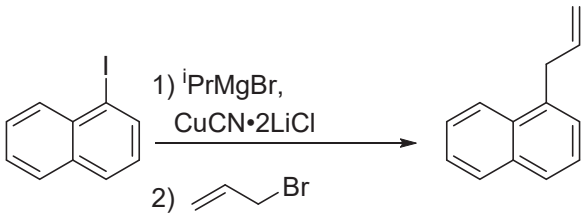

Scheme 2.5. Synthesis of 1-allylnaphthalene.

Synthesis of Polymers

As the tetramers react and form long polymer chains, the mixture changes from a liquid to a gum. After reaction, the polymer is dissolved in hexanes and precipitated with methanol. This removes the more soluble short chains, leaving only the more temperature-stable and less volatile long chains.

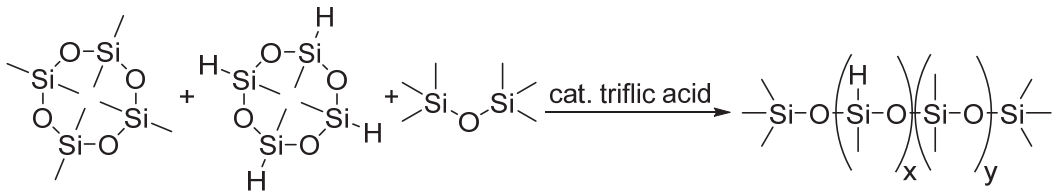

Scheme 2.6. Acid-catalyzed scrambling reaction to synthesize polysiloxane polymer.

It is also possible to generate polymers using a base-catalyzed process (Scheme 2.7). This is potentially advantageous because azulene is acid sensitive; it is easily protonated at the 1-position. By polymerizing with base, the tetramer can undergo hydrosilylation before polymerization. This makes purification easier, because unreacted azulene can be removed from the reaction mixture before polymerization. This was done chromatographically.

To polymerize using base, a small amount of potassium hydroxide is refluxed with a portion of the octamethylcyclotetrasiloxane, which is then mixed with the rest of the tetramers in a toluene solution. The reaction mixture is refluxed, then the toluene

removed, and the polymer precipitated a second time; again by dissolving in hexanes and precipitating with methanol.

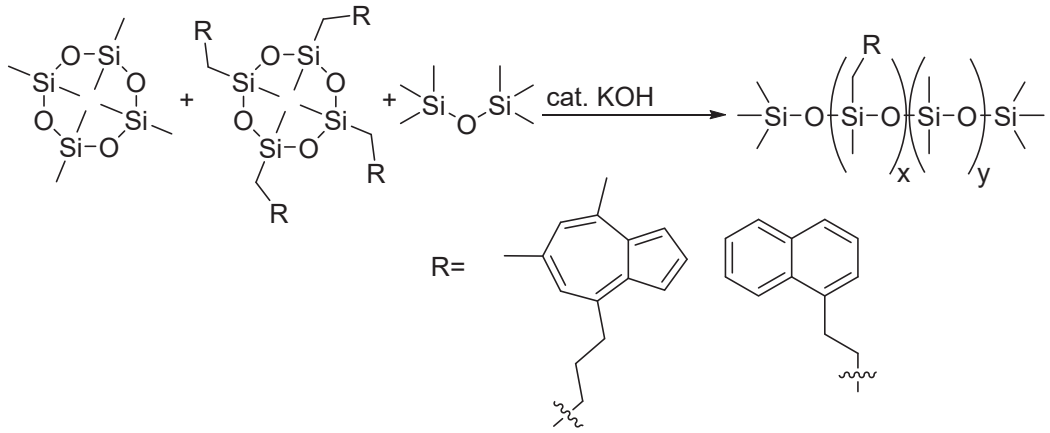

Scheme 2.7. Base-catalyzed scrambling reaction to synthesize substituted polysiloxane polymer.

One problem encountered with this method was an artificial enrichment of the substitution of the polymer. For example, in one reaction aiming for a 10% substitution, a material containing 50% substitution was isolated after purification. We believe this is caused by the purification washes. The lower substitution polymers are somehow washed out more easily, leaving behind an enriched material. While this can be remedied by reacting the polymer in a second round of base-catalyzed scrambling, the ease of the acid-catalyzed method led us to abandon the base-catalyzed method.

Polymer Modification

The polymers were modified using hydrosilylation, reacting an alkene with a silicon hydride (Si-H) group in the presence of a metal catalyst, generally platinum, to form a new silicon-carbon bond (Scheme 2.8). Several catalysts were tested, with the most effective being Karstdedt's catalyst, a well-known platinum catalyst for this

reaction. Hydrosilylations were initially conducted in chloroform at 55°C, but the reaction with allylnaphthalene did not proceed under these conditions. After switching the solvent to benzene, all reactions proceeded to completion within about six hours.

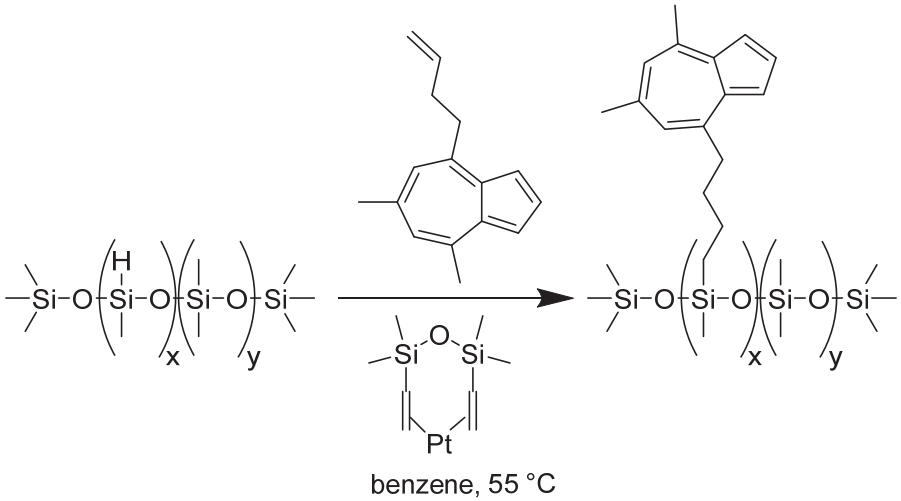

Scheme 2.8. Hydrosilylation of polysiloxane backbone. The same procedure is also used with 1-allylnaphthalene.

The modification reaction was easily monitored using ^{1}H NMR. The Si-H has a distinct peak at approximately 4.8 ppm, and the terminal alkenes used feature peaks between 5.0 and 6.5 ppm. By monitoring the disappearance of these peaks, the progress of the reaction could be tracked.

Column Coating

Columns were coated using the static method, i.e. slow evaporation of a solution of the stationary phase in a volatile solvent.[59] A diagram is shown in Figure 2.2. While uncoated columns are commercially available, they require some preparation before they are ready for coating. The columns were first rinsed with a saturated solution of sodium chloride in methanol to roughen the interior walls of the column; this allows an even film

to form more easily.[60] To remove any residual contaminants, the column was then rinsed with dichloromethane and then dried with flowing nitrogen for several hours.

To coat the columns, a two-neck flask was filled with a dilute solution of the polymer in dichloromethane. The concentration of the solution determines the thickness of the phase in the capillary. This is described by the equation

$$d_f = \frac{rC}{2}$$

where d_f is the film thickness, r is the inner column radius, and C is the concentration of the coating solution. One neck of the flask was attached to an inert gas manifold and the other was covered with a rubber septum. The flask was placed under an inert atmosphere. The capillary was guided through the rubber septum using a 20-gauge needle and pushed into the solution. The gas line to the bubbler was closed, forcing positive nitrogen pressure into the flask, and filling the capillary with the coating solution. After about 10 minutes, the capillary was filled and the bubbler line was reopened. The back end of the capillary was then plugged. Several different methods of plugging the capillary were investigated, including septa, water glass (aqueous sodium silicate), and liquid nitrogen. Ultimately, commercial silicone caulking was found to be the most effective method. It is important to note that only 100% silicone caulking was examined; the column plugging ability of acrylic caulk, which is more prone to cracking and shrinking, have not been investigated. After plugging the column, vacuum was briefly applied to the system to pull the caulking into the capillary. The caulk plug was then allowed to set for at least 12 hours.

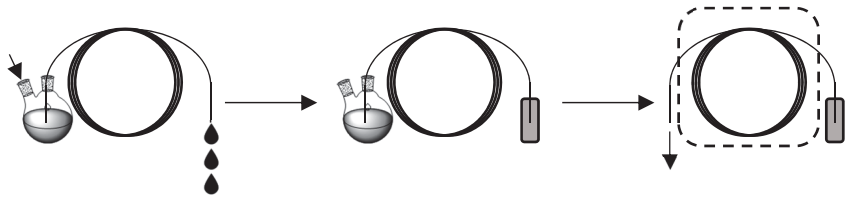

Figure 2.2. Diagram of column coating procedure.

After setting, the capillary was removed from the coating flask and inserted through a septum on a 10 mL round bottom flask. The capillary was transferred to a water bath heated to 35 °C and a vacuum line was inserted into the 10 mL flask. The vacuum was carefully applied. If the coating solution dripped out, the capillary was rinsed with dichloromethane, dried with nitrogen, and the process repeated. If the solution slowly evaporated, the column was left alone until all the solvent had evaporated. This process generally took 10-15 hours. After completion, the columns were removed from the water bath and any length of the column that was out of the water bath during coating was trimmed off.

Initially, column coating attempts failed 95% of the time. However, after much experimentation and consultation with outside sources, success rates rose to approximately 75%. Degassing the solvent via either sonication or sparging with helium had no effect the success or failure of the coating. The most common cause of failure to properly coat was incomplete filling of the back end of the column. If air bubbles were present between the solvent and the caulk plug, the coating solution would immediately exit the capillary upon application of vacuum.

When coating was complete, the column was removed from the water bath and trimmed at the points above the water level. The column was then installed in the GC

injection port and left to run under hydrogen for 30 minutes. The column was then installed in the detector and the column was conditioned to 180 °C. Once this was complete the column was ready for testing.

Column Efficiency

The number of theoretical plates in the columns was evaluated using naphthalene at 120 °C. Evaluation at other temperatures gave nearly identical results. Peak shape was good, as shown in the example chromatogram of the straight chain alkanes heptane through heptadecane (Figure 2.3). All columns gave good plate numbers, indicating the coating had worked sufficiently well for further testing. The number of plates per meter and the retention factor, *k*, of naphthalene at 120 °C are shown in Table 2.1.

Table 2.1. Theoretical plates per meter and retention factor measured for naphthalene at 120 °C.

	N/m	k
15% TMA	2660	4.57
35% TMA	1840	5.25
15% naphthyl	2480	3.41
35% naphthyl	1960	4.37

It should be noted that increasing the percent azulene or naphthalene present in the polymer reduces the number of theoretical plates achieved.Repeating these tests at different temperatures gives the same result. This is because the equation for calculating the theoretical plates is

$$N = 5.54\left(\frac{t_r}{w_{1/2}}\right)^2$$

where N is the number of theoretical plates, t_r is the retention time, and $w_{1/2}$ is the width of the peak at half height. While both the retention time and peak width depend on the temperature, they tend to decrease proportionally to each other as temperature increases.

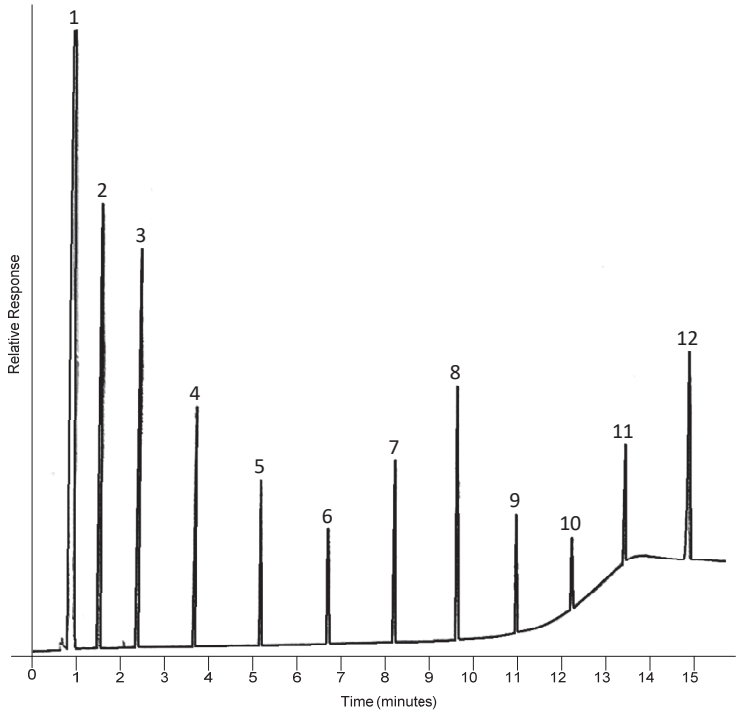

Figure 2.3. Separation of n-alkanes heptane through heptadecane on the 15% trimethylazulene column. Parameters: 40 °C to 180 °C at 10 °C per minute, hold 5 minutes. Peak identification: (1) dichloromethane (solvent), (2) n-heptane (1.517 min), (3) n-octane (2.440 min), (4) n-nonane (3.779 min), (5) n-decane (5.355 min), (6) n-undecane (6.987 min), (7) n-dodecane (8.590 min), (8) n-tridecane (10.122 min), (9) n-tetradecane (11.561 min), (10) n-pentadecane (12.929 min), (11) n-hexadecane (14.239 min), (12) n-heptadecane (15.808 min).

Naphthalene was run at 100 °C at various flow rates on the 15% TMA column. Using these results, a Golay plot was constructed, which shows that efficiency is at its greatest near 1.5 mL/minute, which is expected with the hydrogen carrier gas used.

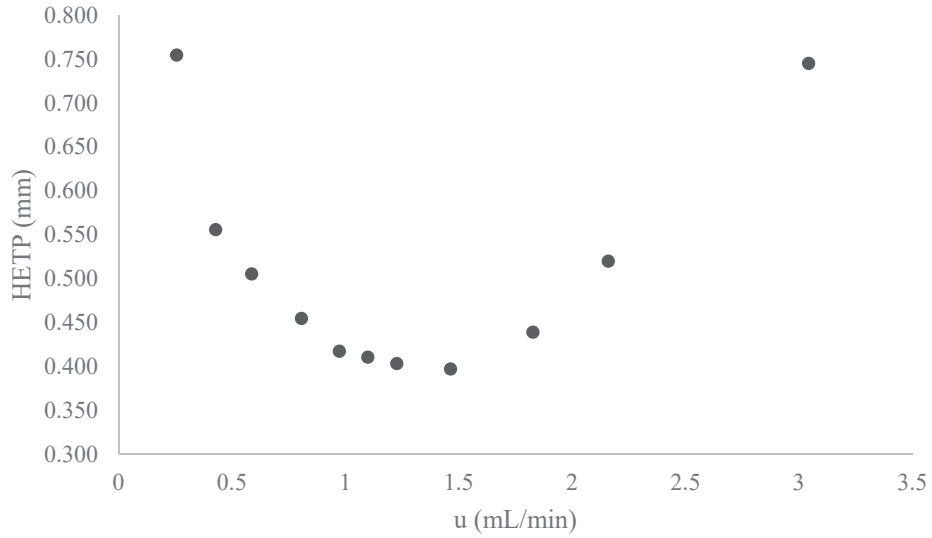

Figure 2.3. Golay plot of the 15% TMA column. Each point represents the height of each theoretical plate from naphthalene at 100 °C.

Temperature Stability

The temperature stability of the 15% TMA column was measured by subjecting the column to one-hour bakes at increasing temperatures, then measuring the efficiency of the column by running naphthalene at 100 °C. A plot of these results is shown in Figure 2.5. As the bake temperature increases from 240 °C to 260 °C, a jump in the efficiency occurs. From this, we can surmise that decay of the stationary phase occurs somewhere in this range and care should be taken not to exceed 240 °C.

Column Polarity

The Kovats retention indices [14] of benzene, pyridine, n-butanol, 2-pentanone, and 1-nitropropane were measured at 40 °C. These were used to calculate the Rohrschneder-McReynolds constants,[13] shown in Table 2.2. Increasing the percentage of azulene

present in the polymer increases the polarity of the stationary phase, particularly in its retention of benzene.

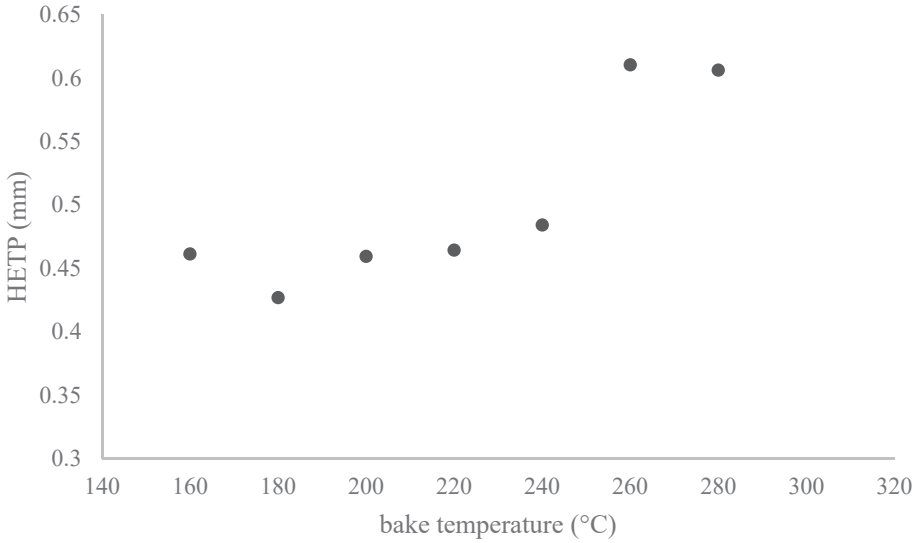

Figure 2.5. Plot of theoretical plate height versus column bake temperature on the 15% TMA column. Each data point represents the efficiency of naphthalene run at 100 °C after which column was subjected to a one-hour bake at the shown temperatures.

The same effect was seen in most cases for naphthalene. Remarkably, the naphthalene phases generally exhibited greater polarity than their azulene analogues. This could partly be due to the difference in chain length used to link the aryl groups to the polymers. The azulenes were linked with a four-carbon chain, while the naphthalene is linked using a three-carbon chain. This longer chain may allow the phase to appear as less polar due to the higher nonpolar character of the alkyl chain.

The enthalpy and entropy of the interaction of a compound with the stationary phase was calculated using the equation [61]

$$\ln k = \frac{\Delta H}{RT} - \frac{\Delta S}{R} + \ln \beta \quad (1)$$

where k is the retention factor, ΔH is the enthalpy of transfer from the mobile phase to the stationary phase, R is the gas constant, T is the absolute temperature, ΔS is the entropy of transfer from the mobile phase to the stationary phase, and β is the phase ratio.

Table 2.2. Rohrschneider-McReynolds parameters for the four stationary phases.

	benzene (X')	n-butanol (Y')	2-pentanone (Z')	nitropropane (U')	pyridine (S')	Sum
15% TMA	18	64	63	74	72	291
35% TMA	44	127	92	117	131	511
15% naphthyl	22	110	113	125	144	514
35% naphthyl	70	126	168	215	228	807

Solvation Thermodynamic Parameters

A variety of analytes were run at different temperatures. By plotting the natural log of the retention factor versus the inverse of the temperature, the enthalpy and entropy can be found from the slope and y-intercept, respectively. Change in entropy and enthalpy govern the movement of analytes between the mobile and stationary phases. The change in enthalpy can be interpreted as the dissolution energy of an analyte moving to the stationary phase. The more negative the value, the more favorable in terms of dissolution energy it is for the analyte to be in the stationary phase. Since entropy is a measure of the degrees of freedom in a molecule, the entropy can be interpreted as a measure of the change in a molecule's degrees of freedom as it moves from mobile to stationary phase. A more negative change in entropy means the molecule has fewer degrees of freedom; therefore, a more positive value of entropy will lead to a higher retention by a stationary phase.

Table 2.3 Thermodynamic parameters of analytes on the columns. The Gibbs free energy was calculated using the formula $\Delta G=\Delta H-T\Delta S$ at T=373 K. The R^2 is the coefficient of determination of the van't Hoff plot.

Analyte	column	Temp. (K) min	Temp. (K) max	ΔH(kJ/mol)	ΔS (J/mol*K)	ΔG (kJ/mol)	R^2
decane	15% TMA	373	423	-29.1	-25.9	-19.4	0.992
	35% TMA			-32.0	-29.5	-21.0	0.997
	15% naphth			-31.6	-32.0	-19.7	0.994
	35% naphth			-31.9	-30.5	-20.5	0.996
undecane	15% TMA	373	423	-36.2	-39.6	-21.4	0.997
	35% TMA			-38.0	-40.1	-23.0	0.998
	15% naphth			-37.7	-43.2	-21.6	0.989
	35% naphth			-38.1	-41.7	-22.5	0.998
dodecane	15% TMA	373	423	-42.4	-50.8	-23.4	0.998
	35% TMA			-43.4	-49.0	-25.1	0.999
	15% naphth			-43.6	-53.3	-23.7	0.998
	35% naphth			-44.9	-54.9	-24.4	0.957
tridecane	15% TMA	373	423	-48.0	-60.3	-25.5	0.999
	35% TMA			-48.1	-56.0	-27.2	0.999
	15% naphth			-48.6	-61.6	-25.7	0.999
	35% naphth			-48.6	-59.1	-26.6	0.999
tetradecane	15% TMA	373	423	-52.9	-68.2	-27.5	0.999
	35% TMA			-52.3	-63.3	-29.3	0.999
	15% naphth			-53.6	-69.5	-27.7	0.999
	35% naphth			-53.0	-65.6	-28.5	0.997
naphthalene	15% TMA	373	423	-38.9	-40.6	-23.7	0.999
	35% TMA			-39.4	-37.6	-25.4	0.999
	15% naphth			-34.3	-29.7	-23.2	0.914
	35% naphth			-41.3	-41.6	-25.8	0.999
azulene	15% TMA	373	413	-40.5	-49.8	-21.9	0.990
	35% TMA			-44.3	-44.1	-27.9	0.999
	15% naphth			-48.3	-58.5	-26.5	0.969
	35% naphth			-46.4	-48.4	-28.4	0.999
nitropropane	15% TMA	313	343	-32.2	-47.9	-14.4	0.998
	35% TMA			-31.9	-43.3	-15.7	0.998
	15% naphth			-29.4	-41.0	-14.1	0.995
	35% naphth			-33.8	-46.6	-16.4	0.999
allyl phenyl ether	15% TMA	363	413	-37.8	-43.6	-21.5	0.998
	35% TMA			-38.2	-40.7	-23.1	0.998
	15% naphth			-50.7	-74.7	-22.9	0.968
	35% naphth			-39.3	-43.3	-23.2	0.955
1-octanol	15% TMA	353	403	-43.9	-59.2	-21.8	0.998
	35% TMA			-43.0	-53.3	-23.1	0.998
	15% naphth			-44.6	-60.5	-22.0	0.999
	35% naphth			-43.8	-55.8	-23.0	0.980

The van't Hoff plots for several analytes were measured on the columns. As can be seen, these were all linear, which suggests that no change in the mechanism of interaction occurs as temperature changes. The Van't Hoff plots for naphthalene and azulene are

shown in Figure 2.6. The linearity is apparent, and this same pattern is found in all analytes' plots on all columns.

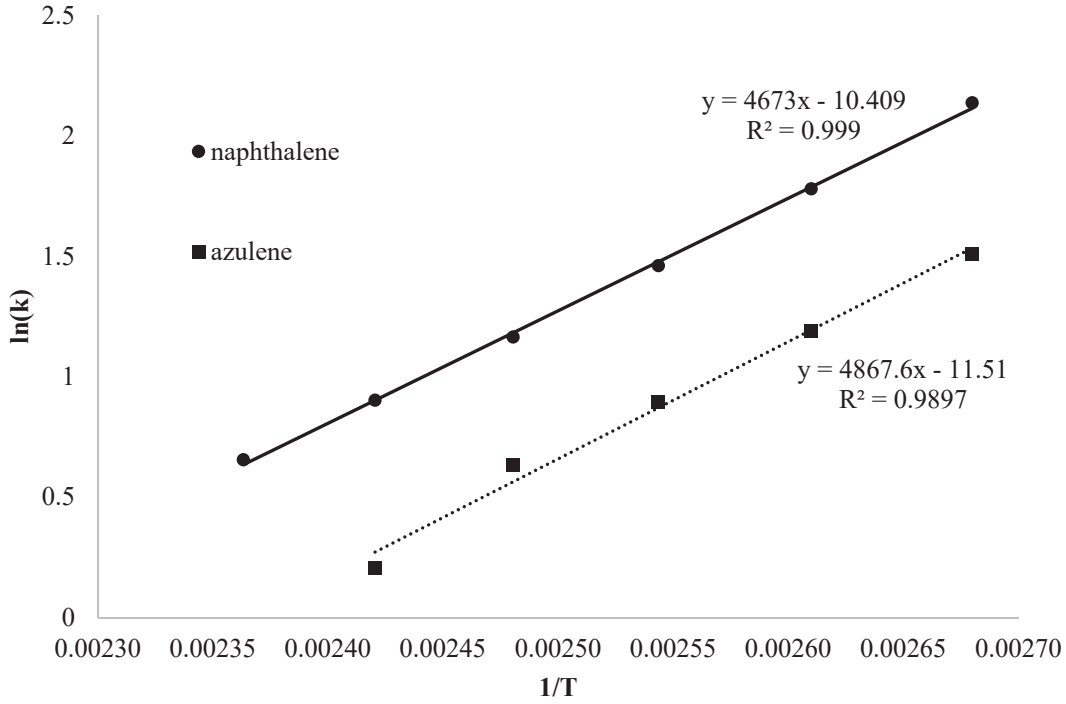

Figure 2.6. Van't Hoff plots of naphthalene and azulene on the 15% TMA stationary phase.

The values of ΔH, ΔS, and ΔG were calculated and are shown in Table 2.3. The enthalpies for decane, azulene, and naphthalene are all similar; however, the entropies vary much more widely. This indicates that entropy primarily controls separation. The more negative value for decane indicates that it is less thermodynamically favored to transfer to the stationary phase than the aromatic ten-carbon molecules examined. Azulene and naphthalene have similar values for both entropy and enthalpy, though azulene has more negative values for both, indicating its transition to the stationary phase is more favored both by entropy and enthalpy.

Isomer Separations

A series of different isomers were separated on the columns to test the phases' abilities against a commercial HP-5 column (30 m length, 0.25 mm ID, 0.25 μm phase thickness). The compounds tested were 2- and 3-phenylpropionaldehyde; 1-, 2-, and 3-octanol; 2-*tert*-butyl- and 4-*tert*-butylcyclohexanone and menthone; 2- and 3-octanone and octanal; 2'-, 3'-, and 4'-methoxyacetophenone; and benzene and cyclohexane. The separation parameters α and resolutions R are shown in Tables 2.4 and 2.5. Example chromatograms from these separations are shown in Figure 2.3.

Table 2.4. Separation factor and resolution of different isomeric mixtures on trimethylazulenyl-derivatized columns, as well as on HP-5. The reported numbers are for the peak vs the preceding peak. In the mixtures with three analytes, the second peak vs the first peak is reported as well as the third vs the second. To compensate for its 30 m length, the resolution of the HP-5 column is corrected by dividing by the square root of 2.

		15% TMA		35% TMA		HP-5	
Analyte	Order	α	R	α	R	α	R
Methoxyacetophenone	2'-, 3'-, 4'-	1.07	2.37	1.10	2.55	1.06	1.64
150 °C		1.33	10.28	1.59	12.28	1.25	7.01
Cyclohexanone	2-tBu, 4-tBu, menthone	1.06	1.86	1.20	2.58	1.05	1.54
150 °C		1.45	11.93	2.20	11.68	1.47	13.48
Octanol	3-, 2-, 1-	1.03	0.80	1.12	1.43	1.20	0.67
100 °C		1.64	14.84	2.20	6.79	1.52	14.42
Octyl carbonyl	3-, 2-, 1-	1.04	1.42	1.12	1.69	1.03	0.70
100 °C		1.06	1.87	1.14	2.06	1.08	2.22
Phenylpropionaldehyde 150 °C	2-, 3-	1.30	7.09	1.78	8.01	1.35	8.37
C6 40 °C	Cy, PhH	1.04	0.91	2.33	1.70	Not separated	

Temperatures were chosen for each separation to provide the minimum retention time with acceptable separation. In general, baseline or very near baseline separation could be achieved on all columns. The higher percentage trimethylazulene and naphthalene

columns did a better job resolving all peaks. Increasing the degree of substitution of either azulene or naphthalene increased the separation factor and resolution in all cases. Cyclohexane and benzene were separated on all azulene and naphthalene columns, but were not separated on the longer HP-5 column, showing potential utility of these phases. In general, only slight differences are seen in the performances between the azulene and naphthalene columns. This could be because the polarizability, while higher for naphthalene, is not different enough to be a factor. Or, the polarizability difference could be masked by the increased dipole moment of azulene.

Table 2.5. Separation factor and resolution of different isomeric mixtures on naphthyl-derivatized columns, as well as on HP-5. The reported numbers are for the peak vs the preceding peak. In the mixtures with three analytes, the second peak vs the first peak is reported as well as the third vs the second. To compensate for its 30 m length, the resolution of the HP-5 column is corrected by dividing by the square root of 2.

		15% Naphthyl		35% Naphthyl		HP-5	
Analyte	Order	α	R	α	R	α	R
Methoxyacetophenone	2'-, 3'-, 4'-	1.08	2.71	1.10	3.00	1.06	1.64
150 °C		1.33	10.00	1.42	11.99	1.25	7.01
Cyclohexanone	2-tBu, 4-tBu, menthone	1.08	2.01	1.11	2.47	1.05	1.54
150 °C		1.48	11.08	1.63	13.09	1.47	13.48
Octanol	3-, 2-, 1-	1.04	1.07	1.05	1.17	1.20	0.67
100 °C		1.60	13.21	1.67	11.16	1.52	14.42
Octyl carbonyl	3-, 2-, 1-	1.06	1.77	1.08	2.01	1.03	0.70
100 °C		1.06	1.76	1.08	2.07	1.08	2.22
Phenylpropionaldehyde 150 °C	2-, 3-	1.31	6.26	1.42	8.31	1.35	8.37
C6 40 °C	Cy, PhH	1.12	2.00	1.49	3.13	Not separated	

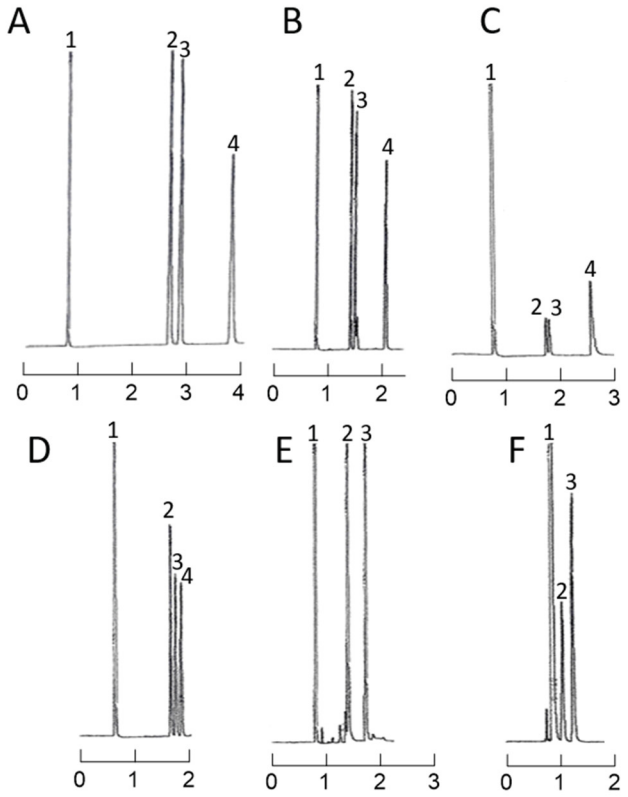

Figure 2.3. Chromatograms of isomeric separations on the 35% naphthalene column. In all cases analyte concentration was 5 mg/mL. A. Run at 150 °C. (1) dichloromethane, (2) 2'-methoxyacetophenone (2.755 min), (3) 3'-methoxyacetophenone (2.960 min), (4) 4'-methoxyacetophenone (3.948 min). B. Run at 150 °C. (1) dichloromethane (solvent), (2) 2-tert-butylcyclohexanone (1.426 min), (3) 4-tert-butylcyclohexanone (1.511 min), (4) menthone (2.073 min). C. Run at 100 °C. (1) dichloromethane (solvent), (2) 3-octanol (1.723 min), (3) 2-octanol (1.780 min), (4) 1-octanol (2.557 min). D. Run at 100 °C. (1) dichloromethane (solvent), (2) 3-octanone (1.776 min), (3) 2-octanone (1.868 min), (4) octanal (1.973 min). E. Run at 150 °C. (1) dichloromethane (solvent), (2) 2-phenylpropionaldehyde (1.410 min), (3) 3-phenylpropionaldehyde (1.739 min). F. Run at 40 °C. (1) dichloromethane (solvent), (2) cyclohexane (1.024 min), (3) benzene (1.220 min).

Development of Chiral Stationary Phases

We also attempted to develop a chiral azulene stationary phase to examine if the diastereomeric separation properties observed in azulene diols would carry over to enantiomeric separations. To synthesize this, azulene was first trifluoroacetylated to form 1-trifluoroacetylazulene, which was then reduced. A variety of reducing agents were

used, both achiral and chiral. An alkene for hydrosilylation could then be added by the etherification of the alcohol using allyl bromide (Scheme 2.9).

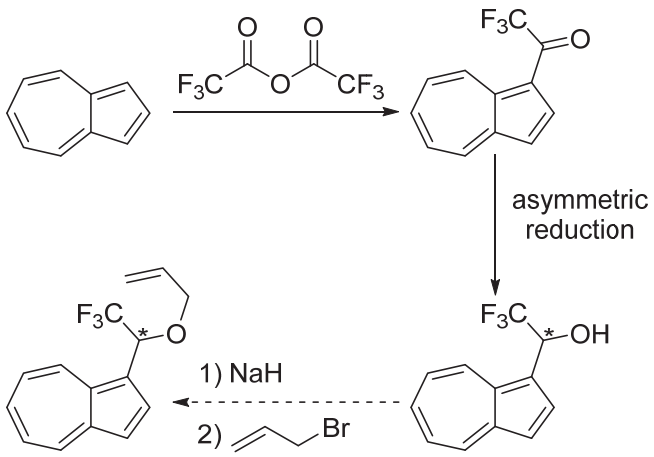

Scheme 2.9. Synthetic pathway of chiral azulene derivative for hydrosilylation.

While achiral reduction using sodium borohydride was straightforward, no chiral reduction conditions could be found that generated an acceptable level of enantiopurity. These include alpine-borane, Meerwein-Ponndorf-Verley reductions using chiral alcohols, various Corey-Bakshi-Shibata reduction catalysts, and reduction using yeast. We also attempted to react the racemic alcohol with the chiral carboxylic acid chlorides (-)-camphanoyl chloride and (-)-menthyl chloroformate to form diastereomers (Scheme 2.10). While these esterifications were successful, the resulting esters could not be separated from each other.

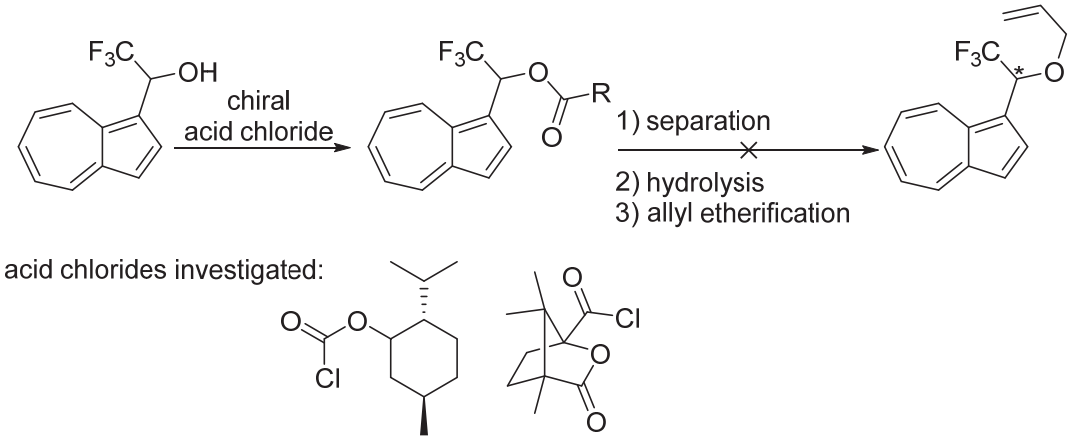

Scheme 2.10. Esterification pathway to chiral azulene derivative.

Conclusions

In summary, polysiloxane modified with 15% or 35% substitution of either a naphthyl- or azulenyl- functionality were synthesized, coated onto capillary GC columns and their separation properties analyzed. All phases exhibited good efficiency and coating ability. Increasing the percent composition of either azulene or naphthalene increases the overall polarity of the phases. Overall, naphthalene columns exhibited greater polarity than azulene columns. All columns exhibited excellent performance in the separation of several groups of isomers, comparing favourably to the results found on an HP-5 column that was twice as long.

Materials

Synthesis of 4-(but-3-en-1-yl)-6,8-dimethylazulene. 4,6,8-Trimethylazulene was prepared by the literature method [52]. A solution of 4,6,8-trimethylazulene (1.7 g, 10 mmol) in freshly distilled THF (30 mL) in a dried round bottom flask under nitrogen was cooled to 0 °C, and n-butyllithium in hexanes (3.86 mL of 2.85 M, 11 mmol) was added slowly. The reaction turned from dark purple to red. After stirring for 10 minutes, allyl bromide (0.952 mL, 11 mmol) was added slowly. The reaction slowly changed from red

to yellow to purple. The reaction was allowed to come to room temperature and stirred for 16 hours. The solvent was removed via rotary evaporation and hexanes was added. The organic layer was washed with water and brine, dried with magnesium sulfate, and the solvent was removed to give a dark purple oil (1.89 g, 90%). Di- and tri-allylated trimethylazulene byproducts were observed by GC-MS, and could be removed via silver nitrate chromatography [62], though a small amount of unreacted starting material was present that could not be removed. The ^{1}H and ^{13}C NMR spectra matched those found in the literature [63].

Synthesis of 1-allylnaphthalene. The synthesis of Boymond et al. was used [64]. A solution of 1-iodonaphthalene (2.92 mL, 20 mmol) in freshly distilled THF (20 mL) in a dried round bottom flask under nitrogen was cooled to -78 °C and 1 M isopropylmagnesium bromide in diethyl ether (60 mL, 60 mmol) was added. The reaction was stirred for 15 minutes. A 1 M solution of copper(I) cyanide di(lithium chloride) complex in THF (60 mL) was added and the reaction was stirred for 15 minutes. Allyl bromide (5.18 mL, 60 mmol) was added and the reaction was allowed to come to room temperature and stirred for 18 hours. The solvent was removed and the product was extracted with dichloromethane. The organic phase was washed with water, 1 M hydrochloric acid, and brine. The organic phase was dried with magnesium sulfate, filtered, and the solvent was removed. The product was purified by Kugelrohr (bulb-to-bulb) distillation under vacuum, followed by flash chromatography with hexanes to give a colorless oil (2.56 g, 76%). The ^{1}H and ^{13}C NMR spectra matched those found in the literature [64].

Preparation of polymers. Tetramethylcyclotetrasiloxane, octamethylcyclotetrasiloxane, and hexamethyldisiloxane (1 mol%) were placed in a round bottom flask, then put under nitrogen. Varying amounts were used to control the final composition of the polymer. Triflic acid (1 mol%) was added and the solvent-free mixture was stirred at room temperature for 6 hours, during which time it thickened greatly. The mixture was dissolved in hexanes (10 mL) and precipitated with methanol (10 mL). This process was repeated five times to ensure purity. The solvent was removed via rotary evaporation to yield a clear, viscous oil. The percentages of hydrogen- and methyl-substitution were obtained by careful integration of the ^{1}H NMR spectrum.

General hydrosilylation procedure. To a solution of the above polysiloxane (500 mg) in chloroform (200 mL) in a dry flask under nitrogen was added a solution of alkene (3.86 mmol) in chloroform (20 mL). A solution of Karstedt's catalyst (240 μL, 3.86 mmol of 2% w/w Pt in xylenes) was added. The reaction was heated to 55 °C. This reaction could be monitored using ^{1}H NMR, watching for the disappearance of the Si-H peak around 4.7 ppm as well as the alkene peaks around 5-6 ppm. It was also possible to monitor using infrared spectroscopy, watching for the disappearance of the Si-H stretch at 2150 cm^{-1}. When the Si-H peak had completely disappeared, the solvent was removed and the mixture was dissolved in hexanes (10 mL). The polymer was precipitated five times with methanol (10 mL) and the solvent was removed to yield a viscous oil. Several catalysts were tested for this reaction, with the most effective being Karstedt's catalyst. The amount of Si-H present on the polymer was calculated based on the integration of the NMR peaks.

Polymer Characterization by NMR Spectroscopy

^{1}H NMR spectra of the polymers in $CDCl_3$ were recorded on either an Agilent VNMRS 500 MHz NMR or a Bruker Ascend 600 MHz NMR. The percent compositions of the polymers were based on the integrations of the proton signals.

Column Preparation

Columns were coated using the static method. A 15 meter 0.25 mm internal diameter column was pretreated by rinsing with a saturated solution of sodium chloride in methanol, followed by dichloromethane. The column was left under flowing nitrogen for 6 hours, then filled with a 0.25% solution (chosen to provide a 0.25 μm film) of the polymer in dichloromethane. The back end of the column was sealed and vacuum was applied to the front while the column was held at 35 °C in a water bath. When all solvent had evaporated, after approximately 10 hours, the column was conditioned under H_2 flow in the GC 40 °C for 1 hour, then 2 °C per minute up to 180 °C and held at this temperature for 90 minutes.

Column Evaluation

Column evaluations were performed with a Hewlett Packard 5890 Series II GC equipped with a flame ionization detector (FID), using hydrogen as the carrier gas with a linear velocity of 40 cm s^{-1}. Samples were injected using the split mode at > 40:1. Injector temperature was held at 280 °C and detector temperature was held at 250 °C. Evaluation of separations on the HP-5 column were performed with an Agilent 7820 GC equipped with an Agilent 5977E MS detector. The carrier gas was helium with a linear velocity of

20 cm s^{-1}. Samples were injected using the split mode at 40:1. Injector temperature was held at 280 °C, MS source at 250 °C and MS quad at 150 °C. Efficiency was expressed as the number of theoretical plates per meter for naphthalene at 120 °C. The polarity was evaluated by measuring the McReynolds constants of the first five standards at 40 °C. The thermodynamic properties were evaluated for the 15% azulene column by generating van't Hoff plots for several different analytes [61].

CHAPTER THREE

Metal Complexes of the Hindered Tridentate Ligand 2,6-bis-(3',5'-diphenylpyrazolyl)pyridine

Introduction

2,6-bis-pyrazolylpyridines (bpp) are an important class of ligand in inorganic chemistry. The use of bpp complexes as catalysts[26, 33-37, 65] is an active area of transition metal chemistry. Historically, bpp ligands have been synthesized by nucleophilic aromatic substitution reactions between pyrazole anions and 2,6-dihalopyridines.[66] However, pyrazole anions react only sluggishly with 2,6-dihalopyridines, requiring long reaction times (~ 72 h) even at elevated temperatures (~ 110 °C), and increasing sterics disfavor the reaction further.[26] Thus, nearly all bpp ligands to date have methyl groups (or H) at the pyrazole 5' positions.[34, 50, 67-70] Another method of synthesizing bpp ligands that tolerates a much wider range of substituents in the 5'- positions of the pyrazole rings has been developed in our research group.[22, 29] This method involves forming the pyrazole rings already in place by the acid-catalyzed condensation of 2,6-bis-hydrazinopyridine with 1,3-diketones. This approach allows groups as large as *tert*-butyl to be placed at the 5' position easily and even selectively.[29] In addition, the regioselective synthesis of 2,6-bis-(1H-indazol-1-yl)pyridines[27] and electron donating- or withdrawing-substituted 2,6-bis-(3,5-diarylpyrazolyl-1-yl)pyridines have been synthesized by this method but are not covered here.[28] In this way, we prepared the modestly bulky 2,6-bis-(3,5-diphenyl-1H-

pyrazol-1-yl)pyridine (bdppp), though it has recently been made by the traditional route in similar yield.[71]

Similar in many ways to the more commonly encountered terpyridine (terpy) ligand,[26, 72] metal-bpp complexes are widely studied because of their interesting physical and chemical properties. The first row transition metal complexes of these type of ligand have been studied for transfer hydrogenation,[33] asymmetric cyclopropanation[38] and epoxidation,[32] the formation of dialkyl ethers,[65] and the polymerization of alkenes[34-36] and caprolactone.[37] These complexes have been examined for use in solar cells.[48] The biological activity has also been investigated, including DNA interaction[50] and anti-cancer activity.[50] Fe complexes have been thoroughly investigated for their spin-crossover properties.[70]

Complexes of bpp ligands with second row transition metals have been evaluated for several uses. Ru complexes with various bpp ligands have been well studied and have been shown to be excellent catalysts for transfer hydrogenation,[30-32] oxidation,[40, 73] and asymmetric epoxidation[32, 74] as well as dye sensitizers in solar cells.[35, 42-47] Similar Ru complexes of bpp with phenyl substituents in the 3-position have been synthesized and their crystal structures determined.[75-76] Chiral Rh-bpp complexes have been used as catalysts for asymmetric cyclopropanation.[38-39] While several research accounts of Pd-bpp complexes have been published,[77-78] to our knowledge no published crystal structures exist.

Herein are reported the synthesis and properties of complexes of bdppp coordinating Mn(II), Fe(II), Co(II), Ni(II), Cu(II), Zn(II), Ru(II), Rh(II) and Pd(II), with the Mn (II)

complex being the first reported bpp complex of that metal and the Pd(II) complex being the first crystal structure reported.

Synthesis

The synthesis of complexes was carried out as shown in Scheme 3.1. Each metal chloride was dissolved in ethanol and was mixed with one equivalent of ligand in dichloromethane. In the case of the Fe salt, two equivalents of ligand were added. In the case of the Pd complex, two equivalent of $PdCl_2$ were added. For the Mn, Co, Ni, Cu, and Zn complexes, the mixture was heated and sonicated briefly. In the cases of the Fe, Ru Rh, and Pd complexes, the reactions were performed in a pressure tube heated to 90°C for two days. The solvent was then removed under rotary evaporation.

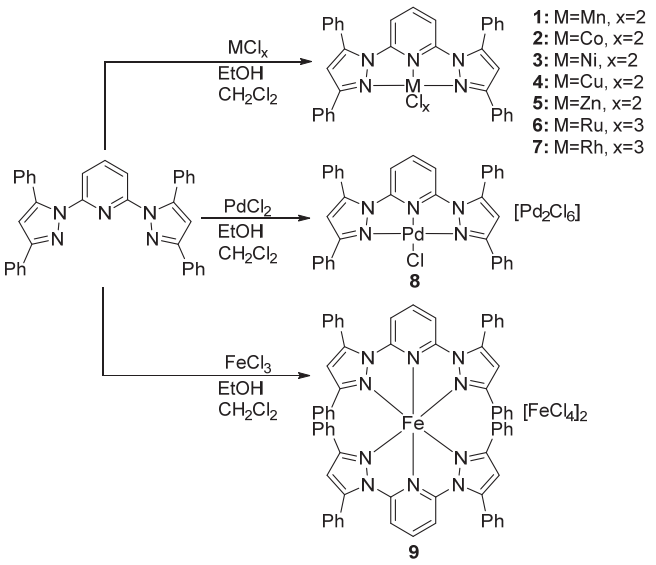

Scheme 3.1. Synthesis of metal complexes.

After dissolution in a minimal amount of dichloromethane, the complexes were crystallized by vapor diffusion of diethyl ether. In all cases, the crystals obtained were suitable for X-ray diffraction studies. A $[Cu(bdppp)_2](NO_3)_2$ and an $[Fe(bdppp)_2](ClO_4)_2$

complex were prepared in a similar manner with copper(II) nitrate and iron(II) perchlorate, respectively, for comparison purposes—though X-ray quality crystals were not obtained for these complexes. The structures were also analyzed by elemental analysis for their percent composition of carbon, nitrogen, and hydrogen. Results are shown in Table 3.1. All complexes matched calculated values within 0.4%, though on storage the Mn and Cu complexes had absorbed one half equivalent of water. Both Fe (III) and Fe (II) chlorides yield the Fe (II) complex, as is well precedented for strong field aromatic ligands, such as pyridines.[79] The synthesis of the Cr complex was attempted using the same methods starting with $CrCl_3$, but no reaction was observed. The synthesized complexes were soluble in dichloromethane, acetonitrile, and methanol, and insoluble in hexanes and ether. The complexes were stable in air and in the solid state.

Table 3.1. Elemental analysis for complexes studied.

entry	compound	color	found (calc)		
			%C	%H	%N
	$[MnLCl_2]$	yellow	62.45 (62.05)	4.10 (4.31)	10.14 (10.34)
	$[CoLCl_2]$	green	64.73 (65.13)	4.16 (3.90)	10.73 (10.85)
	$[NiLCl_2]$	orange	64.76 (65.15)	4.16 (3.91)	10.82 (10.85)
	$[ZnLCl_2]$	colorless	64.09 (64.49)	3.86 (3.87)	10.70 (10.74)
	$[CuLCl_2]$	red	63.78 (63.87)	3.98 (4.00)	10.63 (10.66)
	$[RuLCl_3]$	dark purple	53.52 (53.92)	3.37 (3.47)	8.67 (8.76)
	$[RhLCl_3]$	red-orange	55.25 (55.57)	3.84 (3.97)	9.20 (8.81)
	$[PdLCl]_2[Pd_2Cl_6]$	brown	48.31 (48.14)	2.90 (2.85)	8.05 (7.92)
	$[FeL_2][FeCl_4]_2$	dark yellow	56.46 (56.72)	3.56 (3.40)	9.33 (9.45)

X-ray Crystallography

Crystal data collection and refinement of the first row compounds is summarized in Table 3.2. The SHELX thermal ellipsoid diagrams of the Mn and Fe complexes are displayed in Figure 3.1. Selected bond lengths and angles are listed in Table 3.2. The Mn,

Co, Ni, Cu and Zn complexes have distorted trigonal bipyramidal geometries, with three nitrogen donors (N1, N3, and N5) from the ligand and two chlorine atoms. Consistent with resonance of the pyrazolyl nitrogens with the pyridine ring, in all these cases the metal-pyridine (M(1)-N(1)) bond distances (1.988-2.2193 Å, average 2.09 Å) are shorter than the metal-pyrazole (M(1)-N(3) and M(1)-N(5)) bonds (2.094-2.3932 Å, average 2.24 Å). These are comparable to similar bpp complexes found in the literature.[33-34, 36, 50, 65, 69, 80-84] The metal-chlorine bond lengths range from 2.2071 Å to 2.3329 Å. The metal-chlorine bond distances are similar to those found in the literature.[33, 36, 65, 81-84] The pyridine-pyrazole bond distance ranged from 1.399 Å to 1.420 Å. The N(1)-M(1)-N(3) and N(1)-M(1)-N(5) angles closely match those found in other bpp complexes.[33-34, 36, 48, 50, 65, 81-84] While to our knowledge, no manganese bpp complexes have been reported in the literature, the terpyridine complex has been characterized.[85-87] The Mn-bdppp complex contains shorter Mn-chlorine bonds and Mn-nitrogen bonds than the terpy complex. The Fe complex is hexacoordinate, with a highly distorted octahedral geometry.

In contrast to any of the seven other complexes, the Fe complex features two tridentate ligands coordinated to one Fe atom and two $FeCl_4$ counteranions. The Fe-pyridine distance is 2.1430 Å, and the Fe-pyrazole distances are somewhat longer, 2.1714 Å and 2.2440 Å. The Fe complex features a distorted octahedron, presumably caused by the steric crowding of the phenyl rings. The attachment of the second ligand is done in such a way that there is symmetry around the metal center. While other bulky $Fe(bpp)_2$ complexes are known,[79, 88] the pyrazole rings are only substituted at the 3' position. Those complexes feature much lower levels of distortion than the complexes reported

here. The N(1)-M(1)-N(3) and N(1)-M(1)-N(5) angles are close to those in other bpp complexes.[79]

Table 3.2. Selected bond lengths and angles.

Bond/Angle	**Mn**	**Co**	**Ni**	**Cu**	**Zn**	**Fe**
bond lengths						
M(1)-N(1)	2.2193(16)	2.050(3)	1.988(3)	2.052(3)	2.1224(14)	2.1430(15)
M(1)-N(3)	2.3211(16)	2.270(3)	2.159(3)	2.094(3)	2.2665(16)	2.1714(15)
M(1)-N(5)	2.3687(16)	2.209(3)	2.145(3)	2.120(3)	2.3932(16)	2.2440(15)
M(1)-Cl(1)	2.3023(6)	2.2703(11)	2.2643(10)	2.2507(9)	2.2071(5)	
M(1)-Cl(2)	2.3329(6)	2.2629(10)	2.2583(10)	2.2940(9)	2.2331(5)	
M(1)-Cl(3)						
N(2)-C(1)	1.408(2)	1.420(4)	1.413(4)	1.410(4)	1.404(2)	1.410(2)
N(4)-C(5)	1.416(2)	1.416(4)	1.399(4)	1.417(4)	1.411(2)	1.419(2)
bond angles	**Mn**	**Co**	**Ni**	**Cu**	**Zn**	**Fe**
N(1)-Mn(1)-N(3)	71.24(6)	76.40(11)	77.82(11)	77.45(10)	73.96(5)	73.01(5)
N(3)-Mn(1)-N(5)	71.34(6)	75.67(10)	78.08(11)	76.81(10)	72.65(5)	70.45(5)
N(1)-Mn(1)-N(5)	142.54(6)	151.91(10)	155.85(10)	154.15(10)	146.46(5)	141.05(5)
dihedral angles	**Mn**	**Co**	**Ni**	**Cu**	**Zn**	**Fe**
pyrazole-pyridine	31.57	21.77	25.47	20.03	24.81	28.6
pyrazole-pyridine	26.59	24.26	20.5	26.23	30.23	10.66
5-phenyl-pyrazole	76.73	47.92	40.54	45.88	48.19	88.39
3-phenyl-pyrazole	23.55	34.65	28.37	6.7	18.9	32.54
5-phenyl-pyrazole	46.63	45.09	44.99	42.31	81.18	36.52
3-phenyl-pyrazole	20.59	3.29	5.25	10.28	23.35	19.02
pyridine-[N(1)-N(3)-N(5)]	23.45	19.49	20.85	23.07	20.32	15.35

The dihedral angle between the phenyl and pyrazole rings varies by a larger amount, from nearly parallel to nearly perpendicular. Interestingly, the plane of the pyridine ring is not coplanar with that of the three metal binding nitrogens, with deviations up to 23.45° in the Mn complex. Bis-pyrazolylpyridine complexes with smaller R-groups on the pyrazole rings are very close to planar in this respect, with the pyridine ring being only a few degrees out of the plane of the binding nitrogens—the average angle across 32 literature crystal structures is 4.80°.[33, 35, 50, 71, 81, 83, 89-95] This is attributed to the modest steric requirements of the 5' phenyl rings interacting with the pyridine 3-position hydrogens.

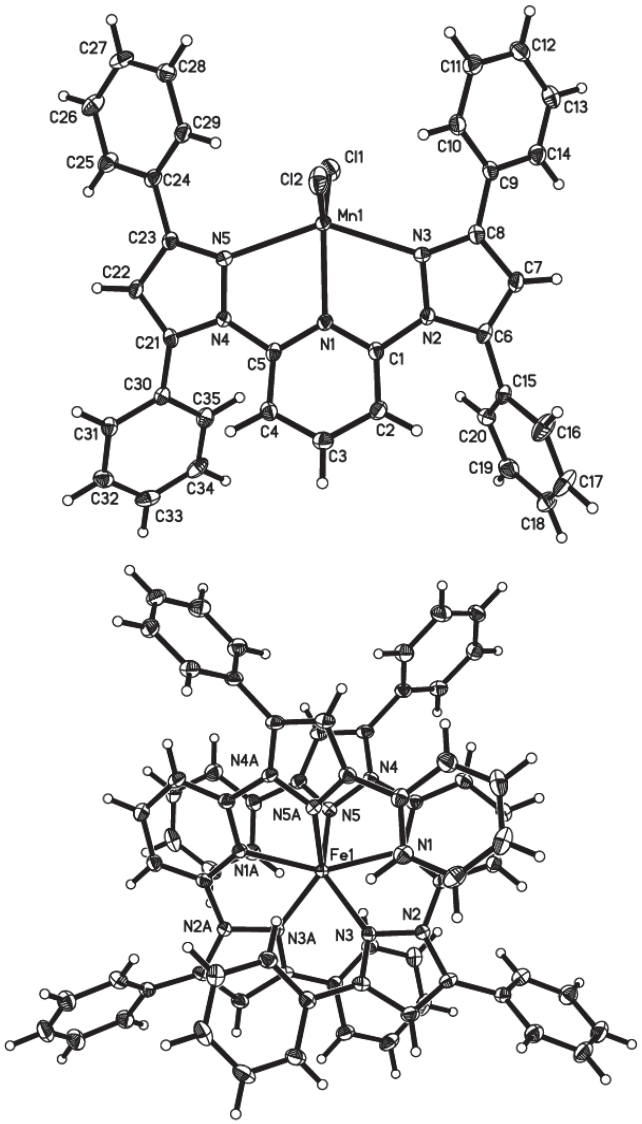

Figure 3.1. Thermal ellipsoid diagrams of the Mn (**1**) and Fe (**5**) complexes. The Co (**2**), Ni (**3**), and Zn (**4**) complexes all share the same general connectivity as **1**. The counteranion of the Fe complex **5** is omitted for clarity.

The second row transition metal complexes is summarized in Table 3.3 and selected bond lengths and angles are summarized in Table 3.4. the SHELX thermal ellipsoid diagrams are displayed in Figure 3.2.

The Ru complex shows octahedral geometry about the Ru atom, with three Ru-Cl bonds and three Ru-N bonds to the ligand. The Ru-pyridine bond is 1.988 Å, and the two

Ru-pyrazole bonds are 2.066 Å and 2.106 Å. The pyrazole and pyridine rings are nearly in the same plane, with dihedral angles of 7.70° and 11.55°. These values are all in line with those reported for other Ru-bpp complexes.[30-31, 72] The phenyl rings are all twisted out of the plane of the pyridine and pyrazoles, due to steric effects. The phenyls in the 5-position are more severely twisted, with dihedral angles of 65.69° and 66.44° with respect to the pyrazole, whereas the 3-position phenyls are 34.53° and 45.39°. This is most likely due to the 5' phenyls avoiding the pyridyl C-3 hydrogens. The pyridine is also tilted out the plane formed by the three Ru-binding nitrogens by 11.06°, again most likely due to the steric hindrance caused by the 5'-position phenyls. Because of the size of the Ru atom, the octahedron about the Ru is slightly distorted, with a pyrazole-Ru-pyrazole angle of 158.40° and pyrazole-Ru-pyridine angles of 78.87° and 79.54°.

Like Ru, the X-ray structure of the Rh complex has octahedral geometry, with one tridentate ligand and three chlorine atoms bound to the metal center. The Rh-pyridine bond distance is 2.040 Å and the pyrazole distances are 2.040 Å and 2.077 Å. The Rh-Cl bond distances are 2.3449 Å, 2.3464 Å, and 2.3398 Å. Again, the pyrazole and pyridine rings are nearly coplanar, with dihedrals between the rings of 10.57° and 8.39°. The phenyl rings are twisted out of the plane of the rest of the ligand, with a dihedral angle between the two phenyl rings in the 3'-position and the pyrazole of 40.22° on average, and a 5'-position phenyl ring/pyrazole dihedral angle averaging 65.90°. We believe this is due to the same causes as in the Ru complex. The octahedron is slightly distorted, with a pyrazole-Rh-pyrazole angle of 160.19°, and pyrazole-Rh-pyridine angles of 79.81° and 80.25°.

Though other bpp-Pd complexes have been reported in the literature, to our knowledge this is the first reported X-ray structure. The Pd structure differs from the other second row transition metal complexes substantially.

Table 3.3. Selected bond lengths and angles of the synthesized complexes.

Bond/Angle	**Ru**	**Rh**	**Pd**
bond lengths (Å)			
M(1)-N(1)	1.988(2)	1.966(2)	1.948(3)
M(1)-N(3)	2.106(2)	2.040(2)	2.033(3)
M(1)-N(5)	2.067(2)	2.077(2)	2.033(3)
M(1)-Cl(1)	2.3441(6)	2.3449(7)	2.2884(8)
M(1)-Cl(2)	2.3571(6)	2.3464(6)	
M(1)-Cl(3)	2.3582(6)	2.3398(6)	
N(2)-C(1)	1.404(3)	1.402(3)	1.396(4)
N(4)-C(5)	1.396(3)	1.414(4)	1.400(4)
bond angles (°)	**Ru**	**Rh**	**Pd**
N(1)-M(1)-N(3)	78.87(8)	80.32(9)	79.90(11)
N(3)-M(1)-N(5)	79.54(8)	79.89(9)	80.07(10)
N(1)-M(1)-N(5)	79.54(8)	160.20(9)	159.72(11)
dihedral angles (°)	**Ru**	**Rh**	**Pd**
pyrazole-pyridine	7.70	10.57	1.93
pyrazole-pyridine	11.55	8.39	3.52
5-phenyl-pyrazole	65.69	65.45	90.03
3-phenyl-pyrazole	34.53	43.43	41.38
5-phenyl-pyrazole	66.44	113.65	78.13
3-phenyl-pyrazole	45.39	37.01	126.99
pyridine-[N(1)-N(3)-N(5)]	11.06	11.11	4.03

Two $[LPdCl]^{+}$ cations are charge balanced by one $[Pd_2Cl_6]^{-2}$ counterion. The crystal structure shows a square planar geometry about the Pd, with the ligand binding through three nitrogen atoms, and one chlorine remaining on the metal. The pyridine-Pd bond length is 1.948 Å and the pyrazole-Pd bond lengths are slightly longer at 2.033 Å for both. The pyrazole and pyridine rings are the closest to coplanarity in this complex, with dihedral angles of 1.93° and 3.52°. While no crystal structure of a Pd-bpp complex has been reported, the similar $[Pd(terpy)Cl]^{+}$ complex has been reported.[96] Compared to the Pd(terpy)Cl complex, the Pd(bdppp)Cl complex features a 0.014 Å shorter bond to the

central pyridine ring and a 0.036 Å shorter Pd-N bonds to the side rings on average. The metal-chlorine bond distance is 2.288 Å, which is 0.027 Å shorter than that of the P(terpy)Cl complex. The pyrazole rings, pyridine, Pd, and chlorine are all nearly coplanar, but the phenyl rings are twisted out of the plane of the rest of the complex. The phenyl's in the 3-position are on average 47.65° out of plane and the 5-phenyl's average 72.40° out of plane. The square planar geometry is slightly distorted, with the pyrazole-Pd-pyrazole angle significantly smaller than the ideal 180° at 160.01° and the pyrazole-Pd-pyridine angles 79.76° and 80.25°.

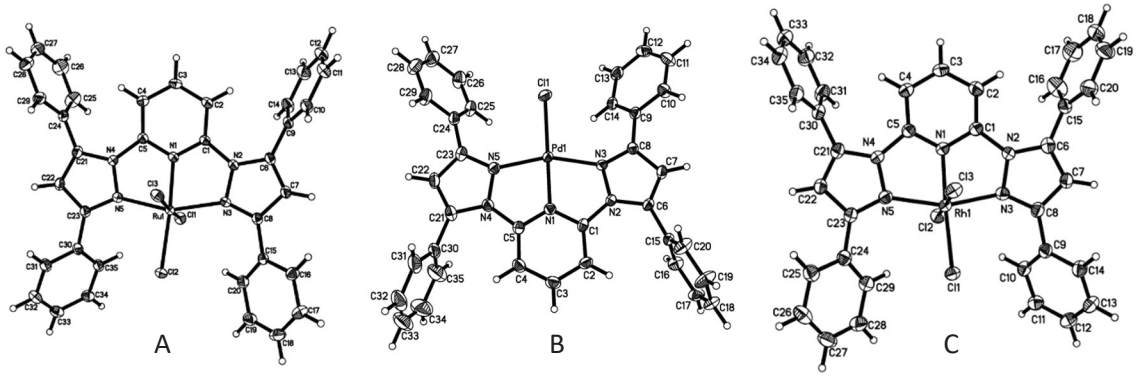

Figure 3.2. Thermal ellipsoid diagrams of complexes studied (A: [Ru], B: [Pd], C: [Rh]). Thermal ellipsoids are shown at the 50% probability level. The Pd complex omits the Pd_2Cl_6 counteranion for clarity.

NMR Spectroscopic Analysis

Proton and carbon NMR spectra were collected for all complexes at room temperature in $CDCl_3$ or DMSO-d_6, shown in Appendix A. The spectra of the Zn, Rh, and Pd complexes show patterns consistent with one ligand bound meridianally to the metal center with C_2 symmetry and are similar to the spectra of other analogous complexes.[81, 89] The resonances of the Pd complex are shifted more downfield than those of the Rh or Zn complexes.

As the Fe complex should also be diamagnetic, the paramagnetic behavior in the NMR spectra was attributed to the $[FeCl_4]^-$. An Fe complex (**6**) with a perchlorate counteranion was synthesized by mixing a solution of the bdppp ligand in dichloromethane with $Fe(ClO_4)_2$ in ethanol. The $[Fe(bdppp)_2](ClO_4)_2$ complex exhibited no paramagnetic behavior in the NMR spectra, as seen in Appendix A.

The NMR spectra of the other compounds exhibited very wide chemical shift ranges and broad peaks, in accordance with the paramagnetic nature of their metals.

ESI Mass Spectrometric Analysis

ESI mass spectra were collected for all complexes from dichloromethane solutions of the complexes. The Mn, Ni, Co, Cu, Zn, Ru, and Rh complexes all ionize by the disassociation of a chloride from the metal, generating $[MLCl\text{-}Cl]^+$ as the major ion. The Pd complex exists as a +1 complex and the Fe complexes exist as +2 complexes, which is observed in the mass spectrum.

To investigate the ligand:metal (L:M) binding ratio with Cu, complexes were synthesized starting from $Cu(NO_3)_2$ and two equivalents of the ligand. Two equivalents of ligand were mixed with one equivalent of $Cu(NO_3)_2$ in dichloromethane. The complex was then precipitated with diethyl ether, filtered, and collected. The Mass spectrum of this complex is solvent dependent. When analyzed in a non-coordinating solvent such as dichloromethane, peaks from the 2:1 L:M species are observed. However, when run in a highly coordinating solvent such as acetonitrile, the 1:1 complex is primarily observed.

UV-Vis Absorption Spectroscopy

Electronic absorption spectra for bdppp and its first row metal complexes are shown in Figure 3.3. All spectra were measured in acetonitrile. All complexes show a strong absorbance in the UV range, particularly around 250 nm, due to the π-π* transitions in the phenyl rings present.

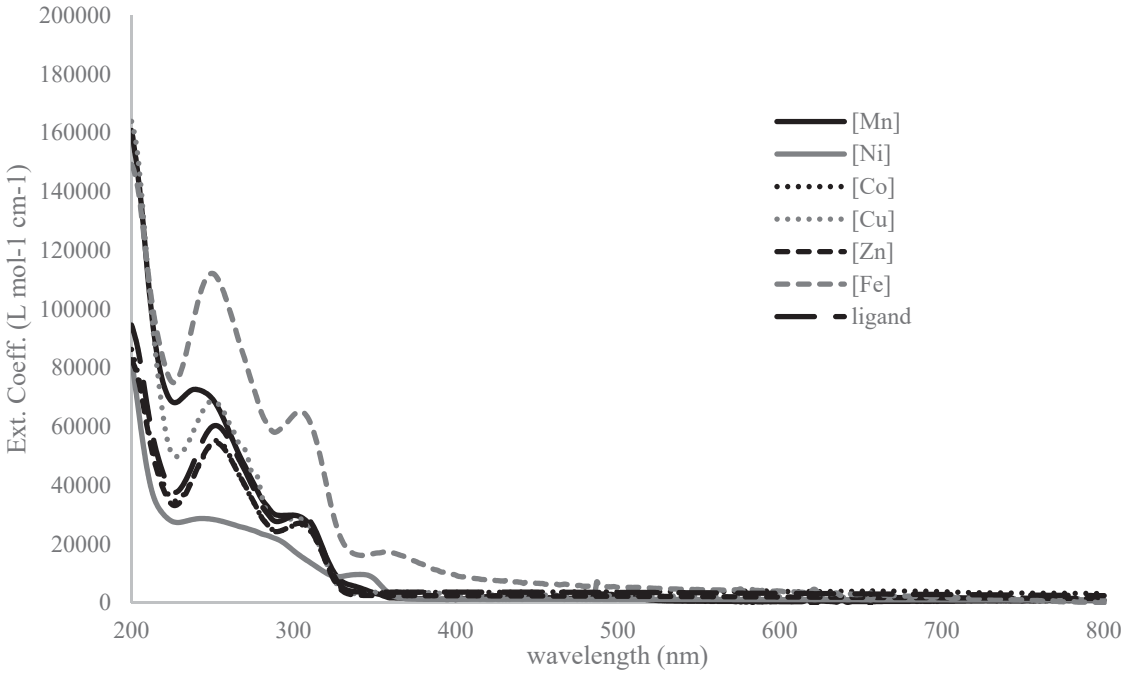

Figure 3.3. UV-Vis spectra of the first-row transition metals.

Of the first row complexes, only the Co and Cu complexes possess significant absorptions in the visible range, as shown in Figure 3.4, caused by d-d transitions. For the Co complex, absorption bands occur at 424, 589 and 685 nm with extinction coefficients of 309, 238 and 308 L mol^{-1} cm^{-1}, respectively. For the Cu complex, absorption bands at 463 and 906 nm are present, with extinction coefficients of 506 and 95 L mol^{-1} cm^{-1}.

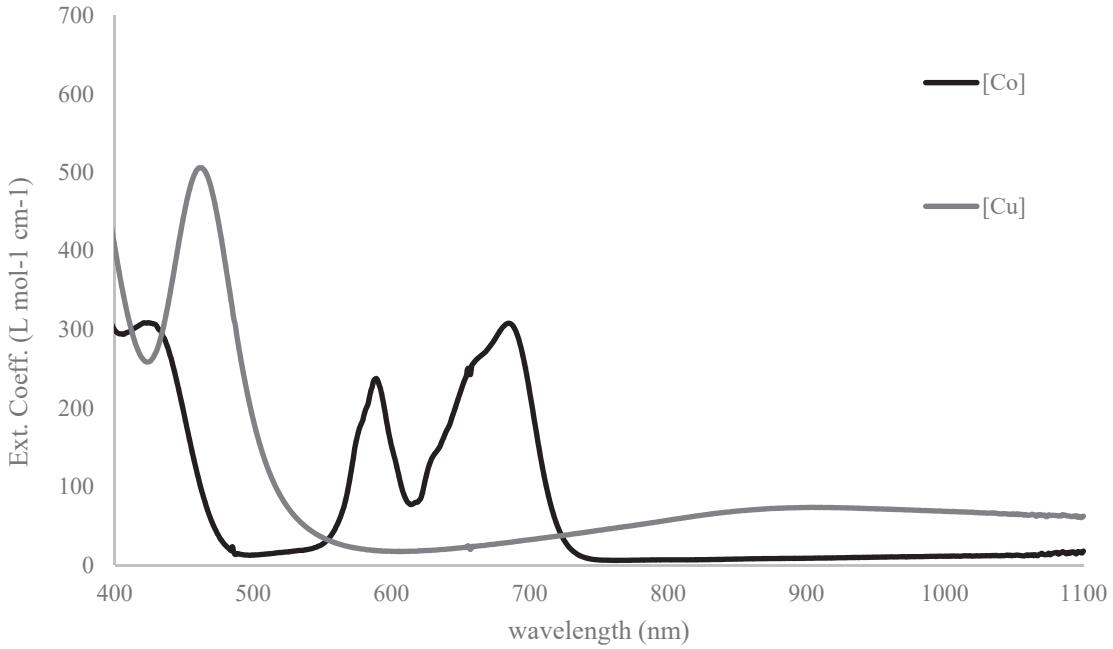

Figure 3.4. Visible normalized absorption spectrum of the Co and Cu complexes.

Job's plots were made for the Cu and Co complexes, shown in Figures 3.5 and 3.6. The plots indicate that in both cases the complexes exhibit a L:M ratio in solution of 2:1, in contrast to the 1:1 ratio observed in the crystal form and implied by the elemental analysis. These results, along with the appearance of ML_2 peaks present in the mass spectra, indicate that the predominant solution form of these two complexes are different than the crystal. Apparently, their propensity to crystallize from solution drives the formation of the 1:1 complexes. Apart from the iron complexes, all attempts to crystallize 2:1 complexes were unsuccessful and produced only 1:1 products. The previously mentioned $[Cu(bdppp)_2][NO_3]_2$ complex shows a different UV-Vis spectrum from the $[Cu(bdppp)Cl_2]$. To ensure the 2:1 complex was measured, the spectrum was collected in dichloromethane instead of acetonitrile. The spectrum is shown in Figure 3.7.

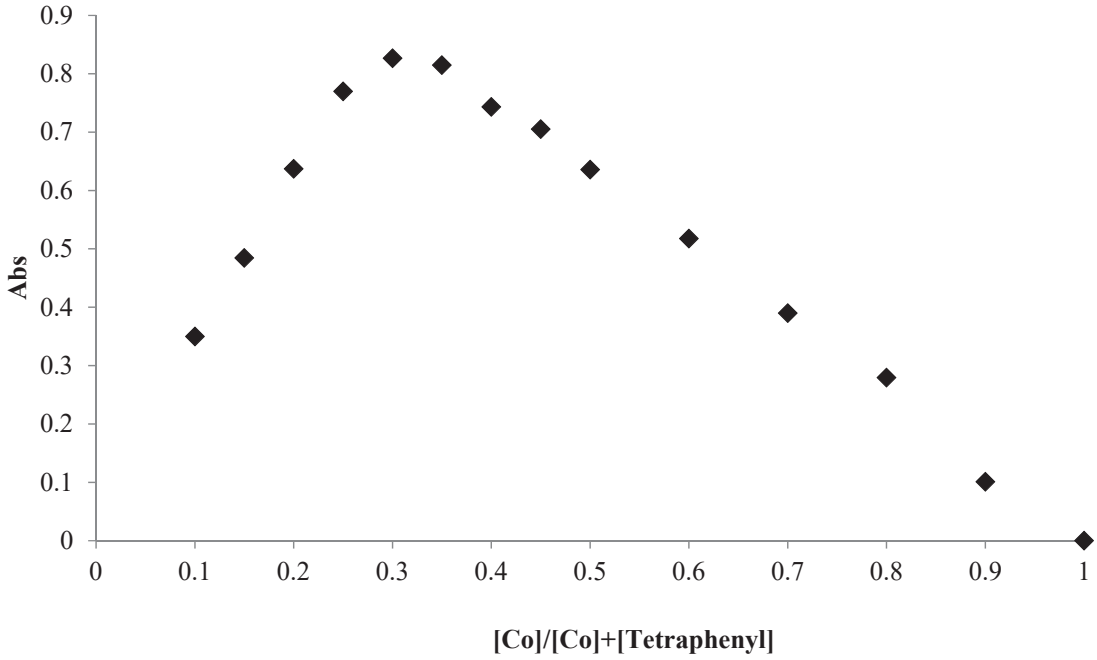

Figure 3.5 Job plot of the Co complex.

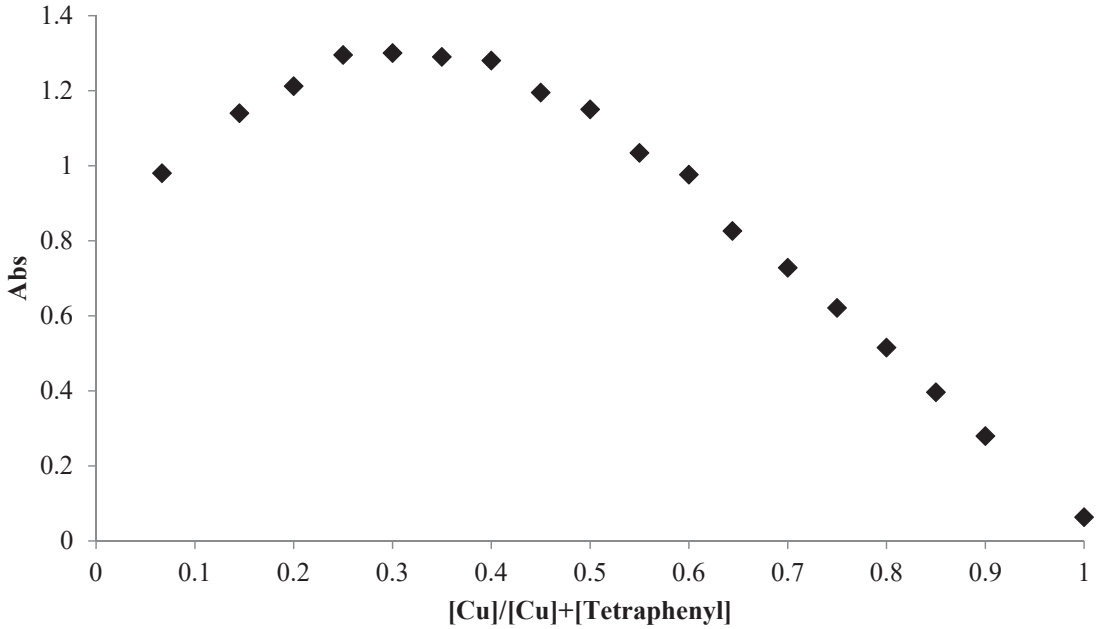

Figure 3.6. Job plot of the Cu complex.

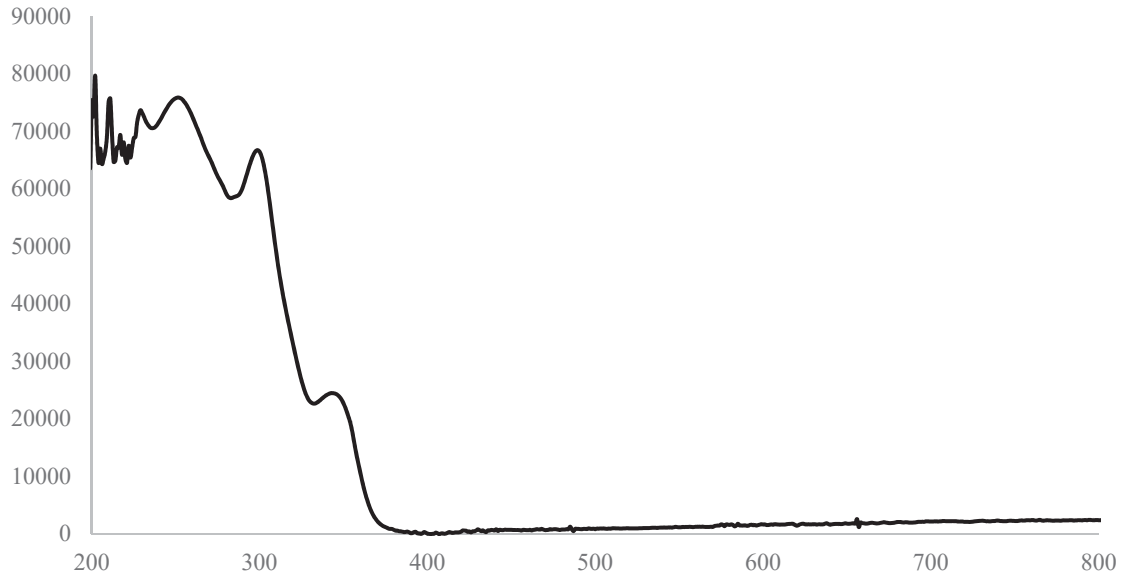

Figure 3.7. UV-Vis spectrum of the 2:1 ligand:copper complex.

In the visible range, this complex shows weak absorption bands at 430 and 761 nm, with extinction coefficients of 292 and 105 L mol^{-1} cm^{-1}, respectively. These are attributed to d-d transitions. The higher energy band at 430 nm is slightly blue-shifted and weaker than the corresponding band in the1:1 complex, which appears at 463 nm and has an extinction coefficient of 506 L mol^{-1} cm^{-1}. The lower energy band is also blue-shifted, from 906 nm, though the intensity is approximately equal.

For the second row complexes, shown in Figures 3.8 and 3.9, the Ru complex shows peaks at longer wavelengths, 400 nm (3524 L mol^{-1} cm^{-1}) and 466 nm (1429 L mol^{-1} cm^{-1}). These are attributed to metal-to-ligand charge transfer (MLCT) processes. The Rh complex has an absorption bands at 438 nm (211 L mol^{-1} cm^{-1}) and 574 nm (574 L mol^{-1} cm^{-1}), which are attributed to d-d transitions. The UV-Vis spectrum of the Pd complex appears very similar to that of the free ligand and shows only strong absorbance bands in the UV region, corresponding to the intra-ligand bands. The peaks are broadened

somewhat, which leads to a slight absorbance that bleeds into the visible range and give the complex its yellow-orange color.

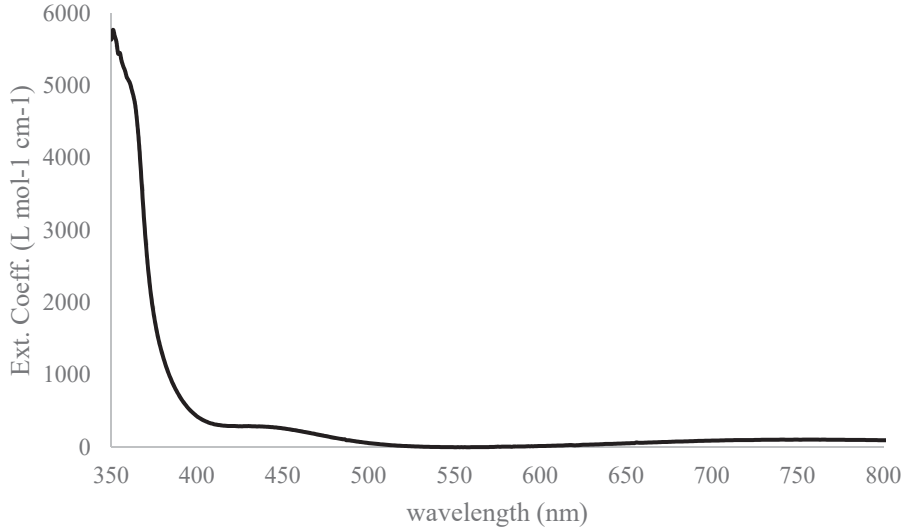

Figure 3.8. UV-Vis spectrum of the 2:1 ligand:copper complex, 350-800 nm.

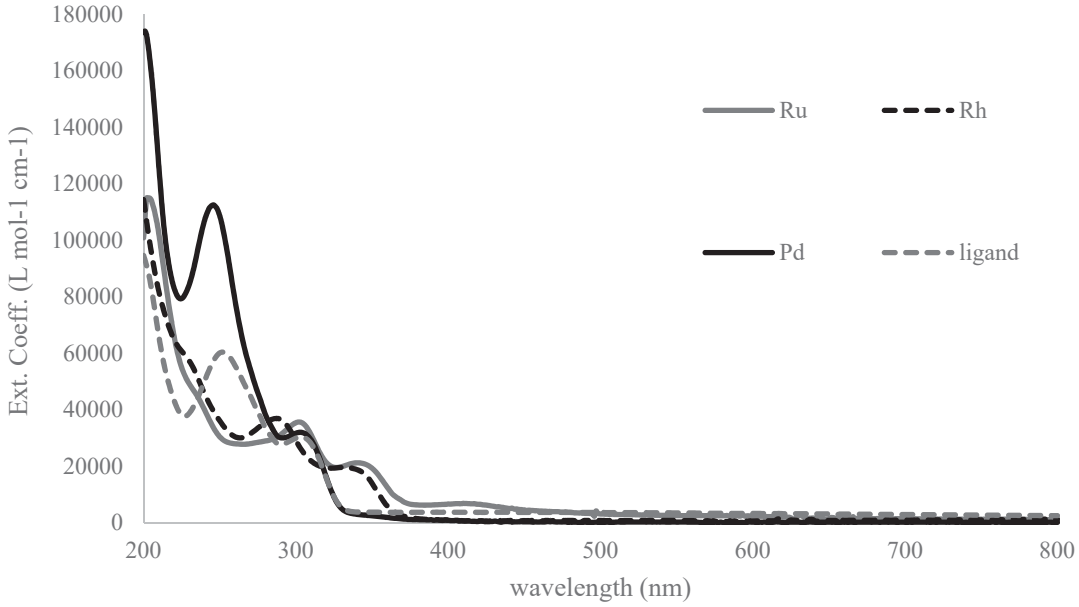

Figure 3.9. UV-Vis spectra of the synthesized metal ligands complexes as well as the free ligand.

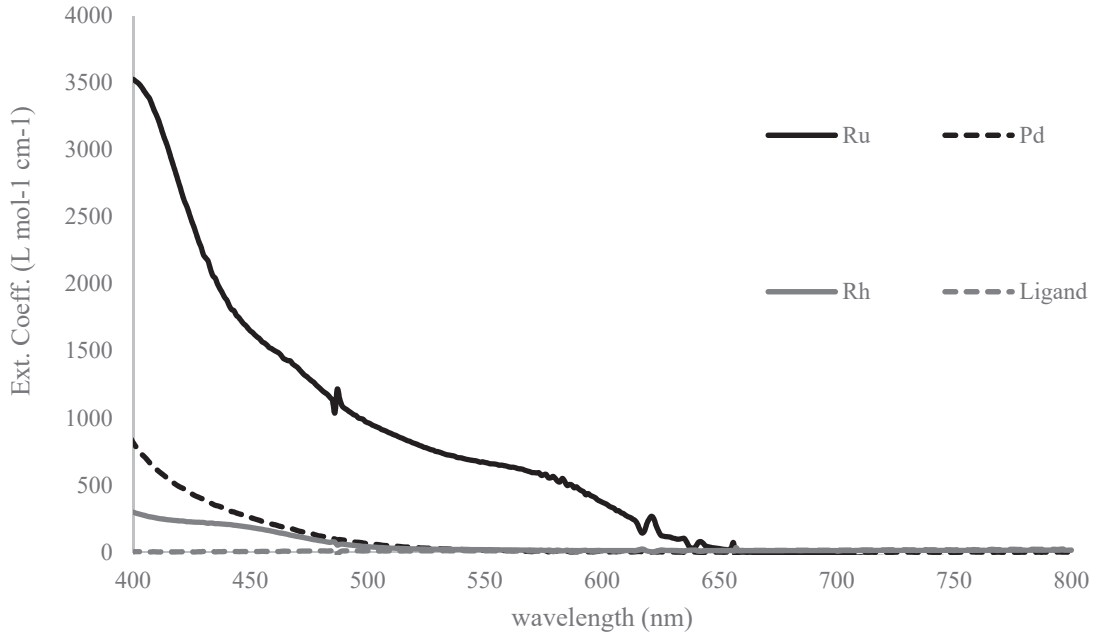

Figure 3.10. UV-Vis spectra of the synthesized metal ligand complexes, 400-800 nm.

Cyclic Voltammetry

Cyclic voltammetry was run in acetonitrile or dichloromethane with 0.1 M tetrabutylammonium hexafluorophosphate (TBAPF6) at room temperature with a 100 mV/s scan rate. $Fe(bdppp)_2(FeCl_4)$ was found to have two quasi-reversible redox couples at 0.05 V (ΔE_p 0.09 V) and 1.28 V (ΔE_p 0.09 V). To determine which Fe redox couple was from the Fe^{2+} in the ligand, the complex with a perchlorate counteranion was synthesized by mixing $Fe(ClO_4)_2$ and the bdppp ligand in ethanol at room temperature, then collecting the resulting precipitate. $Fe(bdppp)_2(ClO_4)_2$, shown in Figure 3.10, was found to have a quasi-reversible redox couple at 1.03 V (ΔEp 0.112 V) with a i_{pa}/i_{pc} of 0.779. Cu, shown in Figure 3.11, was found to have a quasi reversible redox couple centered at 0.50 V (ΔE_p 0.15 V). All the other metal complexes exhibit no redox couples, suggesting that the 2+ state is preferred.

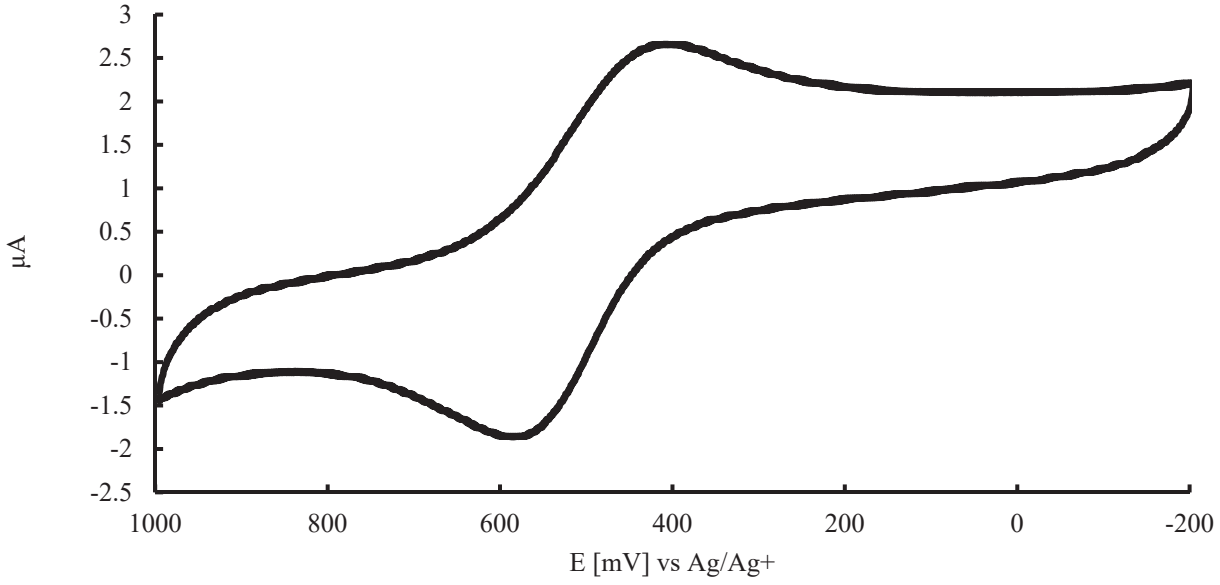

Figure 3.11. Cyclic voltammogram of Cu in ACN with a 100 mV/s scan rate in a 0.1 M solution of $TBAPF_6$.

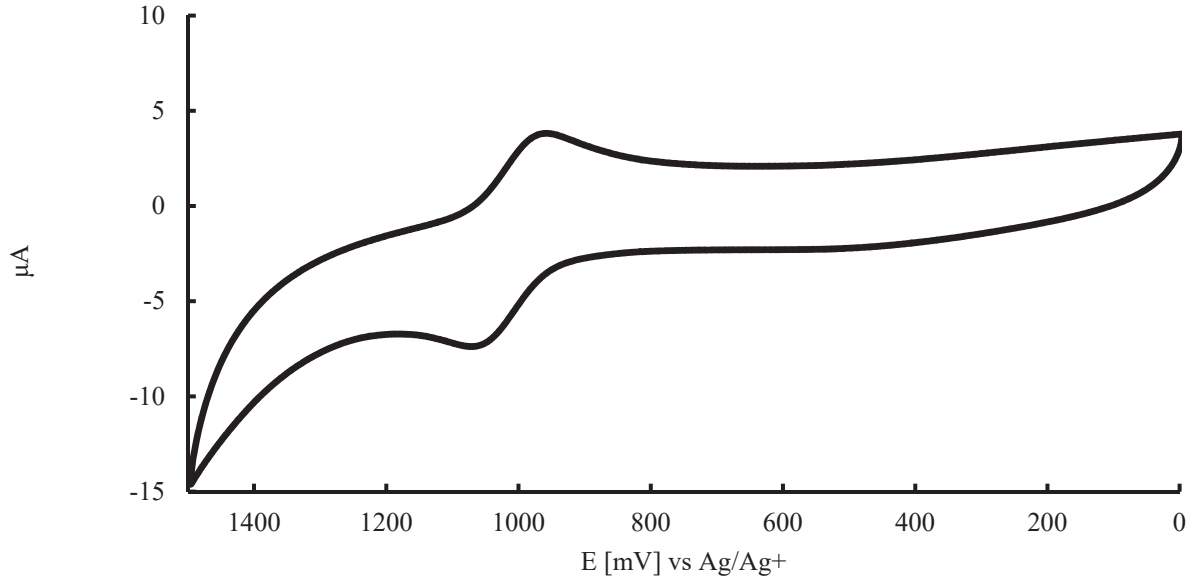

Figure 3.12. Cyclic voltammogram of Ru complex in ACN with a 100 mV/s scan rate in a 0.1 M solution of TBAPF6.

Of the second row complexes, only the Ru complex was found to have a quasi-reversible single electron redox couple centered at ΔE_p of -57 mV and with a i_{pa}/i_{pc} of 0.278. This is shown in Figure 3.12. This was attributed to the Ru(II)/Ru(III) redox couple. As expected, the Pd and Rh complexes did not show any reversibility. The Rh complex featured a reduction at -645 mV and the Pd complex showed a reduction at -577.5 mV.

EPR Spectrsocopy

The room-temperature solid-state EPR spectrum of the 1:1 L:M Cu complex as well as the 2:1 complex were collected, shown in in Figure 3.13. The distinctive pattern clearly indicates the five-coordinate geometry of the complex, with a molecular geometry between a trigonal bipyramide and a square pyramid. The spectrum of the 2:1 L:M material clearly shows six coordinate geometry in the EPR.

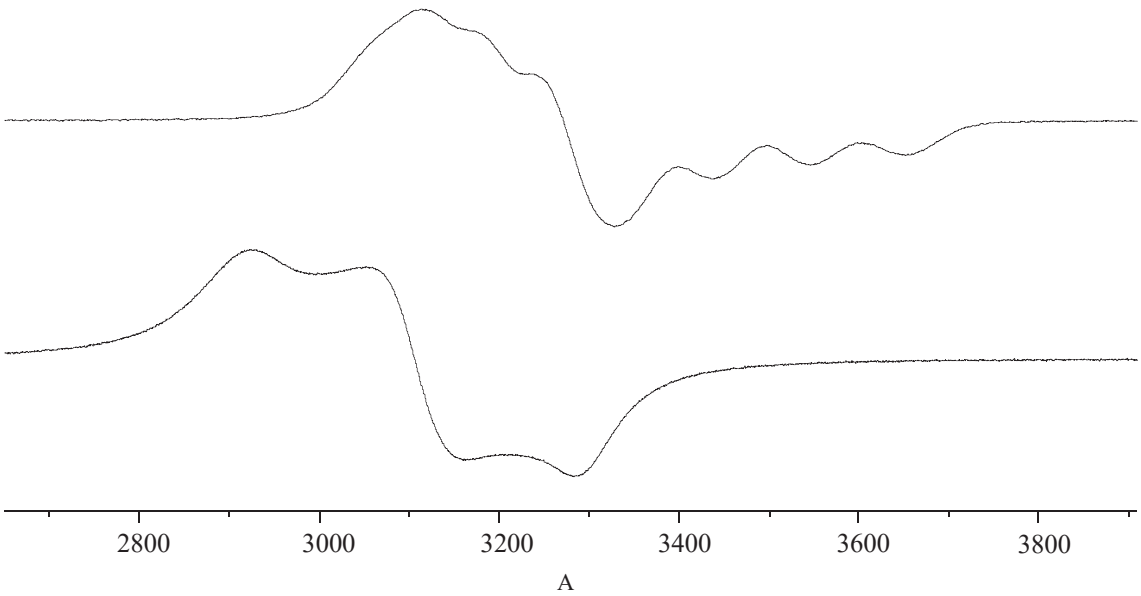

Figure 3.13. Powder EPR spectra of $Cu(bdppp)Cl_2$ (bottom) and $[Cu(bdppp)_2](NO_3)_2$ (top).

Conclusions

The complexes were isolated and analyzed using X-ray crystallography, NMR, and UV-Vis spectroscopy. The first crystal structures of the bdppp ligand reveal two binding modes (1:1 and 2:1) represented by two geometries (distorted trigonal bipyramidal and distorted octahedral). Greater out-of-plane distortions of the pyridine-metal bond vector relative to other reported bpp complexes were observed. This is attributed to the steric interactions between the 5'-phenyl groups and the pyridine 3-position hydrogens.

The NMR spectra of the Zn, Rh and Pd complexes agree with the crystal structure, showing C_2 symmetry, while the other complexes show broad peaks and a wide range of chemical shifts, due to metals' paramagnetic nature. The UV-Vis spectra of the complexes show very strong absorbance bands in the UV-range due to the ligand phenyl substituents. The Co, Cu, and Rh complexes show absorbance bands in the visible range due to both metal-to-ligand and ligand-to-metal charge transfers. The Rh complex shows a charge transfer band in the visible range. The Mn, Ni, Fe, and Pd complexes show only weak absorbance in the visible range due to bleeding over of the UV absorbance bands. The Cu, Fe, and Ru complex show quasi-reversible redox chemistry, while the other complexes show only irreversible reductions.

Experimental Section

$MnCl_2 \cdot 4H_2O$, $FeCl_3 \cdot 6H_2O$, $CoCl_2 \cdot 6H_2O$, $NiCl_2 \cdot 6H_2O$, and $Fe(ClO_4)_2 \cdot H_2O$ were purchased from Aldrich. $FeCl_2$ and $ZnCl_2$ were purchased from Alfa Aesar. 2,6-bis-(3'-5'-diphenylpyrazolyl)pyridine was synthesized according to literature procedures.[29] ^1H and ^{13}C NMR spectra were recorded at room temperature using a Bruker Ascend 600

MHz or an Agilent VNMRS 500 MHz NMR. Spectra obtained in $CDCl_3$ were referenced to TMS (0 ppm) for proton and solvent (77.16 ppm) for carbon. Spectra obtained in DMSO-d_6 were referenced to solvent (2.50 ppm for proton and 39.52 ppm for carbon). Mass spectra were obtained by electrospray ionization using a Thermo Orbitrap Discovery. UV-visible absorption spectra were obtained using a Varian Carey 50 Conc UV-Vis Spectrophotometer. Elemental analyses were performed by Atlantic Microlab (Norcross, GA). Redox potentials were measured via cyclic voltammetry under anaerobic conditions using a CHI-760B potentiostat in dry-degassed CH_2Cl_2 or acetonitrile with 0.1M n-$Bu_4(NPF_6)$ as the supporting electrolyte. The cells consisted of a platinum working electrode (3.0 mm dia.), AgCl/Ag reference, and a coiled Pt auxiliary electrode. The ferrocenium-ferrocene couple (Fc^+/Fc^0) was measured under identical conditions for use as a reference measurement ($E_{1/2}$ = 0.404 V). EPR spectra were recorded in the solid state at room temperature using a Bruker EMX|Plus EPR spectrometer. Crystallographic data were collected on crystals with dimensions of 0.13 x 0.19 x 0.25 mm^3 for Mn, 0.08 x 0.10 x 0.23 mm^3 for Fe, 0.06 x 0.12 x 0.21 mm^3 for Ni, 0.06 x 0.31 x 0.32 mm^3 for Co, and 0.23 x 0.30 x 0.31 mm3 for Zn, 0.496 x 0.331 x 0.068 mm for Ru, 0.06 x 0.31 x 0.33 mm for Rh, and 0.09 x 0.12 x 0.23 mm for Pd. Data for complexes were collected at 110 K on a Bruker/Nonius AXS X8 single crystal X-ray diffractometer except for Rh which was collected at 150 K on a Bruker D8 Quest with IμS microfocus source using Mo K-alpha radiation (λ = 0.71073 Å). All structures were solved by direct methods and refined by full-matrix least-squares refinement on F^2 after multiscan absorption correction of the data using SADABS.[97-98] Crystal data are presented in the appendix. All of the data were processed using the Bruker AXS SHELXTL software,

version 6.14.[99] Unless otherwise noted, all non-hydrogen atoms were refined anisotropically and hydrogen atoms were placed in calculated positions. 1538488 (for Mn), 1538489 (for Fe), 1538490 (for Ni), 1538491 (for Co), 1538492 (for Cu), 1538493, (for Zn) 1569529 (for Ru), 1538494 (for Rh), and 1538495 (for Pd) contain the supplementary crystallographic data for this paper. These data can be obtained free of charge from The Cambridge Crystallographic Data Centre via www.ccdc.cam.ac.uk/data_request/cif.

Synthesis of Metal Complexes, General Procedure: To a vial containing a 5-6 mL of an ethanol solution containing approximately 0.1 mmol of the requisite transition metal chloride was added approximately 1.0 mL of a 0.1 M solution of bdppp in dichloromethane. The reaction was heated briefly with a heat gun and treated with sonication for approximately 60 seconds. The solvent was removed by rotary evaporation and the solid was redissolved in 2-3 mL of dichloromethane then filtered through Celite. Ether was allowed to diffuse into the dichloromethane solution at room temperature until crystals formed (~2 d). If poor quality crystals or a powder was obtained, the solvent was evaporated and the procedure repeated in a freezer rather than at room temperature.

[Mn(bdppp)Cl_2]. From 58.8 mg ligand (0.114 mmol, 1.0 eq) and 25.7 mg $MnCl_2 \cdot 4H_2O$ (0.130 mmol, 1.14 eq) obtained 58.8 mg (0.098 mmol, 80.4%) as yellow trapezoidal scales. UV (ACN) λ_{max} (log ε) 330 (3.94), 295 (4.35), 245 (4.65). HRMS (ESI) for [M-Cl]$^+$: calcd for $C_{35}H_{25}ClMnN_5^+$: 605.1173; found 605.1174. Anal. Calcd for $C_{35}H_{25}Cl_2MnN_5 \cdot \frac{1}{2}H_2O$: C, 62.05; H, 4.31; N, 10.34. Found: C, 62.45; H, 4.10; N, 10.14. IR (FTIR): $\tilde{\nu}$ = 1476 (m), 756 (s).

[Co(bdppp)Cl_2]. From 57.2 mg ligand (0.111 mmol, 1.0 eq) and 30.8 mg $CoCl_2 \cdot 6H_2O$ (0.129 mmol, 1.16 eq) was obtained 67.6 mg (0.105 mmol, 94.6%) as green rhombi. UV (EtOH) λ_{max} (log ε) 415 (2.60), 275 (4.37), 230 (4.31). HRMS (ESI) for $[M\text{-}Cl]^+$: calcd for $C_{35}H_{25}ClCoN_5^+$: 609.1125; found 609.1151. Anal. Calcd for $C_{35}H_{25}Cl_2CoN_5$: C, 65.13; H, 3.90; N, 10.85. Found: C, 64.73; H, 4.16; N, 10.73. IR (FTIR): $\tilde{\nu}$ = 1455 (w), 1467(w), 762 (w).

[Ni(bdppp)Cl_2]. From 51.5 mg ligand (0.100 mmol, 1.0 eq) and 24.5 mg $NiCl_2 \cdot 6H_2O$ (0.103 mmol, 1.03 eq) was obtained 62.5 mg (0.097 mmol, 96.9%) as orange rhombi. UV (EtOH) λ_{max} (log ε) 340 (6.24), 290 (6.42). HRMS (ESI) for $[M\text{-}Cl]^+$: calcd for $C_{35}H_{25}ClN_5Ni^+$: 608.1146; found 608.1163. Anal. Calcd for $C_{35}H_{25}Cl_2NiN_5$: C, 65.15; H, 3.91; N, 10.85. Found: C, 64.76; H, 4.16; N, 10.82 IR (FTIR): $\tilde{\nu}$ = 1455 (s), 763 (s), 695(s).

[Cu(bdppp)Cl_2]. From 56.1 mg ligand (0.109 mmol, 1.0 eq) and 19.4 mg $CuCl_2 \cdot 2H_2O$ (0.114 mmol, 1.04 eq) was obtained 65.4 mg (0.101 mmol, 92.6%) as red rhombi. UV (EtOH) λ_{max} (log ε) 250 (4.89), 205 (5.05). HRMS (ESI) for $[M\text{-}Cl]^+$: calcd for $C_{35}H_{25}CuN_5^+$: 613.1103; found 613.1089. Anal. Calcd for $C_{35}H_{25}Cl_2CuN_5 \cdot ½H_2O$: C, 63.78; H, 3.98; N, 10.63. Found: C, 63.87; H, 4.00; N, 10.66. IR (FTIR): $\tilde{\nu}$ = 1454 (m), 1467(w), 753 (w).

[Cu(bdppp)$_2$][NO_3]$_2$. From 84.6 mg ligand (0.164 mmol, 2.1 eq) and 18.8 mg $Cu(NO_3)_2 \cdot 3H_2O$ (0.078 mmol, 1.0 eq) was obtained 83.4 mg (0.0684 mol, 87.7%). UV (CH_2Cl_2) λ_{max} (log ε) 346 (4.36), 302 (4.82), 255 (4.86). HRMS (ESI) for $[ML_2]^{2+}$: calcd for $C_{70}H_{50}CuN_2^{2+}$: 546.6752; found 546.6815.

[Zn(bdppp)Cl_2]. From 76.2 mg ligand (0.148 mmol, 1.0 eq) and 22.0 mg $ZnCl_2$ (0.161 mmol, 1.16 eq) was obtained 73.6 mg (0.112 mmol, 76.2%) as colorless rhombi. UV (EtOH) λ_{max} (log ε) 305 (4.49), 250 (4.77), 205 (4.86). ^{1}H NMR (600 MHz, $CDCl_3$) δ 8.34 (d, J = 7.2 Hz, 4H), 7.60 – 7.50 (m, 10H), 7.52 – 7.44 (m, 6H), 7.39 (t, J = 8.3 Hz, 1H), 6.90 (s, 2H), 6.63 (d, J = 8.3 Hz, 2H). ^{13}C NMR (151 MHz, $CDCl_3$) δ 155.3, 147.8, 145.2, 142.7, 130.6, 130.2, 129.9, 129.7, 129.5, 129.3, 128.9, 128.8, 112.8, 111.5. HRMS (ESI) for $[M\text{-}Cl]^+$: calcd for $C_{35}H_{25}ClN_5Zn^+$: 614.1084; found 614.1093. Anal. Calcd for $C_{35}H_{25}Cl_2N_5Zn$: C, 64.49; H, 3.87; N, 10.74. Found: C, 64.09; H, 3.86; N, 10.70. IR (FTIR): $\tilde{\nu}$ = 1471 (m), 1456 (m), 765 (s), 749 (s).

[Fe(bdppp)$_2$][$FeCl_4$]$_2$. From 41.2 mg ligand (0.080 mmol, 1.0 eq) and 27.6 mg $FeCl_3$ (0.170 mmol, 2.1 eq) was obtained 48.1 mg of complex (L_2Fe)($FeCl_4$)$_2$ (0.033 mmol, 41%) as dark yellow rhombi. UV (ACN) λ_{max} (log ε) 355 (4.48), 275 (4.59). HRMS (ESI) for $[ML_2]^{2+}$: calcd for $C_{70}H_{50}FeN_{10}$: 543.1779; found 543.1795. Anal. Calcd for $C_{70}H_{50}Cl_8Fe_3N_{10}$: C, 56.72; H, 3.40; N, 9.45. Found: C, 56.46; H, 3.56; N, 9.33. IR (FTIR): $\tilde{\nu}$ = 1463 (w), 763 (s), 749 (s).

[Fe(bdppp)$_2$][ClO_4]$_2$. From 51.3 mg ligand (0.099 mmol, 1.0 eq) and 57.8 mg $Fe(ClO_4)_2 \cdot H_2O$ (0.212 mmol, 2.1 eq) was obtained 105.6 mg of complex $L_2Fe(ClO_4)_2$ (0.082 mmol, 83%) as yellow needles. ^{1}H NMR (600 MHz, DMSO-d6) δ 8.12 (t, J = 7.9 Hz, 2H), 7.90 (d, J = 7.6 Hz, 8H), 7.62 (d, J = 7.9 Hz, 4H), 7.44 (t, J = 7.6 Hz, 8H), 7.36 (t, J = 7.4 Hz, 4H), 7.33 – 7.29 (m, 12H), 7.18 – 7.15 (m, 8H), 7.12 (s, 4H). ^{13}C NMR (151 MHz, DMSO) δ 150.9, 150.0, 144.4, 141.1, 131.6, 129.3, 128.2, 127.88, 127.80, 127.7, 127.6, 127.5, 124.9, 117.9, 105.7. HRMS (ESI) for $[ML_2]^{2+}$: calcd for $C_{70}H_{50}Cl_2FeN_{10}O_8$: 543.1779; found 543.1792.

[Ru(bdppp)Cl_3]. From 52.3 mg ligand (0.102 mmol, 1.0 eq) and 21.2 mg $RuCl_3 \cdot H_2O$ (0.102 mmol, 1.0 eq) was obtained 39.8 mg (0.055 mmol, 53.9**%**) as purple prisms. HRMS (ESI) for $[M\text{-}Cl]^+$: calcd for $C_{35}H_{25}Cl_2N_5Ru^+$: 687.0525; found 687.0557. Anal. Calcd for $C_{35}H_{25}Cl_3N_5Ru \cdot CH_2Cl_2$: C, 53.52; H, 3.37; N, 8.67. Found: C, 53.92; H, 3.47; N, 8.76. IR (FTIR): $\tilde{\nu}$ = 1612 (w), 1471 (s), 979 (m), 822 (m), 798 (w), 758 (m), 697 (s).

[Rh(bdppp)Cl_3]. From 66.1 mg ligand (0.130 mmol, 1.0 eq) and 23.3 mg $RhCl_3$ (0.131 mmol, 1.01 eq) was obtained 58.1 mg (0.080 mmol, 61.7%) as red-orange rhombi. ^{1}H NMR (600 MHz, $CDCl_3$) δ 7.92 – 7.85 (m, 4H), 7.66 (ddd, *J* = 8.8, 3.8, 1.6 Hz, 2H), 7.64 – 7.58 (m, 8H), 7.51 (t, *J* = 8.5 Hz, 1H), 7.41 (dd, *J* = 5.0, 1.8 Hz, 6H), 6.64 (s, 2H), 6.62 (d, *J* = 8.5 Hz, 2H). ^{13}C NMR (151 MHz, $CDCl_3$) δ 162.2, 149.3, 148.1, 141.2, 131.5, 130.9, 130.5, 129.9, 129.7, 127.83, 127.75, 127.72, 114.9, 109.2. HRMS (ESI) for $[M\text{-}Cl]^+$: calcd for $C_{35}H_{25}Cl_2N_5Rh^+$: 688.0537; found 688.0516. Anal. Calcd for $C_{35}H_{25}Cl_3N_5Rh \cdot 2H_2O$: C, 55.25; H, 3.84; N, 9.20. Found: C, 55.57; H, 3.97; N, 8.81. IR (FTIR): $\tilde{\nu}$ = 1617 (w), 1476 (m), 1387 (w), 1094 (w), 991 (w), 756 (w), 695 (m).

$[Pd(bdppp)Cl]_2[Pd_2Cl_6]$. From 29.7 mg ligand (0.058 mmol, 1.0 eq) and 20.5 mg $PdCl_2$ (0.116 mmol, 2.0 eq) was obtained 17.5 mg of $L_2Pd_4Cl_8$ (0.010 mmol, 34.7%) as brown prisms. ^{1}H NMR (600 MHz, DMSO-d_6) δ 8.14 (t, *J* = 7.9 Hz, 1H), 7.92 (d, *J* = 7.2 Hz, 4H), 7.64 (d, *J* = 7.9 Hz, 2H), 7.47 (t, *J* = 7.6 Hz, 4H), 7.38 (t, *J* = 7.4 Hz, 2H), 7.35 – 7.31 (m, 6H), 7.18 (dd, *J* = 7.2, 2.3 Hz, 4H), 7.14 (s, 2H). ^{13}C NMR (151 MHz, DMSO) δ 151.5, 150.6, 145.0, 141.7, 132.2, 129.9, 128.8, 128.49, 128.44, 128.3, 128.2, 125.6, 118.6, 106.3. HRMS (ESI) for $[M]^+$: calcd for $C_{35}H_{25}ClN_5Pd^+$: 656.0828; found 656.0802. Anal. Calcd for $C_{70}H_{50}Cl_8N_{10}Pd_4$: C, 48.31; H, 2.90; N, 8.05. Found: C, 48.14; H, 2.85; N, 7.92. IR (FTIR): $\tilde{\nu}$ = 1483 (m), 1276 (w), 1261 (w), 759 (m), 695 (m).

APPENDICES

APPENDIX A

Selected Spectra

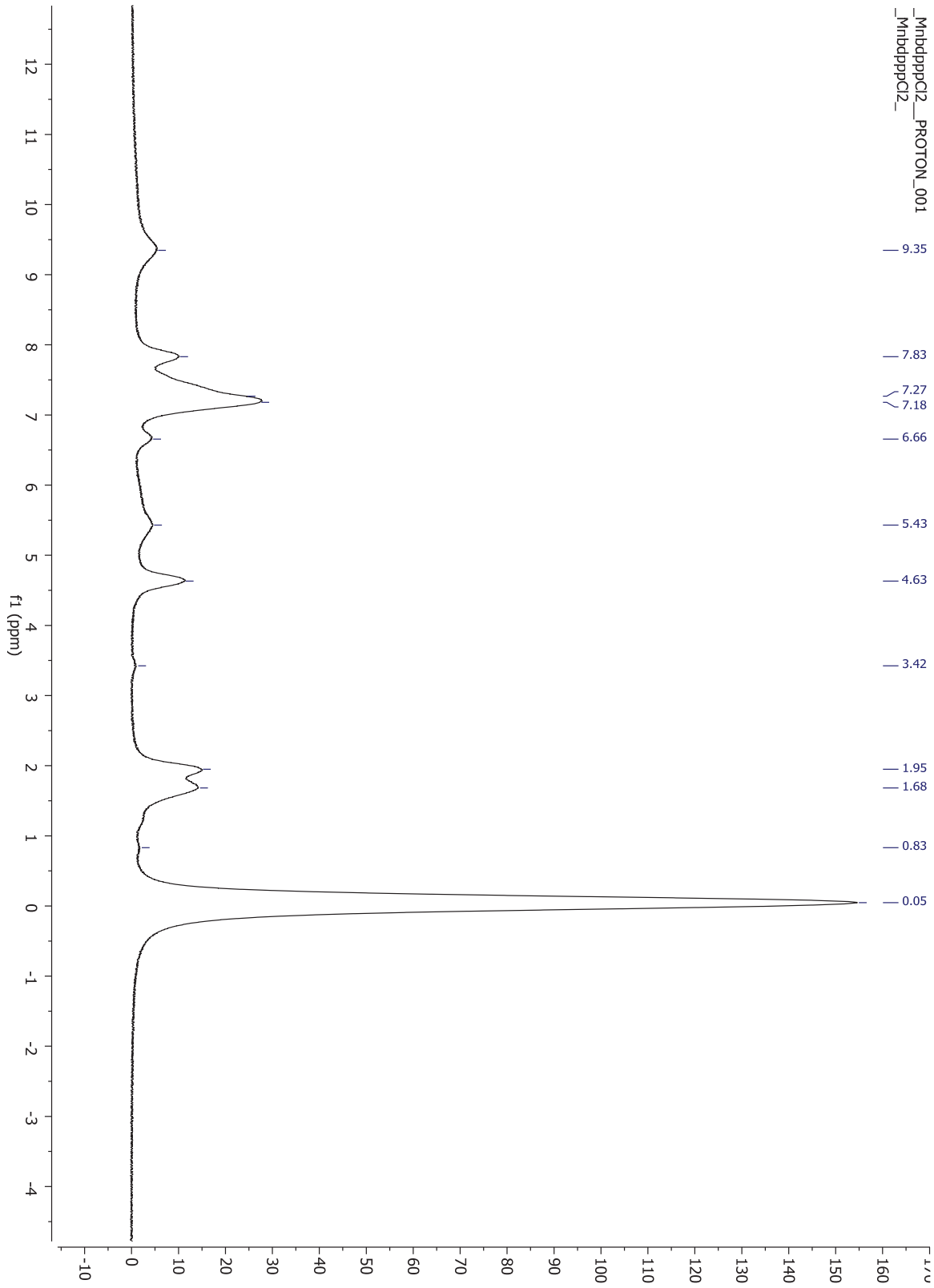

Figure A.1. 1H-NMR Spectrum of the Mn complex in CDCl3.

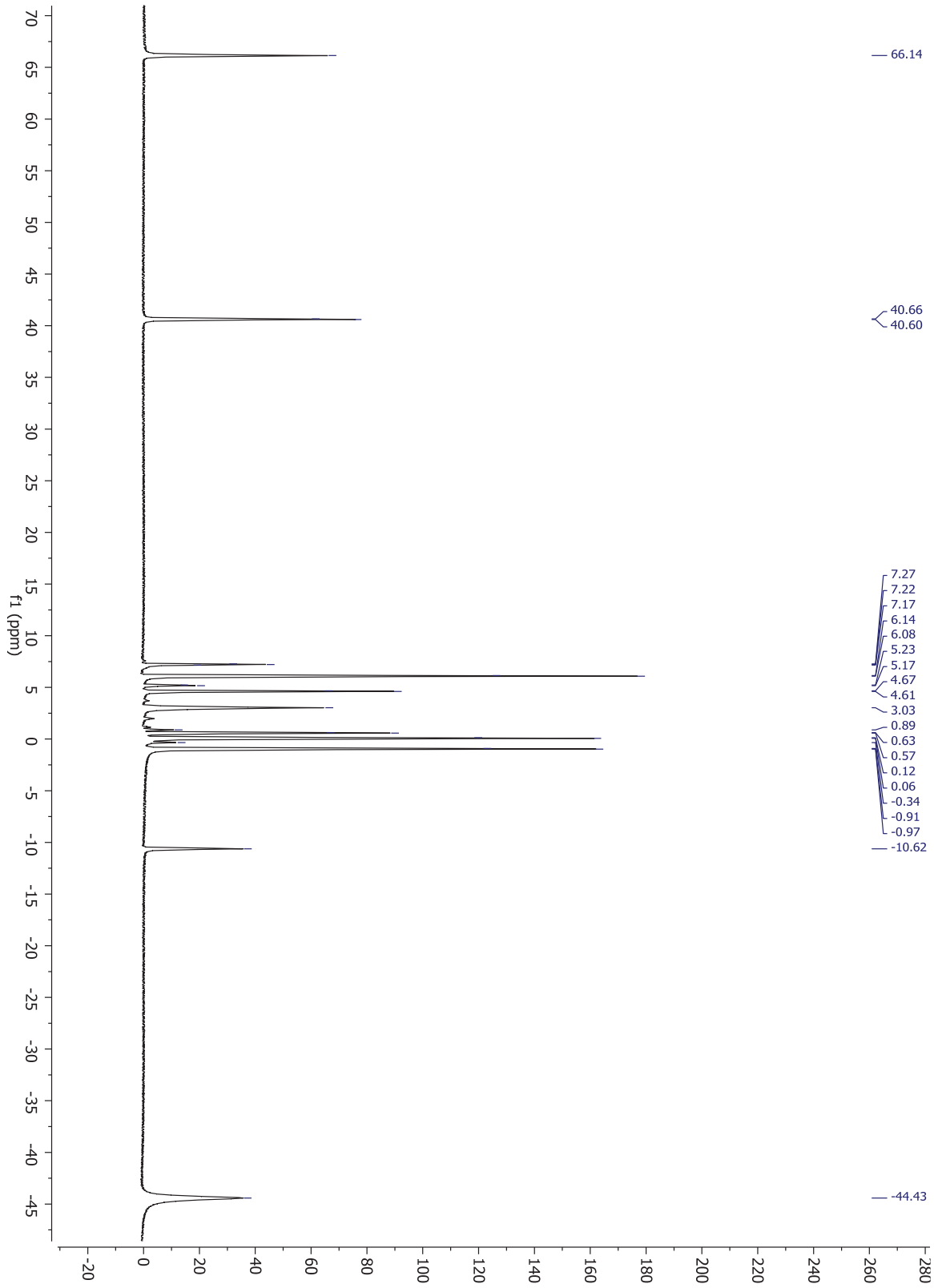

Figure A.2. 1H-NMR Spectrum of the Co complex in CDCl3.

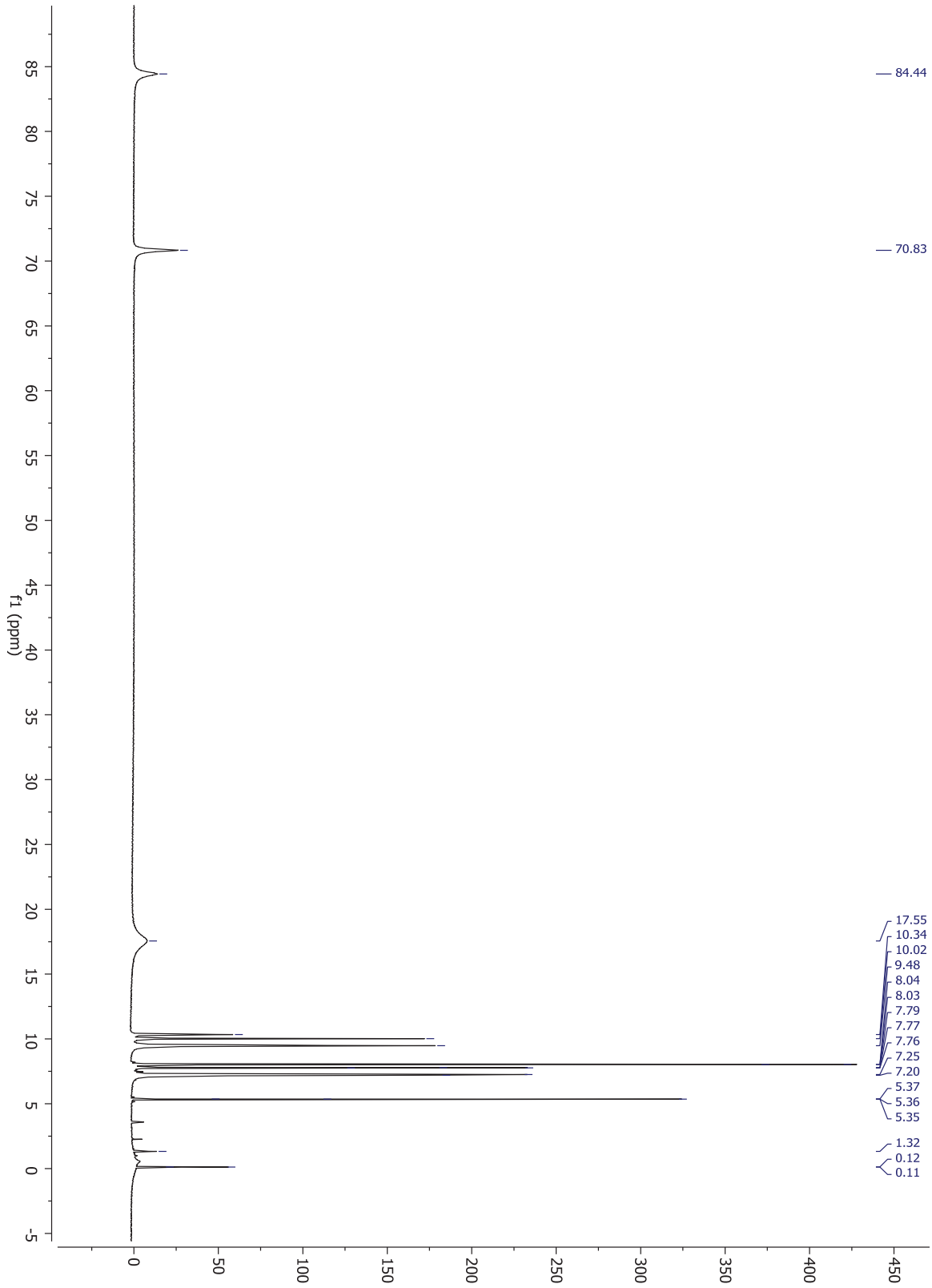

Figure A.3. 1H-NMR Spectrum of the Ni complex in CDCl3.

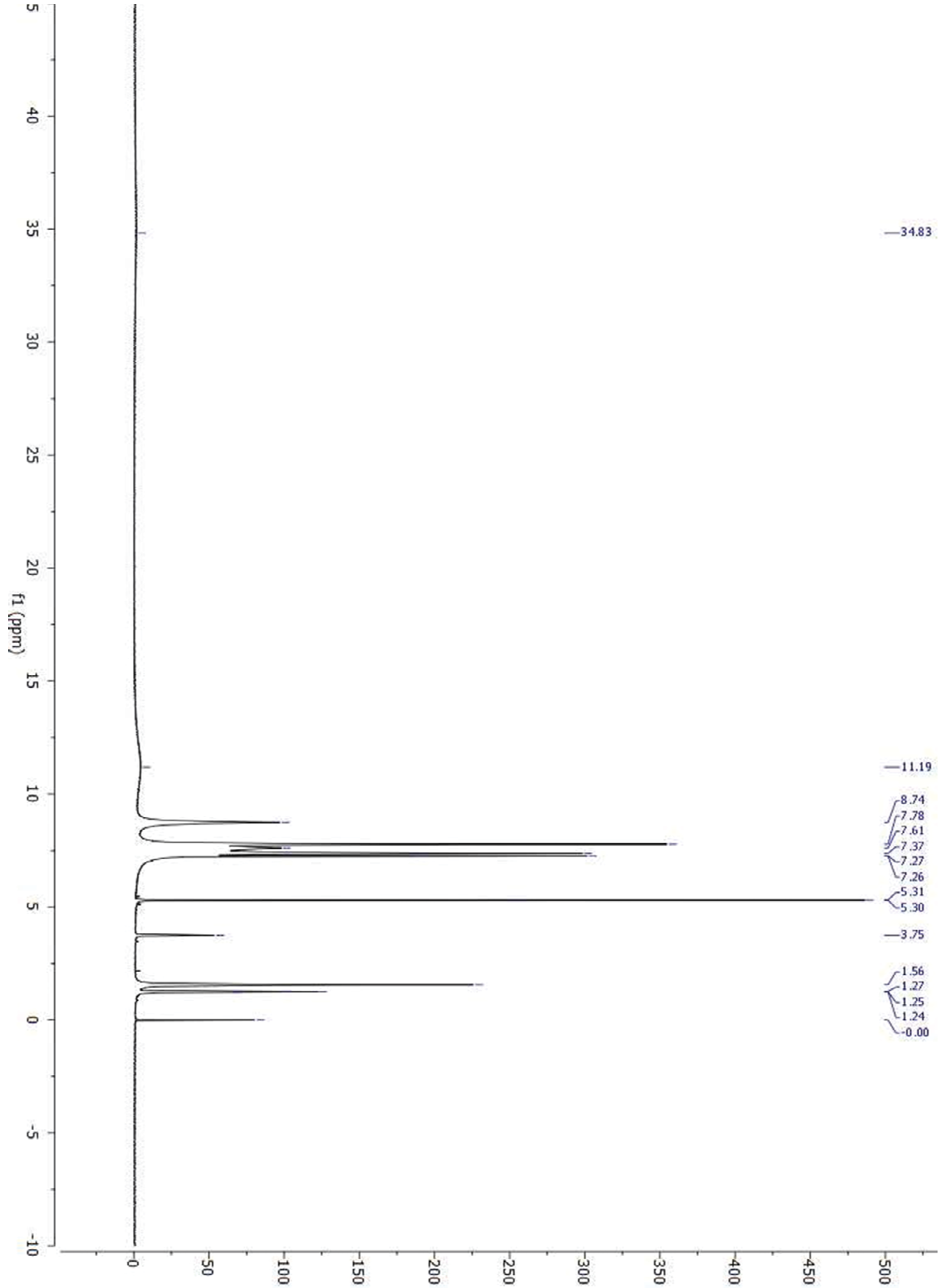

Figure A.4. 1H NMR spectrum of the Cu complex in CDCl3.

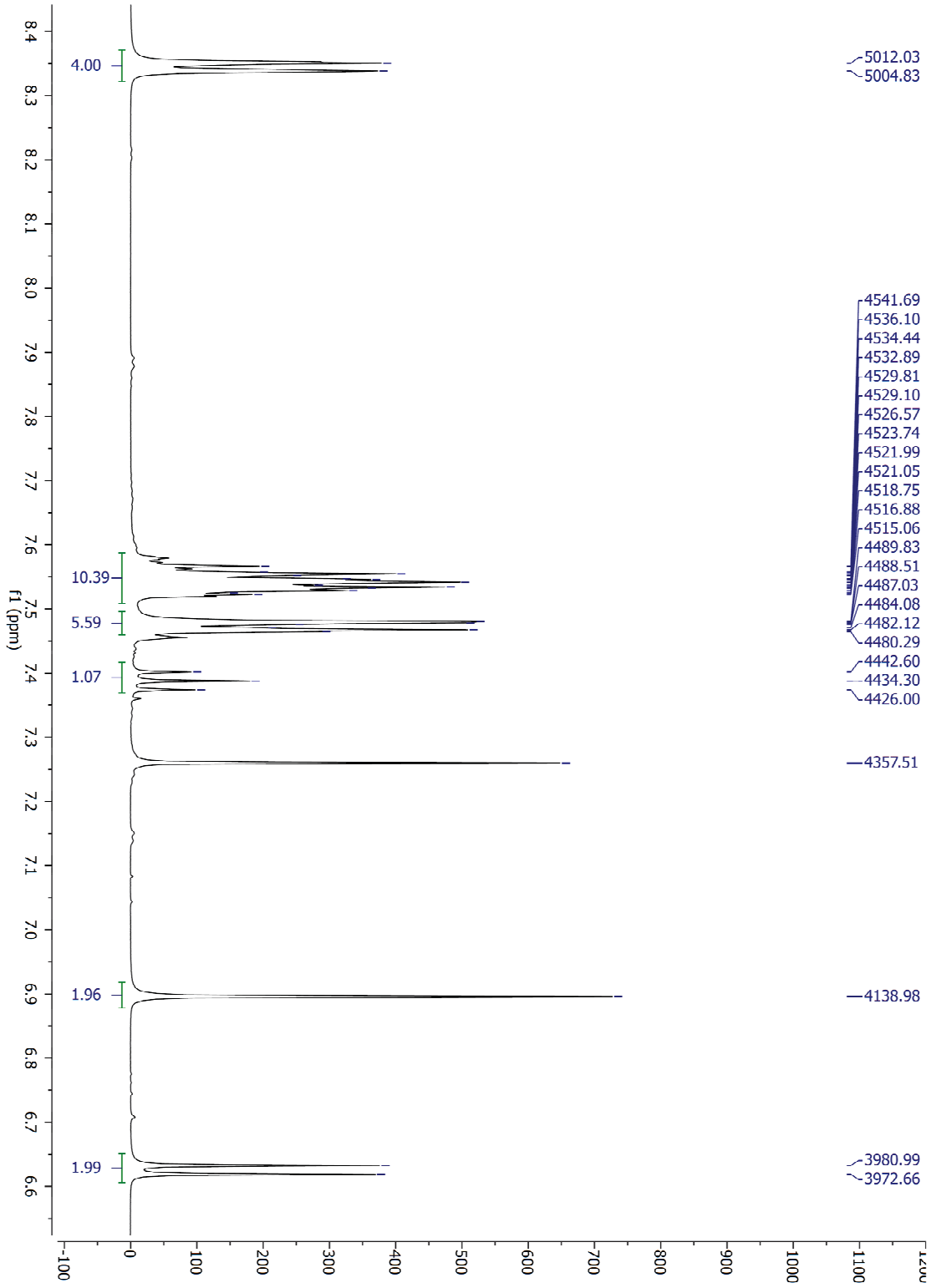

Figure A.5. 1H-NMR Spectrum of the Zn complex in CDCl3.

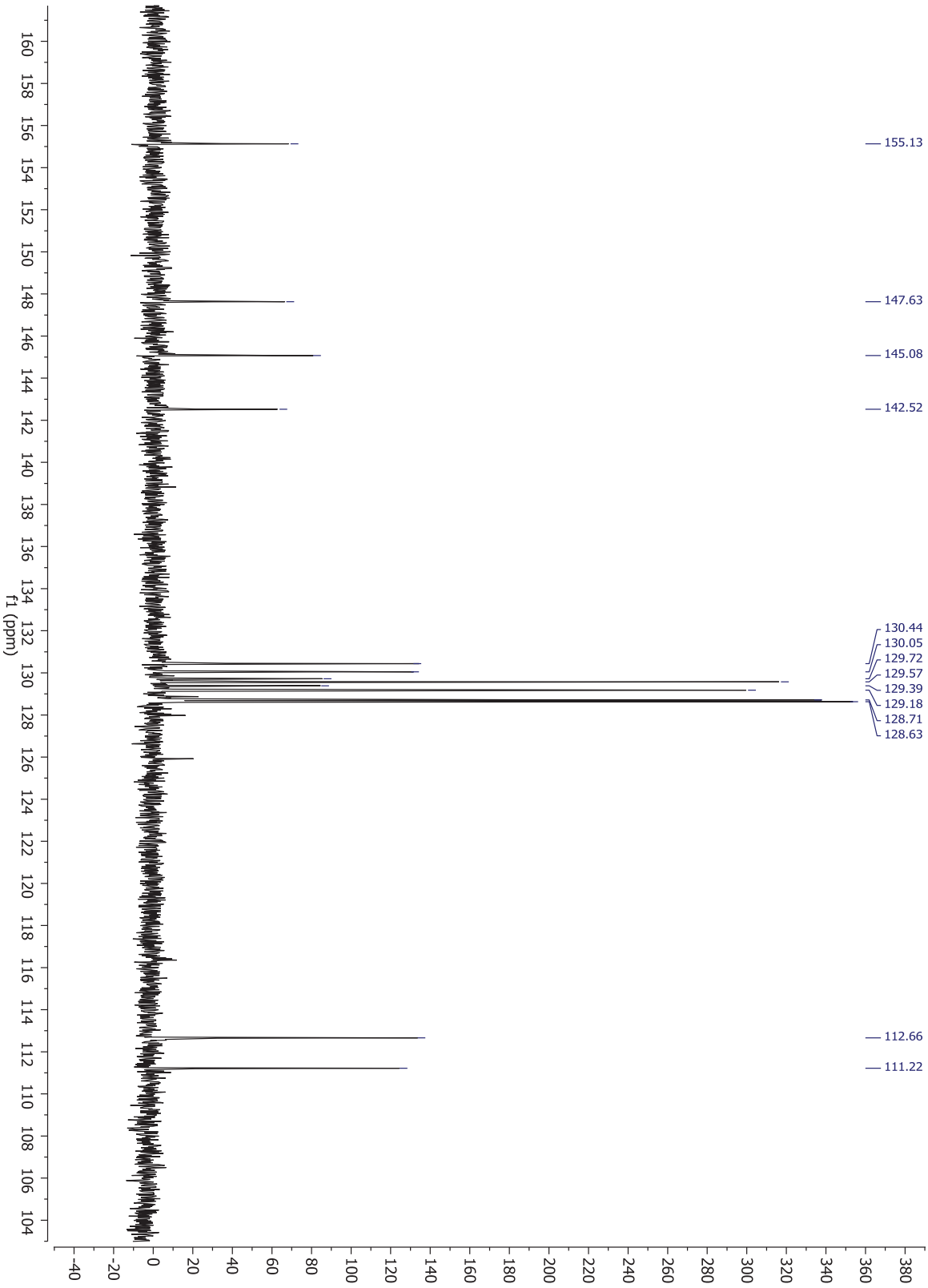

Figure A.6. 13C-NMR Spectrum of the Zn complex in CDCl3.

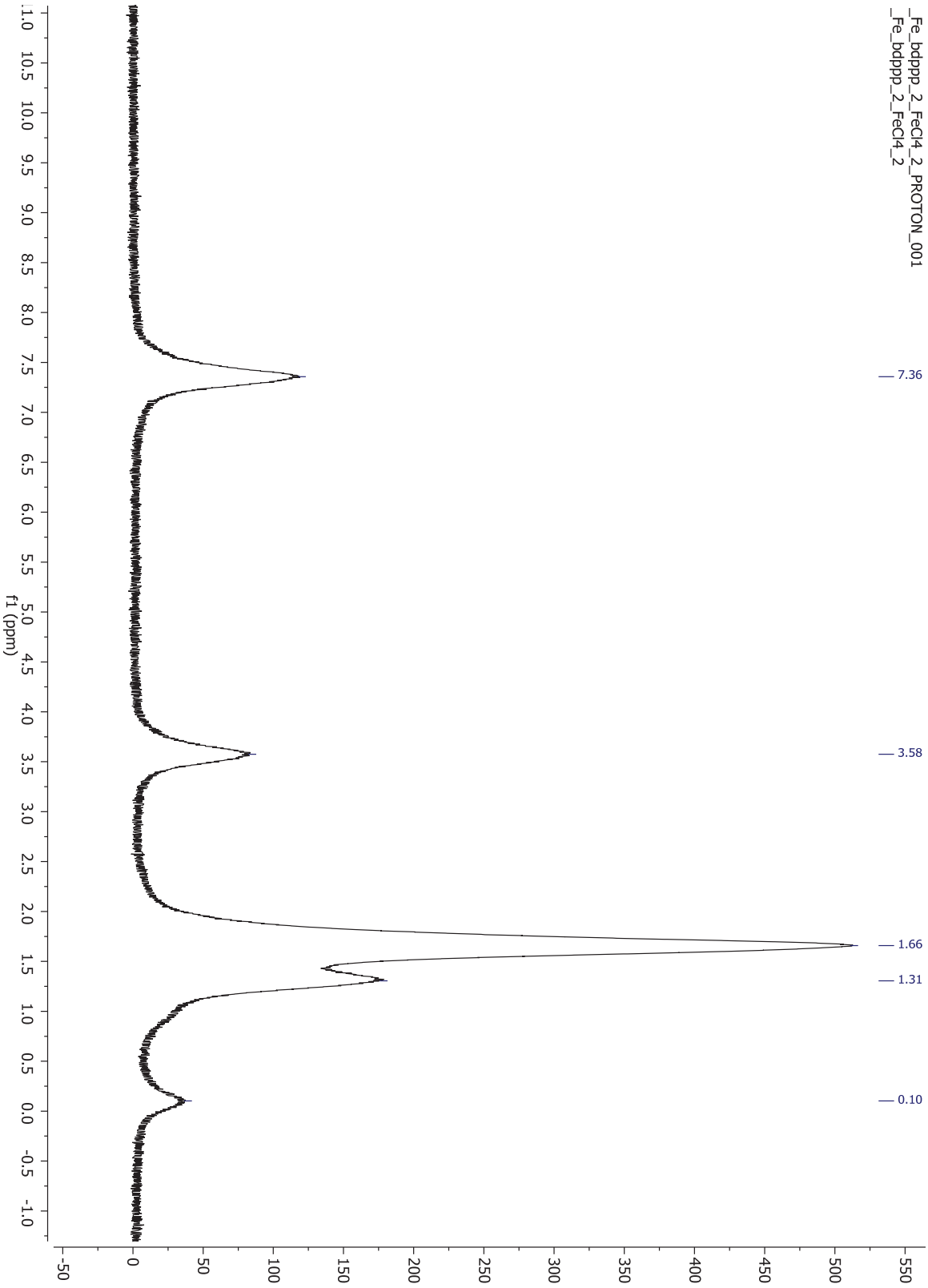

Figure A.7. 1H-NMR Spectrum of [Fe(bdppp)2][FeCl4]2 in CDCl3.

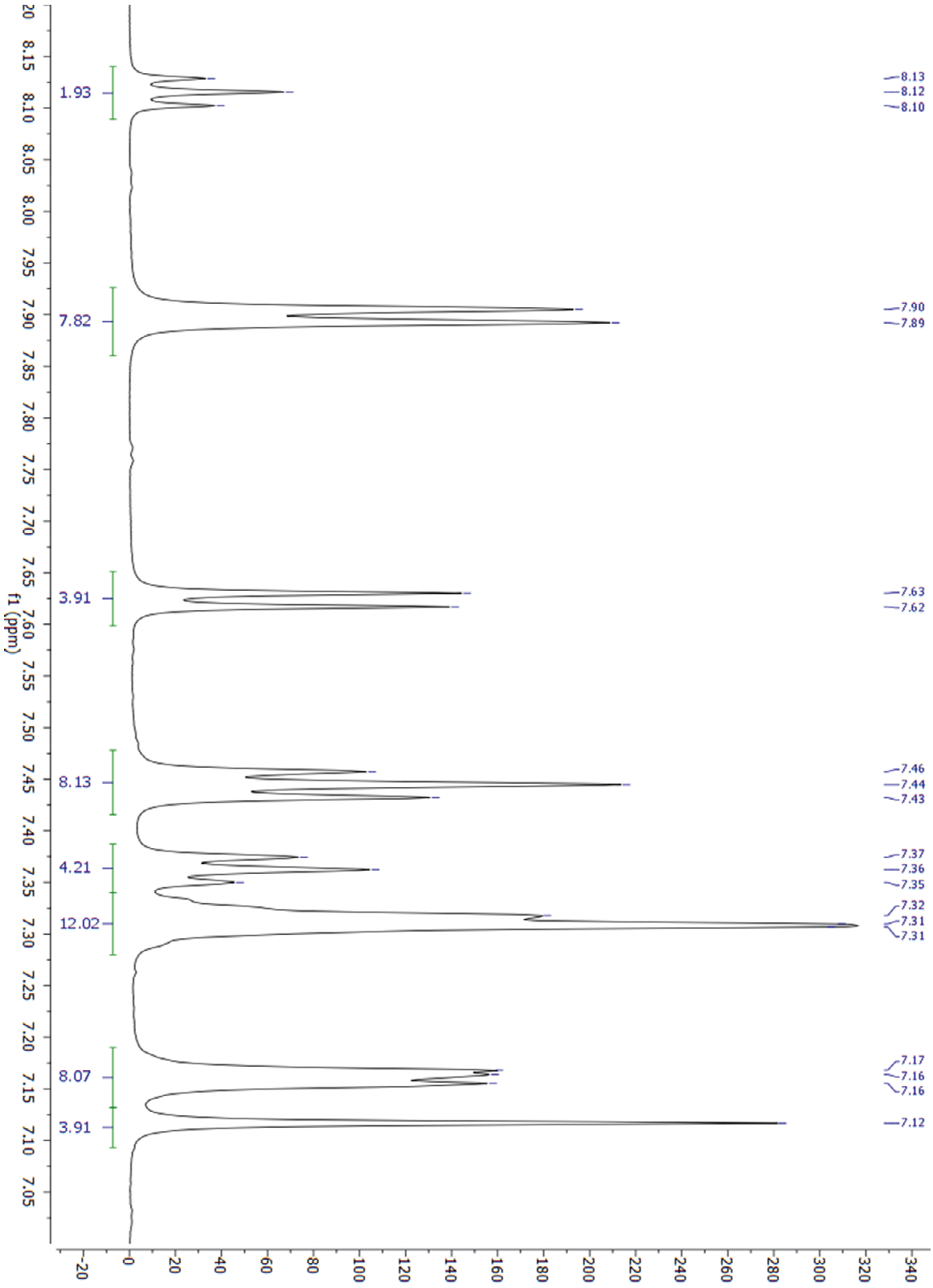

Figure A.8. 1H-NMR Spectrum of [Fe(bdppp)]2[ClO4]2 in DMSO-d6.

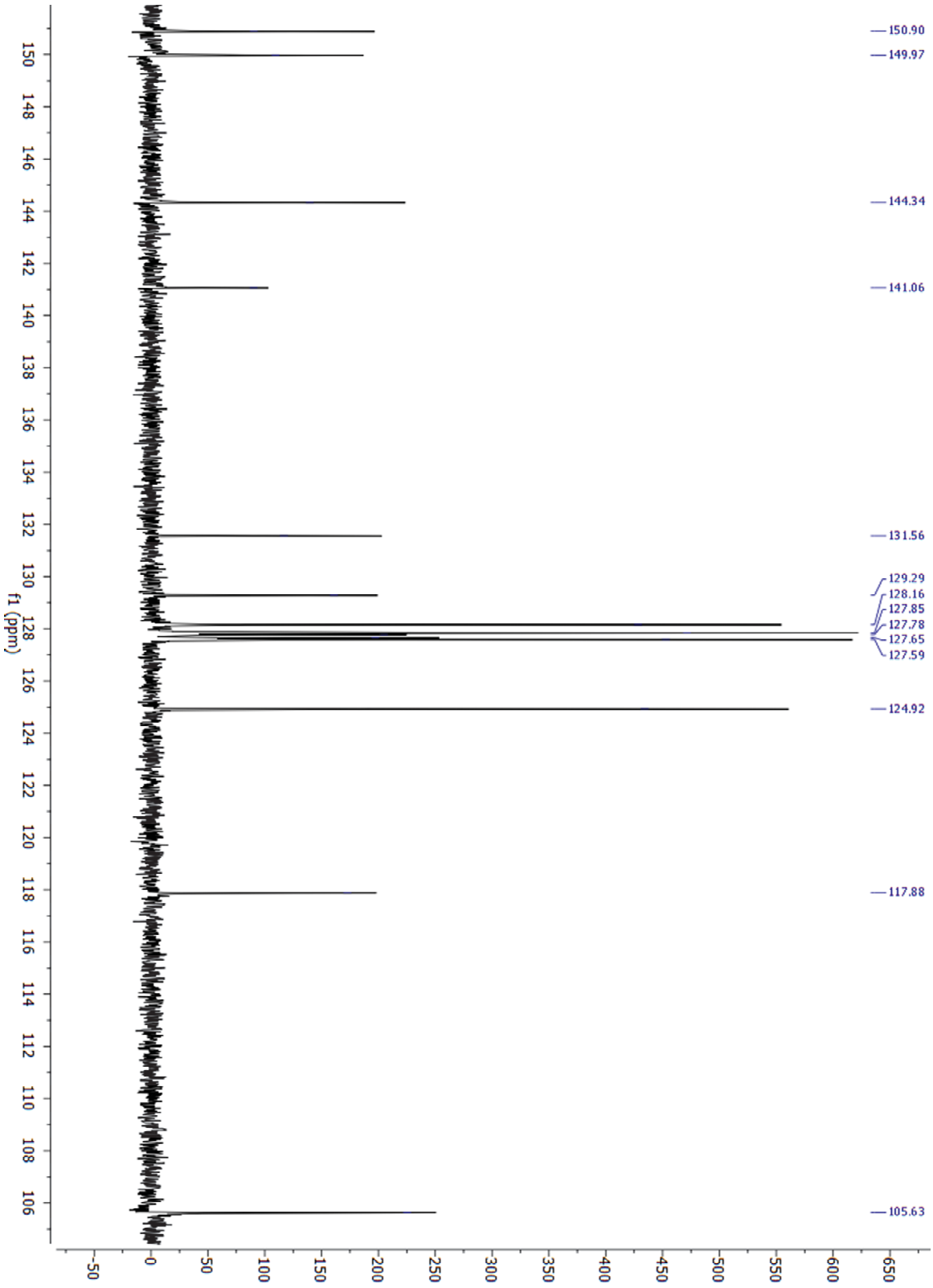

Figure A.9. 13C-NMR Spectrum of [Fe(bdppp)]2[ClO4]2 in DMSO-d6.

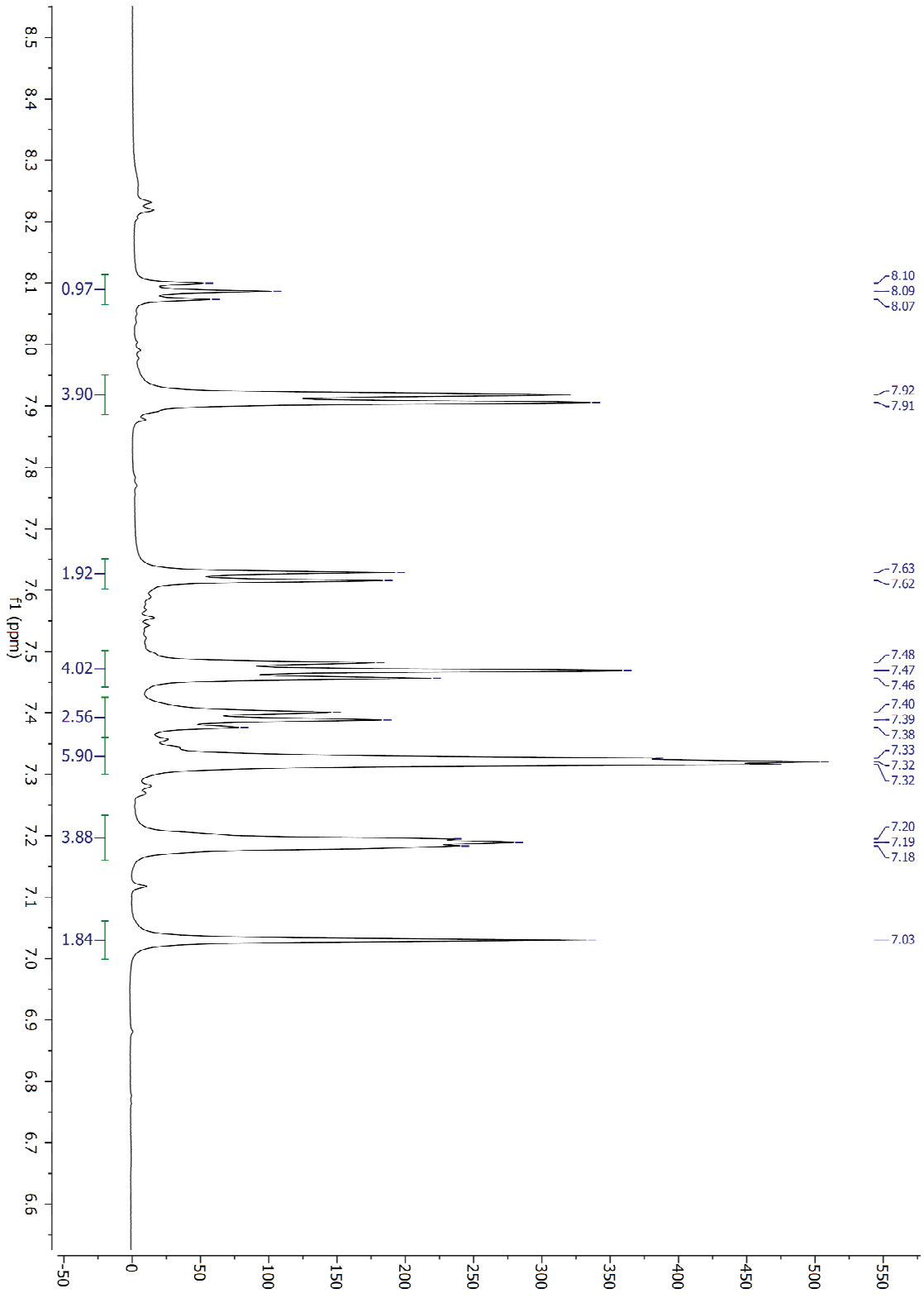

Figure A.10. 1H NMR spectrum of the Pd complex in DMSO-d6.

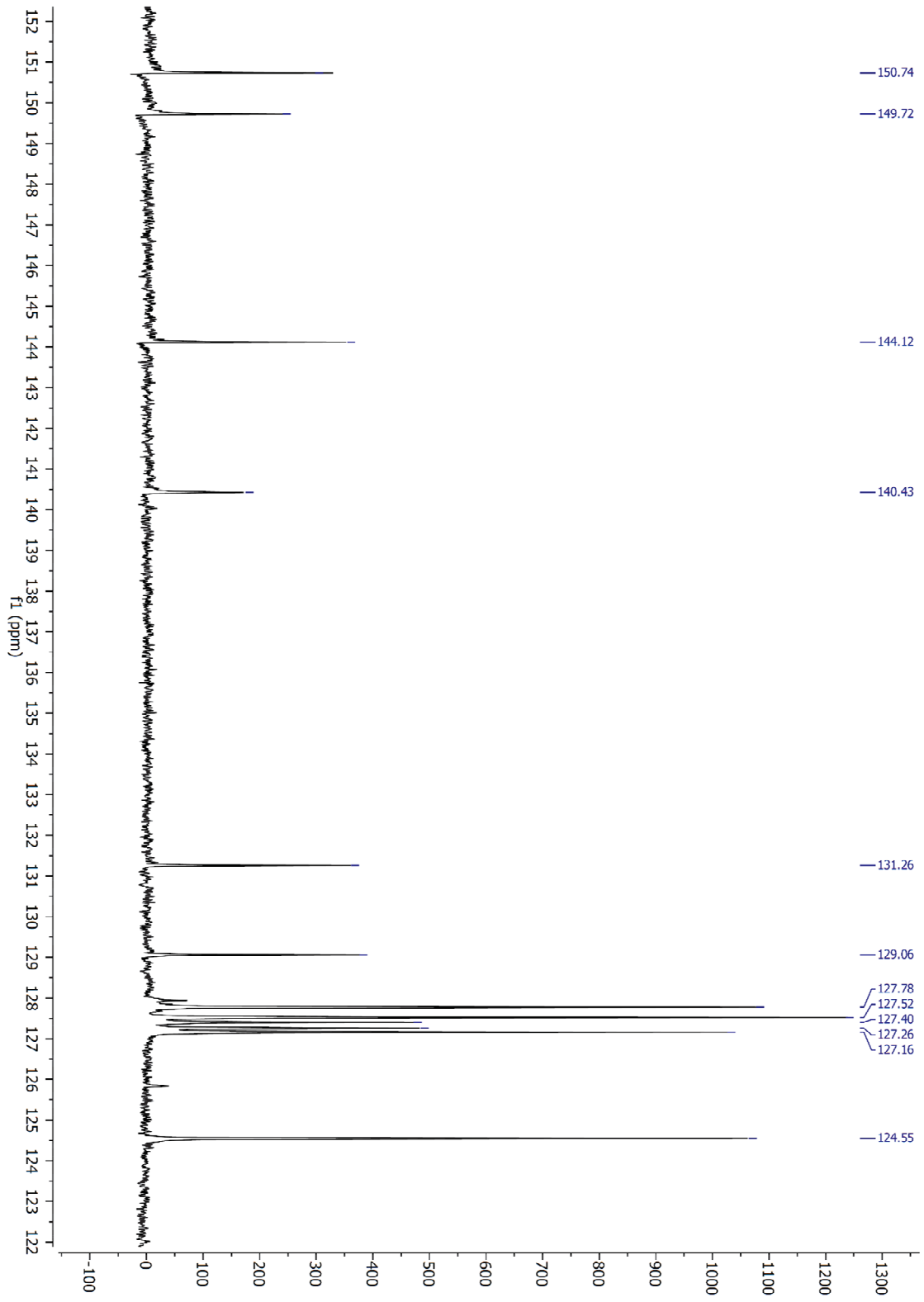

Figure A.11. 13C NMR spectrum of the Pd complex in DMSO-d6.

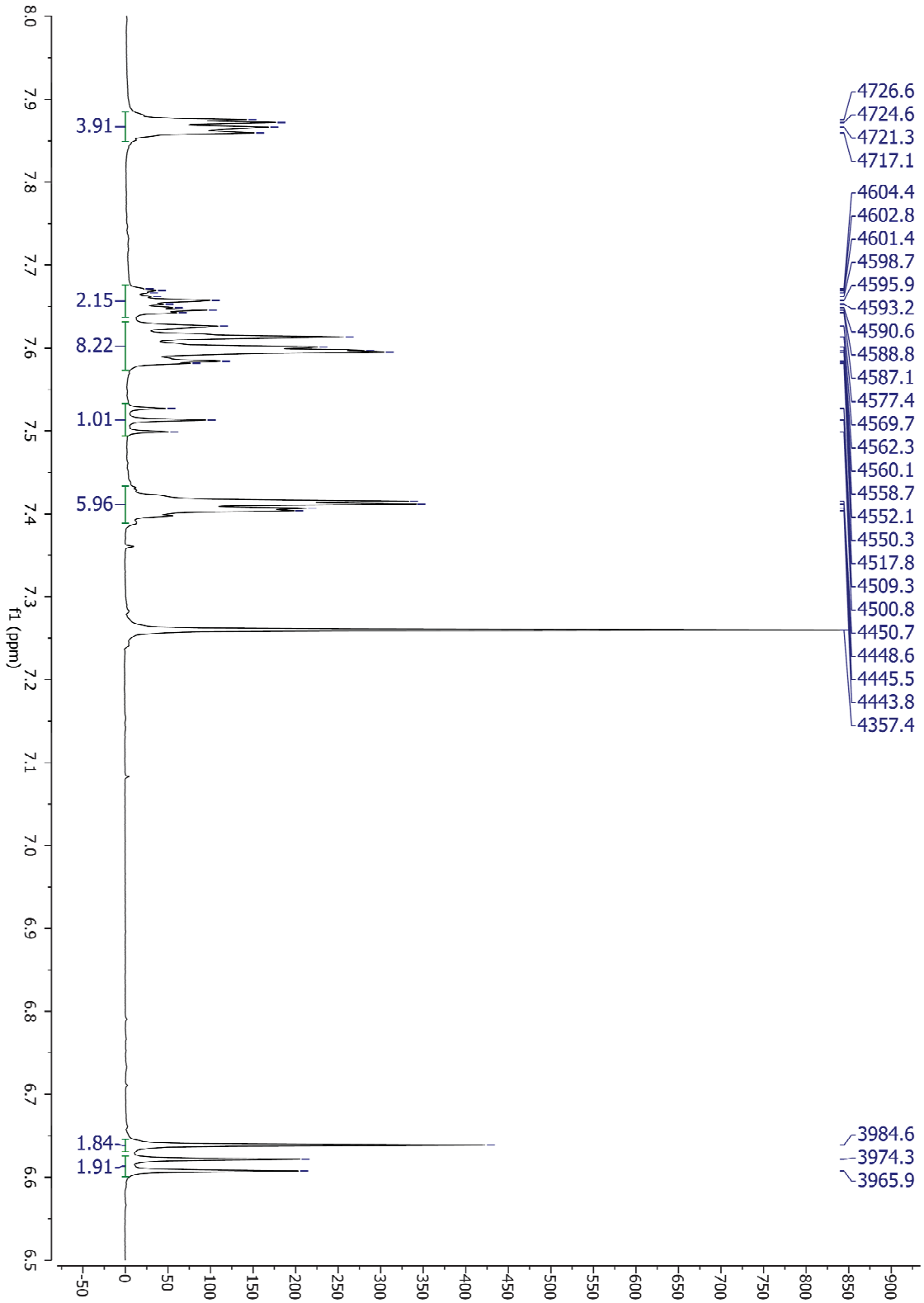

Figure A.12. 1H NMR spectrum of the Rh complex in CDCl3.

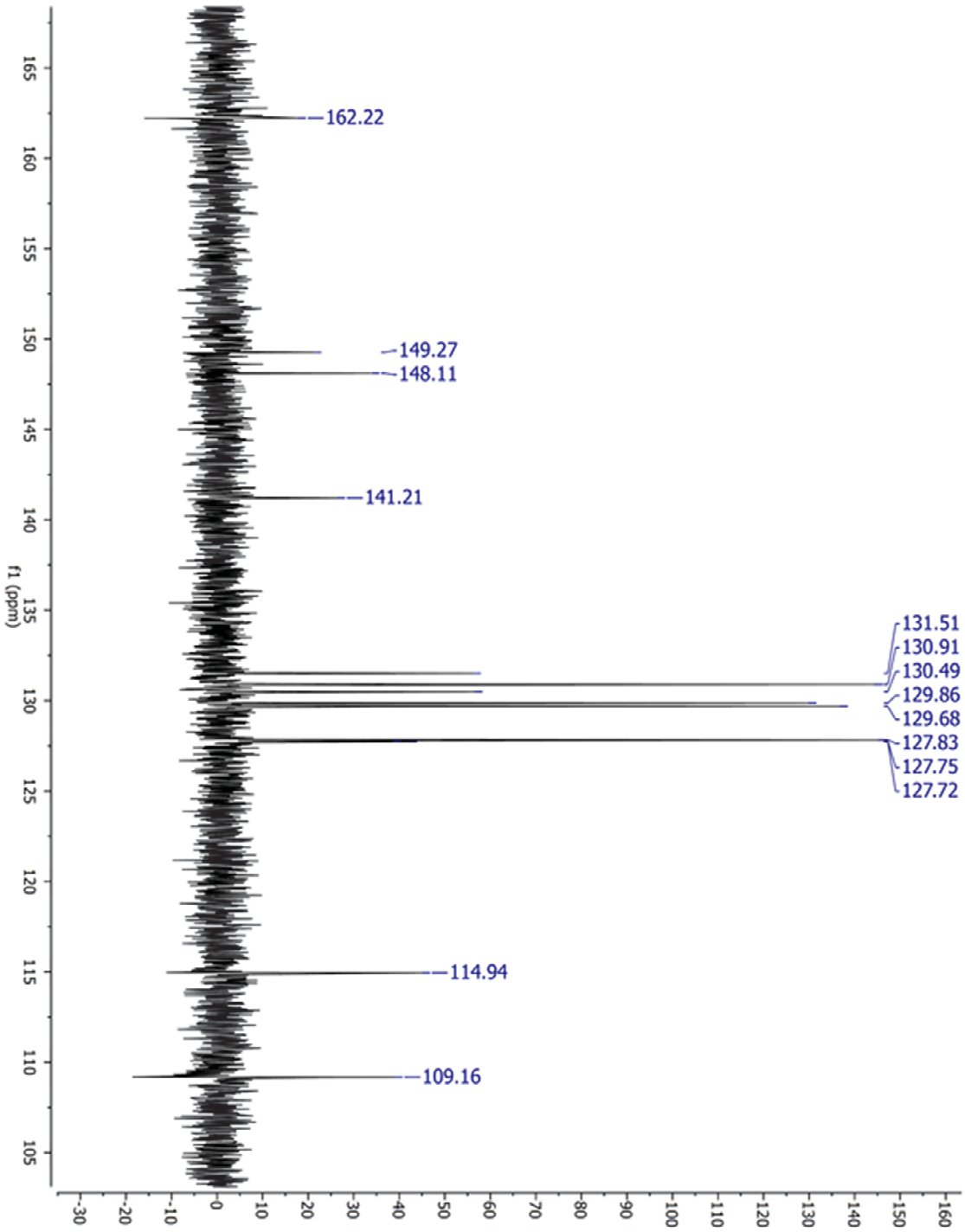

+

Figure A.13. 13C NMR spectrum of the Rh complex in CDCl3.

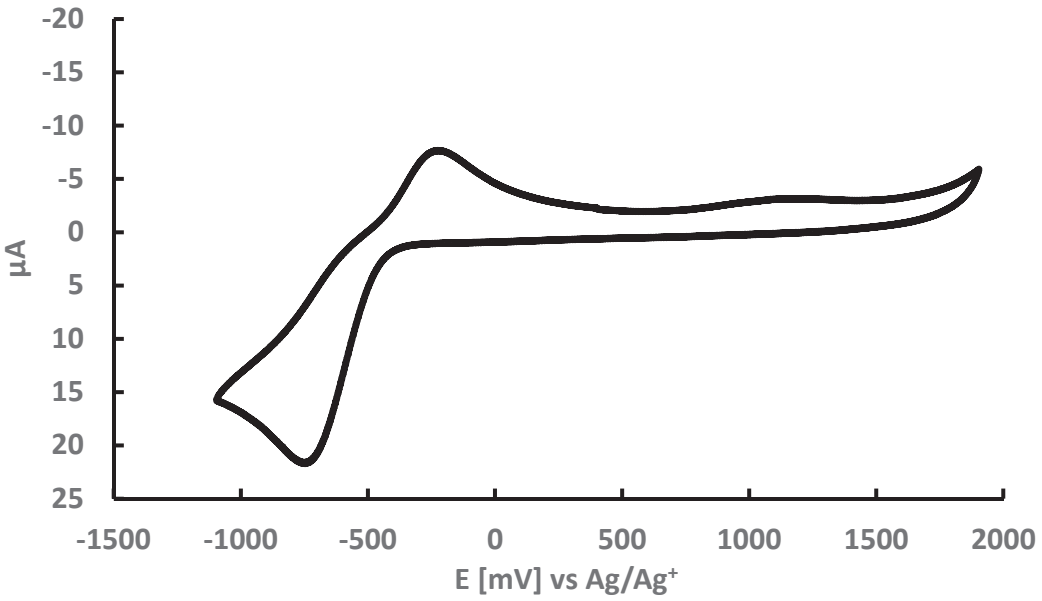

Figure A.14. Cyclic Voltammogram of the bdppp ligand in ACN with a 100 mv/s scan rate in a 0.1M solution of TBAPF6.

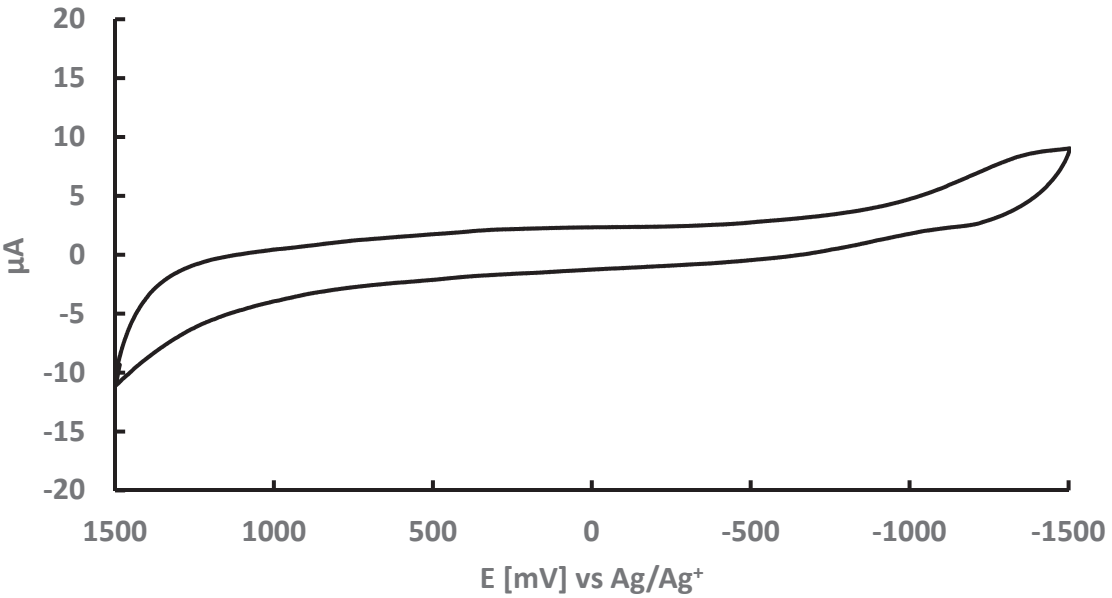

Figure A.15. Cyclic Voltammogram of the Mn complex in ACN with a 100 mv/s scan rate in a 0.1M solution of TBAPF6.

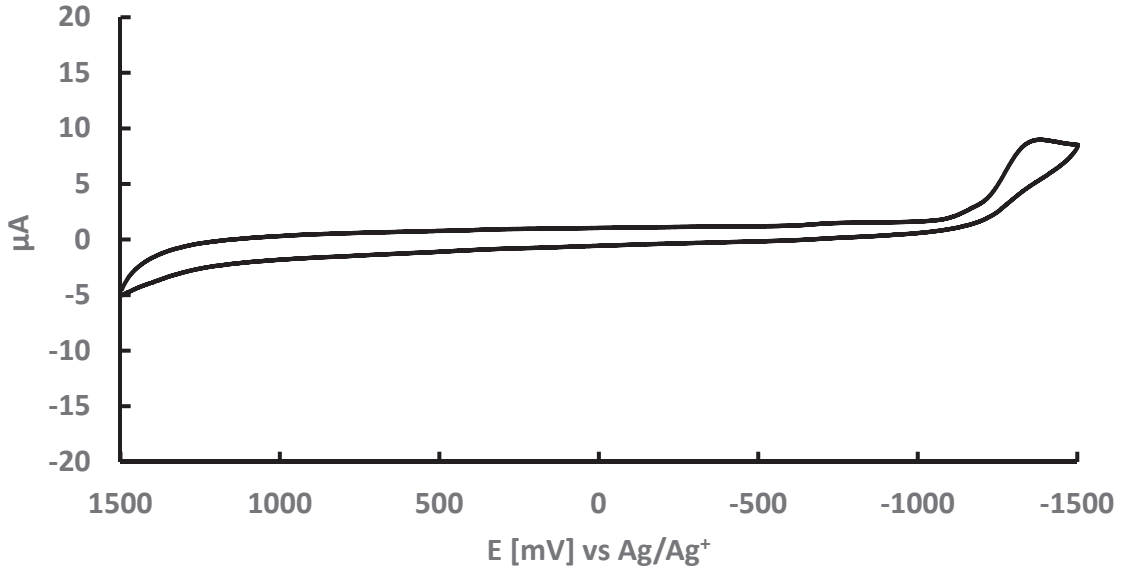

Figure A.16. Cyclic Voltammogram of the Co complex in ACN with a 100 mv/s scan rate in a 0.1M solution of TBAPF6.

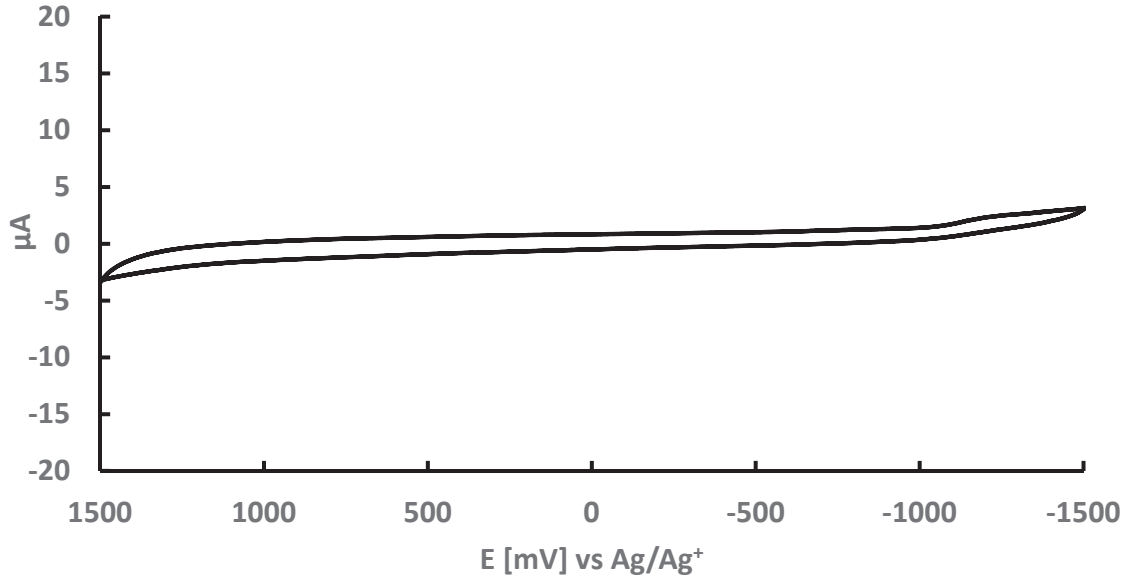

Figure A.17. Cyclic Voltammogram of the Ni complex with a 100 mv/s scan rate in a 0.1M solution of TBAPF6.

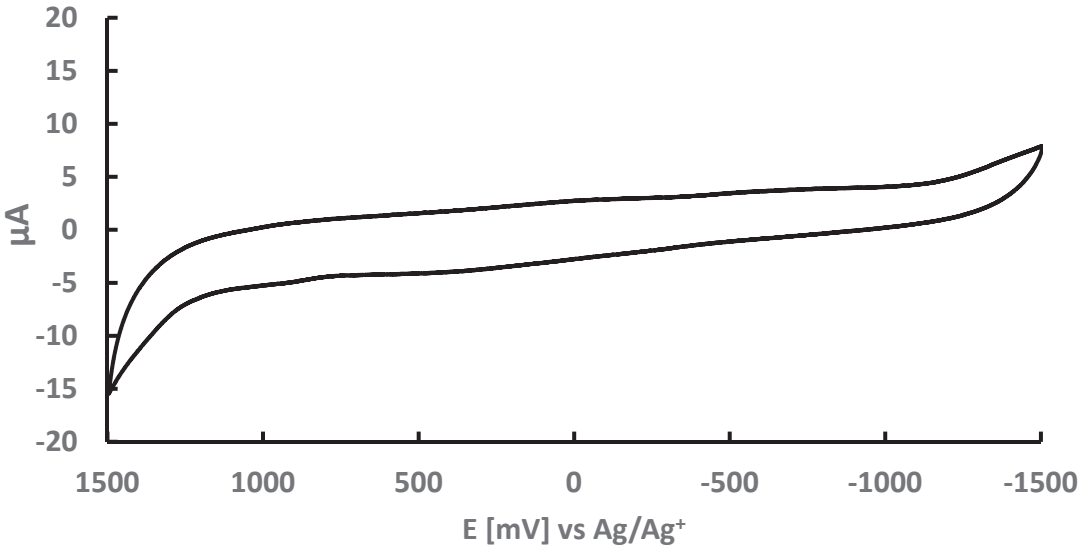

Figure A.18. Cyclic Voltammogram of the Zn complex in ACN with a 100 mv/s scan rate in a 0.1M solution of TBAPF6.

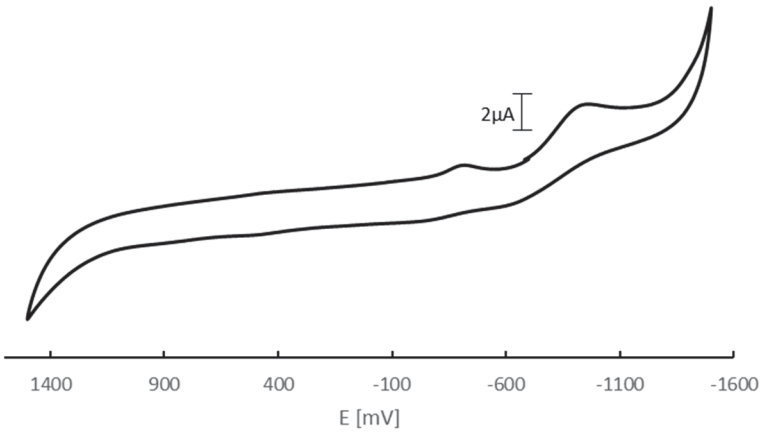

Figure A.19. Cyclic Voltammogram of the Pd complex in ACN with a 100 mv/s scan rate in a 0.1M solution of TBAPF6.

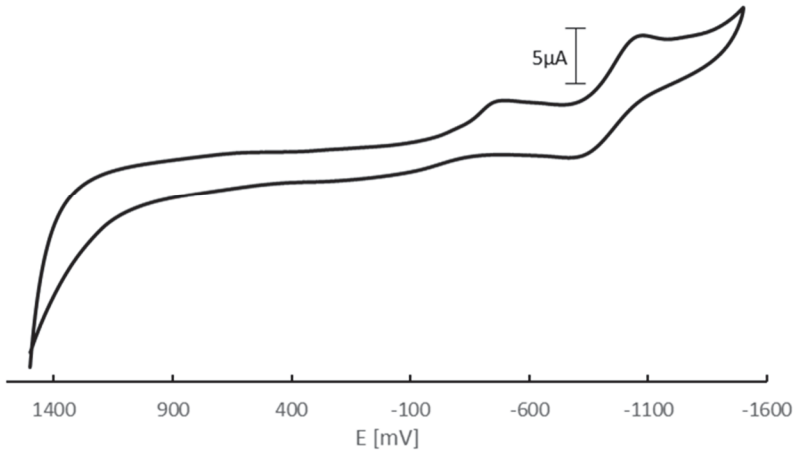

Figure A.20. Cyclic Voltammogram of the Rh complex in ACN with a 100 mv/s scan rate in a 0.1M solution of TBAPF6.

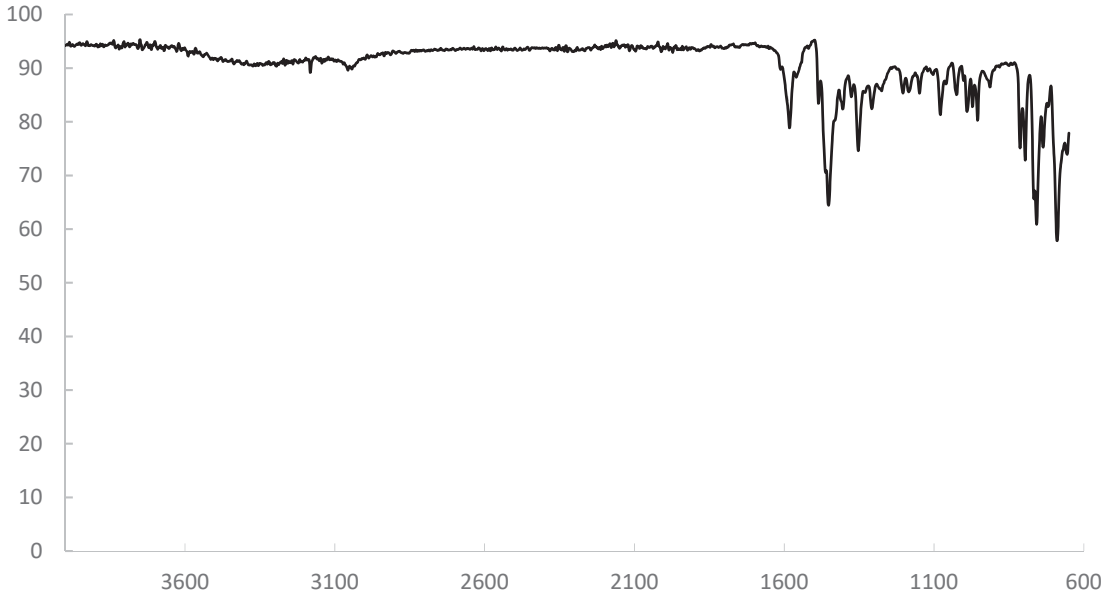

Figure A.21. FTIR spectrum of the Mn complex.

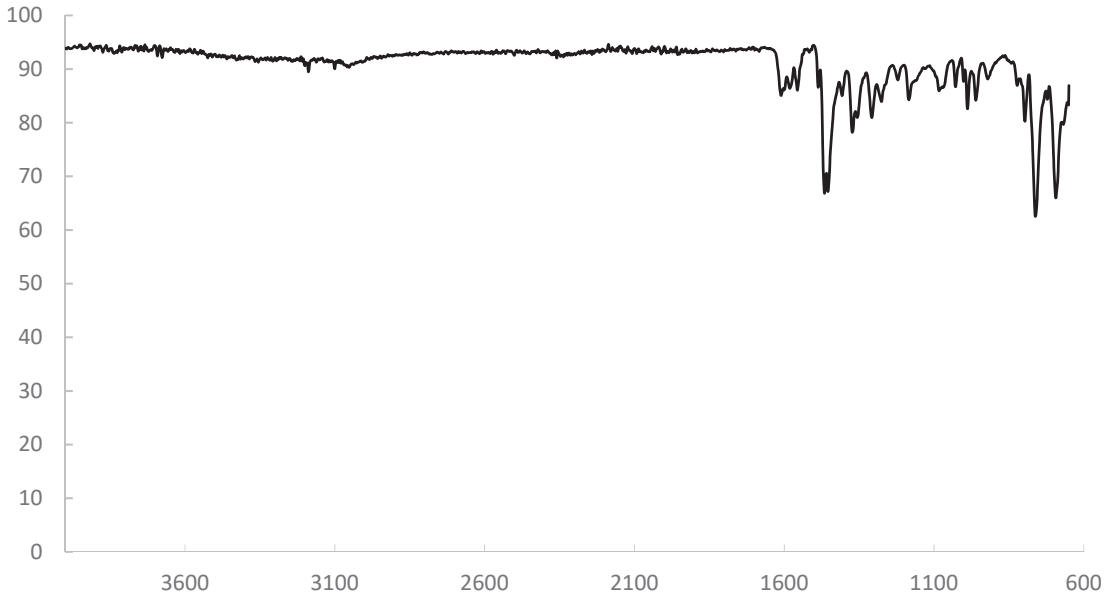

Figure A.22. FTIR spectrum of the Co complex.

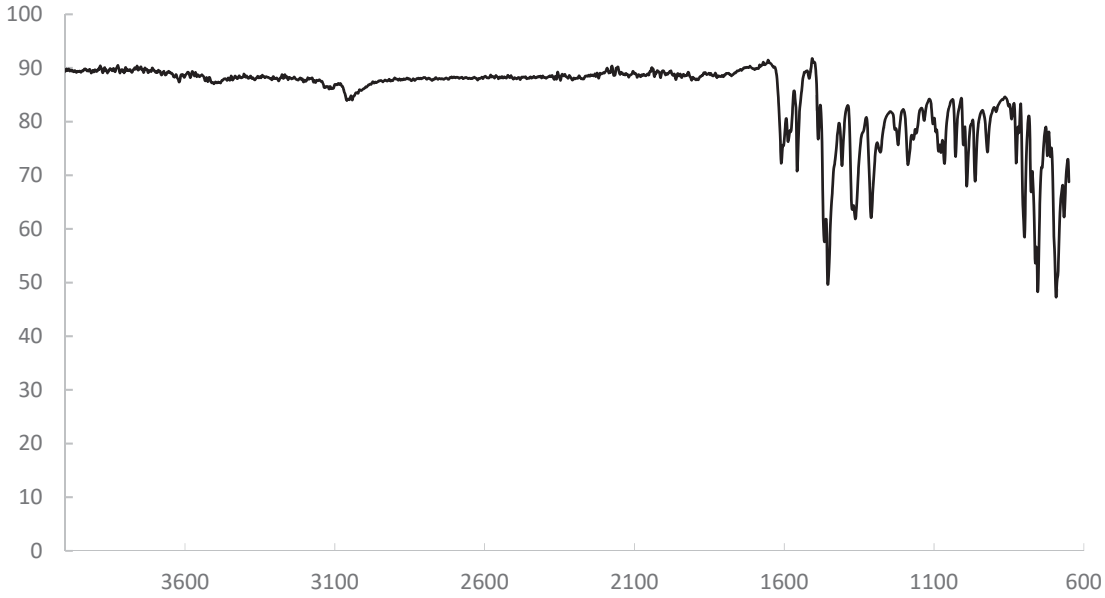

Figure A.23. FTIR spectrum of the Ni complex.

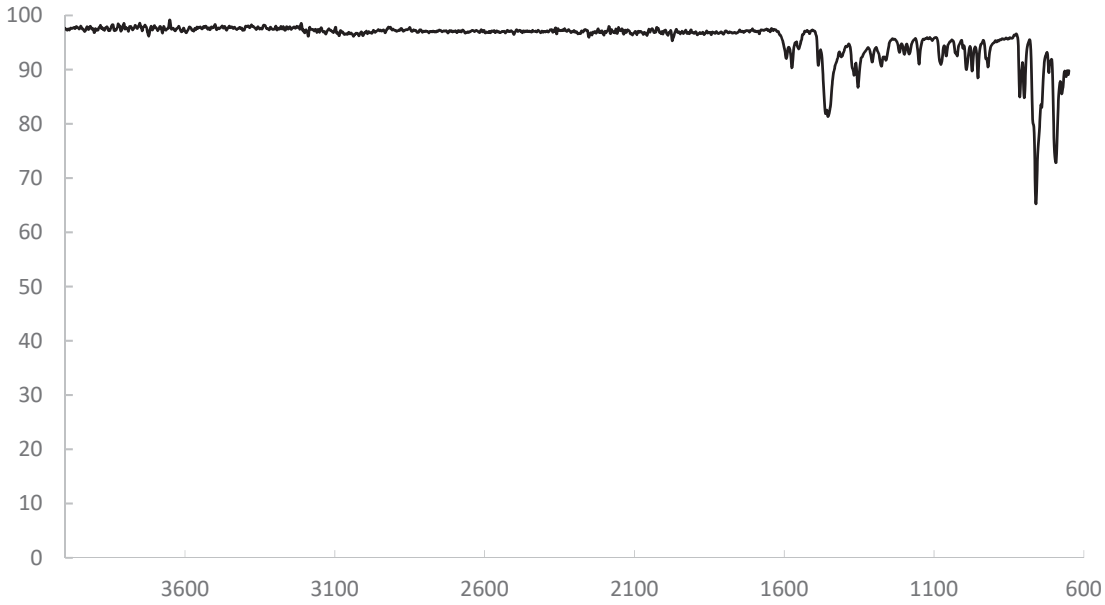

Figure A.24. FTIR spectrum of the Zn complex.

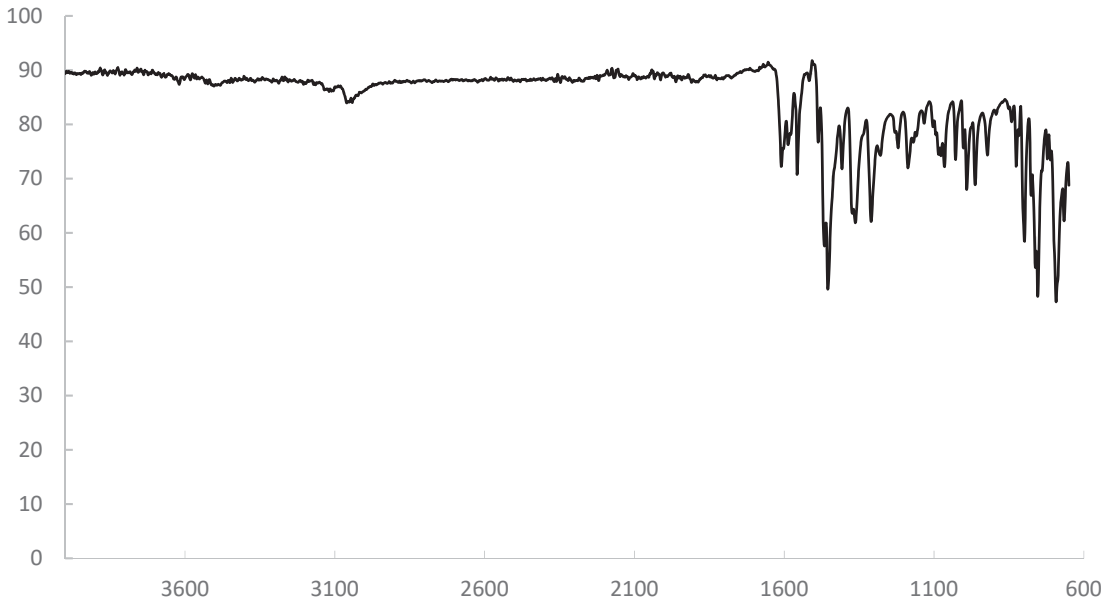

Figure A.25. FTIR spectrum of [Fe(bdppp)2](FeCl4)2 complex.

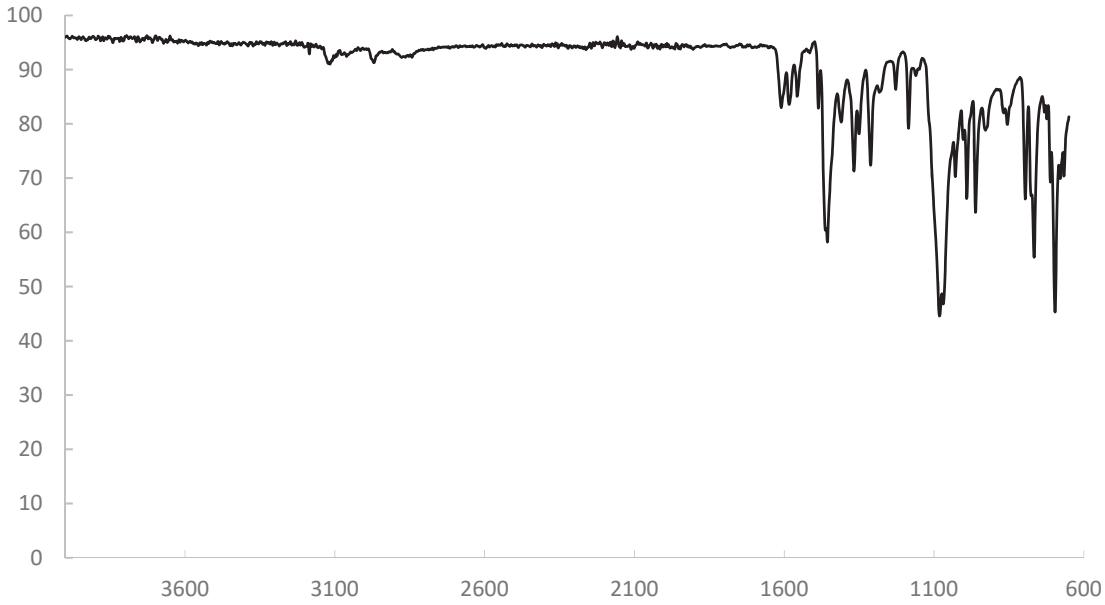

Figure A.26. FTIR spectrum of the [Fe(bdppp)2](FeCl4)2 complex.

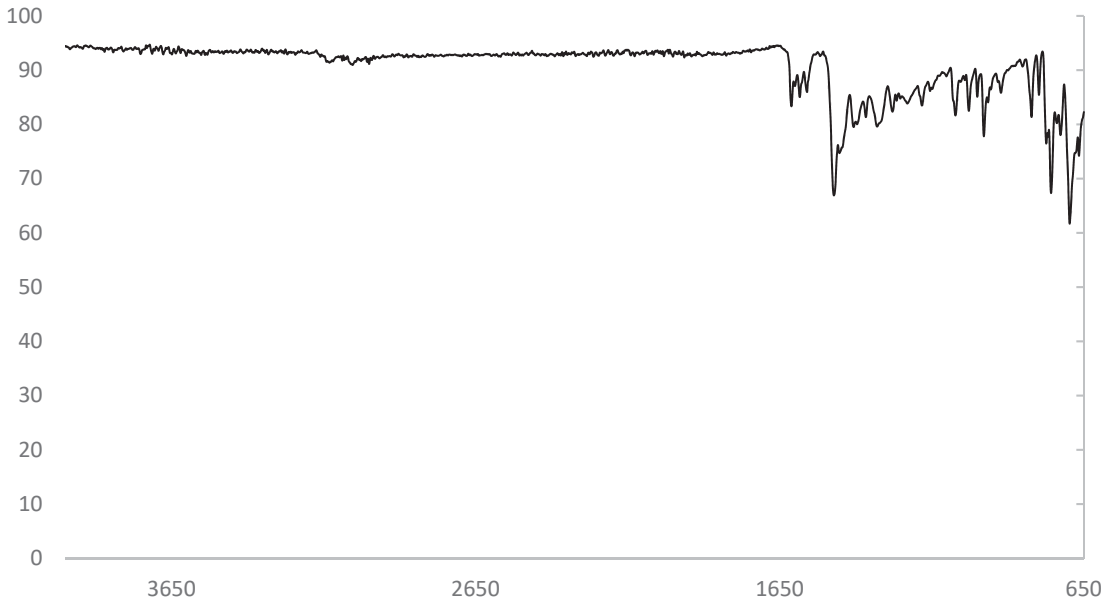

Figure A.27. FTIR spectrum of the Ru complex.

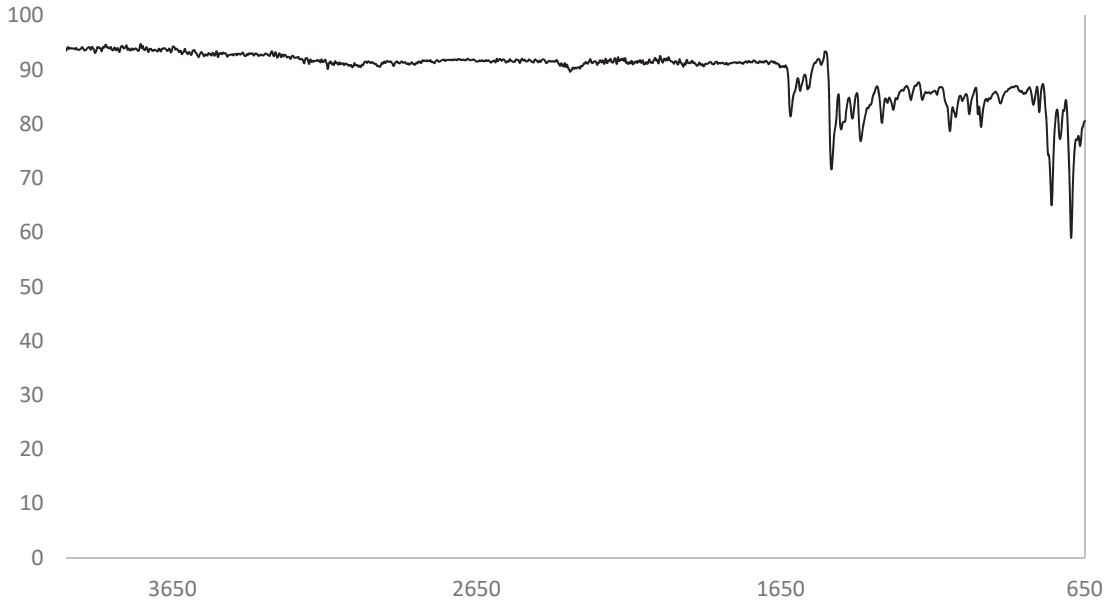

Figure A.28. FTIR spectrum of the Pd complex.

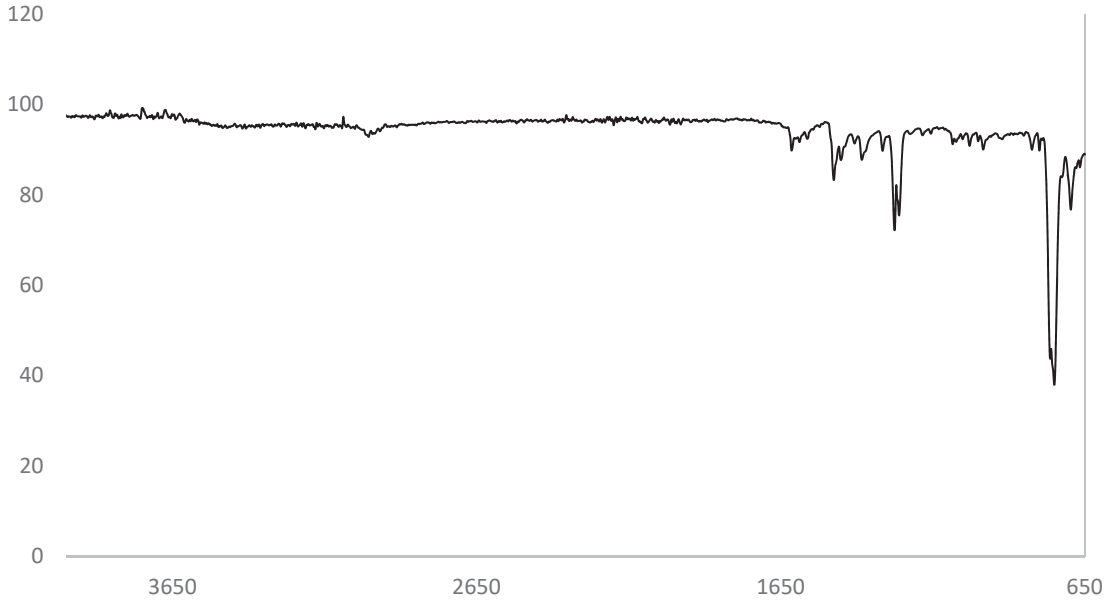

Figure A.29. FTIR spectrum of the Rh complex.

APPENDIX B

Tables of X-ray Crystallographic Data

Table B.1. Crystal data and structure refinement for the Ru complex.

Identification code	CG56	
Empirical formula	C36 H27 Cl5 N5 Ru	
Formula weight	807.94	
Temperature	150(2) K	
Wavelength	0.71073 Å	
Crystal system	Monoclinic	
Space group	$P2_1/c$	
Unit cell dimensions	a = 16.1224(6) Å	α= 90°.
	b = 14.4729(4) Å	β= 111.6091(14)°.
	c = 15.4427(4) Å	γ = 90°.
Volume	3350.11(18) $Å^3$	
Z	4	
Density (calculated)	1.602 Mg/m^3	
Absorption coefficient	0.903 mm^{-1}	
F(000)	1628	
Crystal size	0.496 x 0.331 x 0.068 mm^3	
Theta range for data collection	2.657 to 30.559°.	
Index ranges	-22<=h<=22, -20<=k<=20, -22<=l<=20	
Reflections collected	66321	
Independent reflections	10248 [R(int) = 0.0474]	
Completeness to theta = 25.242°	99.9 %	
Absorption correction	Semi-empirical from equivalents	
Max. and min. transmission	0.807 and 0.569	
Refinement method	Full-matrix least-squares on F^2	
Data / restraints / parameters	10248 / 0 / 424	
Goodness-of-fit on F^2	1.053	
Final R indices [I>2sigma(I)]	R1 = 0.0415, wR2 = 0.1140	
R indices (all data)	R1 = 0.0525, wR2 = 0.1212	
Extinction coefficient	n/a	
Largest diff. peak and hole	1.899 and -1.708 $e.Å^{-3}$	

Table B.2. Atomic coordinates (x 10^4) and equivalent isotropic displacement parameters ($Å^2$x 10^3) for the Ru complex. U(eq) is defined as one third of the trace of the orthogonalized U^{ij} tensor.

Atom number	x	y	z	U(eq)
Ru(1)	2528(1)	1222(1)	4546(1)	14(1)
Cl(1)	1220(1)	613(1)	3438(1)	21(1)
Cl(2)	2310(1)	478(1)	5805(1)	19(1)
Cl(3)	3846(1)	1920(1)	5567(1)	20(1)
Cl(4)	846(1)	8879(1)	385(1)	45(1)
Cl(5)	2048(1)	8906(1)	2314(1)	62(1)
N(1)	2793(1)	1958(1)	3593(1)	16(1)
N(2)	3554(1)	674(2)	3432(1)	17(1)
N(3)	3285(1)	270(1)	4112(1)	16(1)
N(4)	2078(2)	3118(1)	4058(2)	18(1)
N(5)	1876(1)	2439(1)	4592(2)	17(1)
C(1)	3343(2)	1606(2)	3200(2)	16(1)
C(2)	3677(2)	2153(2)	2667(2)	21(1)
C(3)	3440(2)	3081(2)	2578(2)	24(1)
C(4)	2905(2)	3458(2)	3015(2)	23(1)
C(5)	2596(2)	2865(2)	3536(2)	17(1)
C(6)	4087(2)	77(2)	3173(2)	19(1)
C(7)	4159(2)	-708(2)	3685(2)	21(1)
C(8)	3647(2)	-572(2)	4252(2)	18(1)
C(9)	4478(2)	268(2)	2463(2)	20(1)
C(10)	5405(2)	323(2)	2742(2)	24(1)
C(11)	5789(2)	522(2)	2088(2)	31(1)
C(12)	5253(2)	663(2)	1164(2)	35(1)
C(13)	4326(2)	584(2)	878(2)	33(1)
C(14)	3939(2)	385(2)	1524(2)	27(1)
C(15)	3511(2)	-1280(2)	4872(2)	18(1)
C(16)	4208(2)	-1901(2)	5308(2)	23(1)
C(17)	4096(2)	-2594(2)	5876(2)	29(1)
C(18)	3290(2)	-2675(2)	6011(2)	31(1)
C(19)	2596(2)	-2073(2)	5568(2)	28(1)
C(20)	2698(2)	-1381(2)	4988(2)	21(1)

Table B.2. Atomic coordinates (x 10^4) and equivalent isotropic displacement parameters ($Å^2$x 10^3) for the Ru complex. U(eq) is defined as one third of the trace of the orthogonalized U^{ij} tensor, continued.

Atom number	x	y	z	U(eq)
C(21)	1779(2)	3971(2)	4219(2)	20(1)
C(22)	1397(2)	3830(2)	4866(2)	22(1)
C(23)	1439(2)	2875(2)	5062(2)	19(1)
C(24)	1796(2)	4824(2)	3698(2)	20(1)
C(25)	1291(2)	4866(2)	2746(2)	33(1)
C(26)	1297(2)	5661(3)	2243(2)	38(1)
C(27)	1793(3)	6414(2)	2691(3)	38(1)
C(28)	2292(3)	6382(2)	3642(3)	39(1)
C(29)	2285(2)	5588(2)	4143(2)	28(1)
C(30)	943(2)	2413(2)	5575(2)	19(1)
C(31)	870(2)	2852(2)	6355(2)	23(1)
C(32)	264(2)	2526(2)	6731(2)	27(1)
C(33)	-266(2)	1765(2)	6340(2)	26(1)
C(34)	-178(2)	1311(2)	5585(2)	23(1)
C(35)	425(2)	1632(2)	5202(2)	21(1)
C(36)	924(3)	9005(4)	1521(3)	58(1)

Table B.3. Bond lengths [Å] and angles [°] for the Ru complex.

Atom Number	Å (°)
Ru(1)-N(1)	1.988(2)
Ru(1)-N(5)	2.067(2)
Ru(1)-N(3)	2.106(2)
Ru(1)-Cl(1)	2.3441(6)
Ru(1)-Cl(3)	2.3571(6)
Ru(1)-Cl(2)	2.3582(6)
Cl(4)-C(36)	1.722(4)
Cl(5)-C(36)	1.780(4)
N(1)-C(5)	1.346(3)
N(1)-C(1)	1.347(3)
N(2)-C(6)	1.378(3)
N(2)-N(3)	1.403(3)
N(2)-C(1)	1.404(3)
N(3)-C(8)	1.335(3)
N(4)-C(21)	1.381(3)
N(4)-N(5)	1.396(3)
N(4)-C(5)	1.405(3)
N(5)-C(23)	1.341(3)
C(1)-C(2)	1.386(3)
C(2)-C(3)	1.390(4)
C(3)-C(4)	1.387(4)
C(4)-C(5)	1.388(4)
C(6)-C(7)	1.364(4)
C(6)-C(9)	1.478(3)
C(7)-C(8)	1.421(4)
C(8)-C(15)	1.473(4)
C(9)-C(10)	1.396(4)
C(9)-C(14)	1.400(4)
C(10)-C(11)	1.396(4)
C(11)-C(12)	1.384(5)
C(12)-C(13)	1.398(5)
C(13)-C(14)	1.388(4)

Table B.3. Bond lengths [Å] and angles [°] for the Ru complex, continued.

Atom Number	Å (°)
C(15)-C(20)	1.395(4)
C(15)-C(16)	1.402(4)
C(16)-C(17)	1.387(4)
C(17)-C(18)	1.396(4)
C(18)-C(19)	1.384(4)
C(19)-C(20)	1.393(4)
C(21)-C(22)	1.369(4)
C(21)-C(24)	1.479(4)
C(22)-C(23)	1.412(4)
C(23)-C(30)	1.476(4)
C(24)-C(29)	1.385(4)
C(24)-C(25)	1.394(4)
C(25)-C(26)	1.389(5)
C(26)-C(27)	1.378(5)
C(27)-C(28)	1.391(5)
C(28)-C(29)	1.387(4)
C(30)-C(35)	1.398(4)
C(30)-C(31)	1.404(4)
C(31)-C(32)	1.391(4)
C(32)-C(33)	1.388(4)
C(33)-C(34)	1.391(4)
C(34)-C(35)	1.390(4)
N(1)-Ru(1)-N(5)	79.54(8)
N(1)-Ru(1)-N(3)	78.87(8)
N(5)-Ru(1)-N(3)	158.40(8)
N(1)-Ru(1)-Cl(1)	92.37(6)
N(5)-Ru(1)-Cl(1)	90.72(6)
N(3)-Ru(1)-Cl(1)	89.60(6)
N(1)-Ru(1)-Cl(3)	83.03(6)
N(5)-Ru(1)-Cl(3)	87.51(6)
N(3)-Ru(1)-Cl(3)	90.45(6)

Table B.3. Bond lengths [Å] and angles [°] for the Ru complex, continued.

Atom Number	Å (°)
Cl(1)-Ru(1)-Cl(3)	175.31(2)
N(1)-Ru(1)-Cl(2)	173.32(6)
N(5)-Ru(1)-Cl(2)	97.40(6)
N(3)-Ru(1)-Cl(2)	104.14(6)
Cl(1)-Ru(1)-Cl(2)	93.61(2)
Cl(3)-Ru(1)-Cl(2)	90.93(2)
C(5)-N(1)-C(1)	121.3(2)
C(5)-N(1)-Ru(1)	117.51(16)
C(1)-N(1)-Ru(1)	119.18(17)
C(6)-N(2)-N(3)	110.7(2)
C(6)-N(2)-C(1)	130.3(2)
N(3)-N(2)-C(1)	118.57(19)
C(8)-N(3)-N(2)	105.30(19)
C(8)-N(3)-Ru(1)	144.66(17)
N(2)-N(3)-Ru(1)	109.98(15)
C(21)-N(4)-N(5)	110.4(2)
C(21)-N(4)-C(5)	131.0(2)
N(5)-N(4)-C(5)	118.3(2)
C(23)-N(5)-N(4)	105.8(2)
C(23)-N(5)-Ru(1)	142.64(18)
N(4)-N(5)-Ru(1)	110.31(15)
N(1)-C(1)-C(2)	121.1(2)
N(1)-C(1)-N(2)	112.7(2)
C(2)-C(1)-N(2)	126.1(2)
C(1)-C(2)-C(3)	117.3(2)
C(4)-C(3)-C(2)	122.0(2)
C(3)-C(4)-C(5)	117.4(2)
N(1)-C(5)-C(4)	120.9(2)
N(1)-C(5)-N(4)	113.1(2)
C(4)-C(5)-N(4)	126.0(2)
C(7)-C(6)-N(2)	106.5(2)
C(7)-C(6)-C(9)	128.1(2)

Table B.3. Bond lengths [Å] and angles [°] for the Ru complex, continued.

Atom Number	Å (°)
N(2)-C(6)-C(9)	125.4(2)
C(6)-C(7)-C(8)	107.3(2)
N(3)-C(8)-C(7)	110.2(2)
N(3)-C(8)-C(15)	125.4(2)
C(7)-C(8)-C(15)	124.3(2)
C(10)-C(9)-C(14)	119.9(2)
C(10)-C(9)-C(6)	118.8(2)
C(14)-C(9)-C(6)	121.3(2)
C(9)-C(10)-C(11)	119.9(3)
C(12)-C(11)-C(10)	120.1(3)
C(11)-C(12)-C(13)	120.1(3)
C(14)-C(13)-C(12)	120.1(3)
C(13)-C(14)-C(9)	119.8(3)
C(20)-C(15)-C(16)	119.7(2)
C(20)-C(15)-C(8)	121.9(2)
C(16)-C(15)-C(8)	118.3(2)
C(17)-C(16)-C(15)	120.0(3)
C(16)-C(17)-C(18)	119.9(3)
C(19)-C(18)-C(17)	120.1(3)
C(18)-C(19)-C(20)	120.4(3)
C(19)-C(20)-C(15)	119.8(3)
C(22)-C(21)-N(4)	106.2(2)
C(22)-C(21)-C(24)	128.7(2)
N(4)-C(21)-C(24)	124.8(2)
C(21)-C(22)-C(23)	107.6(2)
N(5)-C(23)-C(22)	109.8(2)
N(5)-C(23)-C(30)	125.1(2)
C(22)-C(23)-C(30)	124.4(2)
C(29)-C(24)-C(25)	119.5(3)
C(29)-C(24)-C(21)	121.2(2)
C(25)-C(24)-C(21)	119.3(2)
C(26)-C(25)-C(24)	120.3(3)

Table B.3. Bond lengths [Å] and angles [°] for the Ru complex, continued.

Atom Number	Å (°)
C(27)-C(26)-C(25)	119.8(3)
C(26)-C(27)-C(28)	120.4(3)
C(29)-C(28)-C(27)	119.7(3)
C(24)-C(29)-C(28)	120.3(3)
C(35)-C(30)-C(31)	119.6(2)
C(35)-C(30)-C(23)	120.2(2)
C(31)-C(30)-C(23)	119.3(2)
C(32)-C(31)-C(30)	119.9(3)
C(33)-C(32)-C(31)	120.2(3)
C(32)-C(33)-C(34)	120.1(3)
C(35)-C(34)-C(33)	120.1(3)
C(34)-C(35)-C(30)	120.0(2)
Cl(4)-C(36)-Cl(5)	111.5(2)

Table B.4. Anisotropic displacement parameters (Å2x 103) for the Ru complex. The anisotropic displacement factor exponent takes the form: -2□2[h2 a*2U11 + ... + 2 h k a* b* U12]

Atom Number	U^{11}	U^{22}	U^{33}	U^{23}	U^{13}	U^{12}
Ru(1)	15(1)	14(1)	14(1)	0(1)	7(1)	0(1)
Cl(1)	19(1)	22(1)	20(1)	-2(1)	6(1)	-2(1)
Cl(2)	22(1)	21(1)	18(1)	2(1)	11(1)	0(1)
Cl(3)	17(1)	26(1)	18(1)	-2(1)	7(1)	-3(1)
Cl(4)	49(1)	42(1)	47(1)	-3(1)	19(1)	-4(1)
Cl(5)	48(1)	72(1)	58(1)	-26(1)	10(1)	6(1)
N(1)	18(1)	17(1)	14(1)	0(1)	8(1)	0(1)
N(2)	19(1)	18(1)	17(1)	1(1)	10(1)	2(1)
N(3)	19(1)	17(1)	15(1)	1(1)	9(1)	0(1)
N(4)	22(1)	14(1)	20(1)	1(1)	11(1)	1(1)
N(5)	19(1)	17(1)	18(1)	1(1)	9(1)	-1(1)
C(1)	19(1)	18(1)	13(1)	0(1)	7(1)	0(1)
C(2)	27(1)	23(1)	20(1)	2(1)	14(1)	2(1)
C(3)	33(1)	22(1)	22(1)	5(1)	16(1)	0(1)
C(4)	32(1)	18(1)	24(1)	4(1)	16(1)	2(1)
C(5)	18(1)	17(1)	16(1)	0(1)	7(1)	1(1)
C(6)	18(1)	22(1)	19(1)	-1(1)	9(1)	3(1)
C(7)	22(1)	22(1)	21(1)	4(1)	11(1)	8(1)
C(8)	17(1)	19(1)	18(1)	0(1)	7(1)	2(1)
C(9)	25(1)	20(1)	18(1)	0(1)	12(1)	4(1)
C(10)	23(1)	27(1)	24(1)	1(1)	12(1)	4(1)
C(11)	30(2)	34(2)	38(2)	1(1)	23(1)	3(1)
C(12)	50(2)	34(2)	34(2)	4(1)	31(2)	8(1)
C(13)	45(2)	38(2)	21(1)	2(1)	17(1)	7(1)
C(14)	26(1)	34(2)	20(1)	-1(1)	10(1)	5(1)
C(15)	20(1)	17(1)	18(1)	-2(1)	8(1)	0(1)
C(16)	21(1)	22(1)	24(1)	3(1)	7(1)	2(1)
C(17)	30(1)	24(1)	28(1)	7(1)	7(1)	2(1)
C(18)	39(2)	28(1)	27(1)	6(1)	14(1)	-4(1)
C(19)	30(1)	26(1)	32(2)	-1(1)	18(1)	-5(1)

Table B.4. Anisotropic displacement parameters (Å2x 103) for the Ru complex. The anisotropic displacement factor exponent takes the form: -2□2[h2 a*2U11 + ... + 2 h k a* b* U12], continued.

Atom Number	U^{11}	U^{22}	U^{33}	U^{23}	U^{13}	U^{12}
C(20)	22(1)	20(1)	23(1)	-2(1)	10(1)	0(1)
C(21)	19(1)	16(1)	24(1)	-2(1)	8(1)	0(1)
C(22)	24(1)	16(1)	28(1)	-4(1)	14(1)	0(1)
C(23)	20(1)	17(1)	22(1)	-2(1)	10(1)	0(1)
C(24)	20(1)	17(1)	25(1)	0(1)	11(1)	2(1)
C(25)	30(2)	31(2)	30(2)	2(1)	0(1)	0(1)
C(26)	39(2)	42(2)	28(2)	11(1)	7(1)	12(1)
C(27)	56(2)	24(1)	45(2)	13(1)	32(2)	11(1)
C(28)	64(2)	21(1)	42(2)	-3(1)	30(2)	-10(1)
C(29)	41(2)	21(1)	24(1)	-3(1)	16(1)	-6(1)
C(30)	18(1)	19(1)	21(1)	1(1)	10(1)	3(1)
C(31)	24(1)	23(1)	24(1)	-3(1)	12(1)	-1(1)
C(32)	29(1)	33(2)	23(1)	-2(1)	15(1)	-1(1)
C(33)	22(1)	32(1)	25(1)	4(1)	13(1)	-1(1)
C(34)	20(1)	26(1)	25(1)	2(1)	10(1)	-2(1)
C(35)	21(1)	21(1)	22(1)	-2(1)	10(1)	0(1)
C(36)	40(2)	93(4)	43(2)	-5(2)	19(2)	7(2)

REFERENCES

1. Poole, C., *Gas Chromatography : Gas Chromatography*. Elsevier Science: Saint Louis, UNITED STATES, 2012.

2. Grob, K., *Split and Splitless Injection for Quantitative Gas Chromatography : Concepts, Processes, Practical Guidelines, Sources of Error*. John Wiley & Sons, Incorporated: Berlin, GERMANY, 2008.

3. Miller, J. M., *Chromatography: concepts and contrasts*. Wiley: New York, 1988; p xii, 297 p.

4. Sparkman, O. D.; Penton, Z.; Kitson, F. G., *Gas Chromatography and Mass Spectrometry: A Practical Guide*. Elsevier Science: San Diego, UNITED STATES, 2011.

5. Armstrong, D. W.; He, L.; Liu, Y.-S., Examination of Ionic Liquids and Their Interaction with Molecules, When Used as Stationary Phases in Gas Chromatography. *Analytical Chemistry* **1999,** *71* (17), 3873-3876.

6. Malik, A.; Reese, S. L.; Morgan, S.; Bradshaw, J. S.; Lee, M. L., Dicyanobiphenyl Polysiloxane Stationary Phases for Capillary Column Gas Chromatography. *Chromatographia* **1997,** *46* (1/2), 79-84.

7. Kuei, J. C.; Shelton, J. I.; Castle, L. W.; Kong, R. C.; Richter, B. E.; Bradshaw, J. S.; Lee, M. L., Polarizable Biphenyl Polysiloxane Stationary Phase for Capillary Column Gas Chromatography. *J. High Resolut. Chromatogr. Chromatogr. Commun.* **1984,** *7*, 13-18.

8. Bradshaw, J. S.; Adams, N. W.; Johnson, B. J.; Tarbet, C. M.; Schregenberger, M. A.; Pulshiper, M. A.; Andrus, M. B.; Markides, K. E.; Lee, M. L., Prepararation of Polysiloxane Stationary Phases for Capillary Column Chromatography: a New Methoxyphenyl Phase. *Journal of High Resolution Chromatography & Chromatography Commnucations* **1985,** *8*, 678-683.

9. Bradshaw, J. S.; Aggarwal, S. K.; Rouse, C. A.; Tarbet, B. J.; Markides, K. E.; Lee, M. L., Polysiloxanes containing thermally stable chiral amide side-chains for capillary gas and supercritical fluid chromatography. *J. Chromatogr.* **1987,** *405*, 169-77.

10. Zhao, P.; Liu, L.; Yu, M.; Niu, N.; Wu, B.; Wang, G., A 3,4-2(trifluoromethyl phenyl)-2,5-diphenyl phenyl grafted polysiloxane as a stationary phase for gas chromatography. *Anal. Methods* **2014,** *6* (16), 6278.

11. Han, X.; He, X.; Wang, B.; Wu, B., Polarizable polysiloxane stationary phase containing a cyano unit attached to an aromatic side group for highly selective separation of H-bonding and aromatic analytes. *RSC Adv.* **2016,** *6* (111), 109786-109792.

12. Zhao, P.; Teng, S.; Yu, M.; Niu, N.; He, X.; Wu, B., Synthesis and characterization of diphenyl–phenyl polysiloxane as a high-temperature gas chromatography stationary phase. *Anal. Methods* **2015,** *7* (4), 1333-1338.

13. Rohrschneider, L., Method of characterization for gas chromatographic separation of liquids. *J. Chromatogr.* **1966,** *22* (1), 6-22.

14. McReynolds, W. O., Characterization of Some Liquid Phases. *J. Chromatogr. Sci.* **1970,** *8* (12), 685-691.

15. Kováts, E., Gas-chromatographische Charakterisierung organischer Verbindungen. Teil 1: Retentionsindices aliphatischer Halogenide, Alkohole, Aldehyde und Ketone. *Helvetica Chimica Acta* **1958,** *41* (7), 1915-1932.

16. Blice-Baum, A.; Van Dyke, A.; Sigmon, I.; Salter, E. A.; Wierzbicki, A.; Pocker, Y.; Spyridis, G. T., Computational and spectroscopic studies concerning the solvatochromic behavior of 1,3-disubstituted azulenes. *International Journal of Quantum Chemistry* **2006,** *106* (11), 2331-2338.

17. St. Pfau, A.; Plattner, P. A., Zur Kenntnis der flüchtigen Pflanzenstoffe VIII. Synthese des Vetivazulens. *Helvetica Chimica Acta* **1939,** *22* (1), 202-208.

18. Guarrera, M.; Turbino, L.; Rebora, A., The anti-inflammatory activity of azulene. *Journal of the European Academy of Dermatology and Venereology* **2001,** *15* (5), 486-487.

19. Yanagisawa, T.; Wakabayashi, S.; Tomiyama, T.; Yasunami, M.; Takase, K., Synthesis and Anti-ulcer Activities of Sodium Alkylazulene Sulfonates. *CHEMICAL & PHARMACEUTICAL BULLETIN* **1988,** *36* (2), 641-647.

20. Akatsu, Y.; Ohshima, N.; Yamagishi, Y.; Nishishiro, M.; Wakabayashi, H.; Kurihara, T.; Kikuchi, H.; Tadashi, K.; Motohashi, N.; Shoji, Y.; Nakashima, H.; Sakagami, H., Apoptosis-inducing Activity of Trihaloactylazulenes against Human Oral Tumor Cell Lines. *Anticancer Research* **2006,** *26*, 1917-1924.

21. Lusk, M. T.; Wu, D. T.; Carr, L. D., Graphene nanoengineering and the inverse Stone-Thrower-Wales defect. *Physical Review B* **2010,** *81* (15), 155444.

22. Brien, K. A.; Garner, C. M.; Klausmeyer, K. K.; Feazell, R. P., Crystal structure of 2,6-bis-hydrazinopyridine dihydrate, its tosylate salt and 2,6-bis(3,5-di-tert-butylpyrazolyl)pyridine. *J. Chem. Crystallogr.* **2005,** *35* (11), 875-883.

23. Garst, M. E.; Hochlowski, J.; Douglass, III; Sasse, S., The synthesis of 4,6,8-trimethylazulene: an organic laboratory experiment. *Journal of Chemical Education* **1983,** *60* (6), 510.

24. Horgen, D.; Garner, C., Influence of the Azulene Ring on the Enantioseparation of 1,5-Diols. *Chromatography* **2014,** *1* (2), 65.

25. Constable, E. C., The Coordination Chemistry of 2,2′:6′,2″-Terpyridine and Higher Oligopyridines. *Chemical Reviews* **1986,** *30*, 69-121.

26. Halcrow, M. A., The synthesis and coordination chemistry of 2,6-bis(pyrazolyl)pyridines and related ligands — Versatile terpyridine analogues. *Coordination Chemistry Reviews* **2005,** *249* (24), 2880-2908.

27. Duncan, N. C.; Garner, C. M., Regiospecific synthesis of 2,6-bis-indazol-1-ylpyridines from 2,6-bis-hydrazinopyridine. *Tetrahedron Lett.* **2011,** *52* (41), 5214-5216.

28. Duncan, N. C.; Garner, C. M.; Nguyen, T.; Hung, F.; Klausmeyer, K., Electronic effects in the reaction of 1,3-diaryl-1,3-diketones with hydrazinopyridines. *Tetrahedron Lett.* **2008,** *49* (40), 5766-5769.

29. Brien, K. A.; Garner, C. M.; Pinney, K. G., Synthesis and characterization of 2,6-bis-hydrazinopyridine, and its conversion to 2,6-bis-pyrazolylpyridines. *Tetrahedron* **2006,** *62* (15), 3663-3666.

30. Deng; Yu; Dong; Wu, 2,6-Bis(3,5-dimethylpyrazol-1-yl)pyridine: A Useful Pseudo-N3 Ligand in Efficient Ruthenium(II)-Catalyzed Transfer Hydrogenation of Ketones. *Organometallics* **2005,** *24* (17), 4110-4112.

31. Du, W.; Wang, Q.; Wang, L.; Yu, Z., Ruthenium Complex Catalysts Supported by a Bis(trifluoromethyl)pyrazolyl-Pyridyl-Based NNN Ligand for Transfer Hydrogenation of Ketones. *Organometallics* **2014,** *33* (4), 974-982.

32. Fung, W.-H.; Cheng, W.-C.; Yu, W.-Y.; Che, C.-M.; Mak, T. C. W., Enantioselective epoxidation of unfunctionalized alkenes by a chiral monooxoruthenium(IV) complex [RuL(bpy)O]2+ {L = 2,6-bis[(4S,7R)-7,8,8-trimethyl-4,5,6,7-tetrahydro-4,7-methanoindazol-2-yl]pyridine; bpy = 2,2'-bipyridine}. *J. Chem. Soc., Chem. Commun.* **1995,** (19), 2007-8.

33. Magubane, M. N.; Nyamato, G. S.; Ojwach, S. O.; Munro, O. Q., Structural, kinetic, and DFT studies of the transfer hydrogenation of ketones mediated by (pyrazole)pyridine iron(II) and nickel(II) complexes. *RSC Adv.* **2016,** *6* (69), 65205-65221.

34. Gong, D.; Jia, X.; Wang, B.; Zhang, X.; Huang, K.-W., Trans-1,4 selective polymerization of 1,3-butadiene with symmetry pincer chromium complexes activated by MMAO. *Journal of Organometallic Chemistry* **2014,** *766*, 79-85.

35. Gong, D.; Jia, X.; Wang, B.; Zhang, X.; Jiang, L., Synthesis, characterization, and butadiene polymerization of iron(III), iron(II) and cobalt(II) chlorides bearing 2,6-bis(2-benzimidazolyl)pyridyl or 2,6-bis(pyrazol)pyridine ligand. *Journal of Organometallic Chemistry* **2012,** *702*, 10-18.

36. Karam, A. R.; Catari, E. L.; Lopez-Linares, F.; Agrifoglio, G.; Albano, C. L.; Diaz-Barrios, A.; Lehmann, T. E.; Pekerar, S. V.; Albornoz, L. A.; Atencio, R.; Gonzalez, T.; Ortega, H. B.; Joskowics, P., Synthesis, characterization and olefin polymerization studies of iron(II) and cobalt(II) catalysts bearing 2,6-bis(pyrazol-1-yl)pyridines and 2,6-bis(pyrazol-1-ylmethyl)pyridines ligands. *Appl. Catal., A* **2005,** *280* (2), 165-173.

37. Zikode, M.; Ojwach, S. O.; Akerman, M. P., Structurally rigid bis(pyrazolyl)pyridine Zn(II) and Cu(II) complexes: Structures and kinetic studies in ring-opening polymerization of ε-caprolactone. *Appl. Organomet. Chem.* **2017,** *31* (2), n/a.

38. Christenson, D. L.; Tokar, C. J.; Tolman, W. B., New Copper and Rhodium Cyclopropanation Catalysts Supported by Chiral Bis(pyrazolyl)pyridines. A Metal-Dependent Enantioselectivity Switch. *Organometallics* **1995,** *14* (5), 2148-50.

39. Kwong, H.; Wong, W.; Lee, W.; Cheng, L.; Wong, W., New chiral 2,2':6',2''-terpyridine ligands from the chiral pool: synthesis, crystal structure of a rhodium complex and uses in copper- and rhodium-catalyzed enantioselective cyclopropanation of styrene. *Tetrahedron-Asymmetr.* **2001,** *12*, 2683-2694.

40. Yamaguchi, M.; Tomizawa, M.; Takagaki, K.; Shimo, M.; Masui, D.; Yamagishi, T., Photooxidation of alkane under visible light irradiation catalyzed by ruthenium complexes. *Catal. Today* **2006,** *117* (1-3), 206-209.

41. Shin, M. S.; Oh, B. J.; Ryu, J. Y.; Park, M. H.; Kim, M.; Lee, J.; Kim, Y., Synthesis, characterization, and cycloaddition reaction studies of zinc(II) acetate complexes containing 2,6-bis(pyrazol-1-yl)pyridine and 2,6-bis(3,5-dimethylpyrazol-1-yl)pyridine ligands. *Polyhedron* **2016**, Ahead of Print.

42. Motaung, M. P.; Ajibade, P. A., Ru(II) and Co(II) complexes of bis(pyrazolyl)pyridine and pyridine-2,6-dicarboxylic acid: synthesis, photo physical studies and evaluation of solar cell conversion efficiencies. *Int. J. Electrochem. Sci.* **2015,** *10* (10), 8087-8096.

43. Kontos, A. G.; Stergiopoulos, T.; Tsiminis, G.; Raptis, Y. S.; Falaras, P., In situ micro- and macro-Raman investigation of the redox couple behavior in DSSCS. *Inorg. Chim. Acta* **2008,** *361* (3), 761-768.

44. Sivakumar, R.; Marcelis, A. T. M.; Anandan, S., Synthesis and characterization of novel heteroleptic ruthenium sensitizer for nanocrystalline dye-sensitized solar cells. *J. Photochem. Photobiol., A* **2009,** *208* (2-3), 154-158.

45. Stergiopoulos, T.; Bernard, M.-C.; Hugot-Le Goff, A.; Falaras, P., Resonance micro-Raman spectrophotoelectrochemistry on nanocrystalline TiO2 thin film electrodes sensitized by Ru(II) complexes. *Coord. Chem. Rev.* **2004,** *248* (13-14), 1407-1420.

46. Chryssou, K.; Stergiopoulos, T.; Falaras, P., Synthesis and spectroscopic properties of a new bipyridine-bipyrazoyl(pyridine)-thiocyanato-ruthenium(II) complex. *Polyhedron* **2002,** *21* (27-28), 2773-2781.

47. Philippopoulos, A. I.; Terzis, A.; Raptopoulou, C. P.; Catalano, V. J.; Falaras, P., Synthesis, Characterization, and Sensitizing Properties of Heteroleptic RuII Complexes Based on 2,6-Bis(1-pyrazolyl)pyr-idine and 2,2′-Bipyridine-4,4′-dicarboxylic Acid Ligands. *European Journal of Inorganic Chemistry* **2007,** *2007* (36), 5633-5644.

48. Halcrow, M. A.; Kilner, C. A.; Thornton-Pett, M., Bis{2,6-bis[3-(2,4,6-trimethylphenyl)-pyrazol-1-yl-jN2]pyridine-KN}zinc(II) diperchlorate bis(nitromethane) solvate. *Acta Crystallographia Section C* **2000**, 1425-1426.

49. Kalyanasundaram, K., Photophysics, photochemistry and solar energy conversion with tris(bipyridyl)ruthenium(II) and its analogues. *Coordination Chemistry Reviews* **1982,** *46* (Supplement C), 159-244.

50. Hopa, C.; Kurtaran, R.; Hopa, E.; Cetin, G.; Dundar, E.; Kara, H.; Alkan, M., Nitrito complexes of nickel(II), copper(II) and cobalt(II) with tridentate pyrazole based planer ligand: Structure, spectroscopy, thermal properties and imitative nuclease activity. *Inorg. Chim. Acta* **2015,** *429*, 15-21.

51. Anderson, A. G., Jr.; Steckler, B. M., Azulene. VIII. A study of the visible absorption spectra and dipole moments of some 1- and 1,3-substituted azulenes. *J. Am. Chem. Soc.* **1959,** *81*, 4941-6.

52. Hafner, K.; Kaiser, H., 4,6,8-Trimethylazulene. *Org. Synth.* **1964,** *44*, 94-8.

53. Elizalde-Gonzalez, M. P.; Hutfliess, M.; Hedden, K., Retention index system, adsorption characteristics, and structure correlations of polycyclic aromatic hydrocarbons in fuels. *J. High Resolut. Chromatogr.* **1996,** *19* (6), 345-352.

54. Engewald, W.; Wennrich, L.; Ritter, E., Molecular structure and retention behavior. XII. Retention behavior of alkylnaphthalenes by gas-partition and gas-adsorption chromatography. *J. Chromatogr.* **1979,** *174* (2), 315-23.

55. Reiter, S. E.; Dunn, L. C.; Houk, K. N., Synthesis of azulenes by the [6 + 4] cycloadditions of 6-aminofulvenes to thiophene S,S-dioxides. *Journal of the American Chemical Society* **1977,** *99* (12), 4199-4201.

56. Yamanoi, Y.; Nishihara, H., Direct and Selective Arylation of Tertiary Silanes with Rhodium Catalyst. *The Journal of Organic Chemistry* **2008,** *73* (17), 6671-6678.

57. Murata, M.; Ishikura, M.; Nagata, M.; Watanabe, S.; Masuda, Y., Rhodium(I)-Catalyzed Silylation of Aryl Halides with Triethoxysilane: Practical Synthetic Route to Aryltriethoxysilanes. *Organic Letters* **2002,** *4* (11), 1843-1845.

58. Murata, M.; Suzuki, K.; Watanabe, S.; Masuda, Y., Synthesis of Arylsilanes via Palladium(0)-Catalyzed Silylation of Aryl Halides with Hydrosilane. *The Journal of Organic Chemistry* **1997,** *62* (24), 8569-8571.

59. Bouche, J.; Verzele, M., Static coating procedure for glass capillary columns. *J. Gas Chromatogr.* **1968,** *6* (10), 501-5.

60. Peng, J.; Sun, T.; Wu, L.; Qi, M.; Huang, X., Separation performance of dithienyl benzothiadiazole-based stationary phases for capillary gas chromatography. *RSC Advances* **2017,** *7* (72), 45408-45415.

61. Poole, C., *Handbook of Methods and Instrumentation in Separation Science*. Elsevier Science: 2009.

62. Morris, L. J., Separations of lipids by silver-ion chromatography. *J. Lipid Res.* **1966,** *7* (6), 717-32.

63. Hafner, K.; Hartung, J.; Syren, C., Isomerization of dihydroazulenes to substituted azulenes - naked eye observation of a novel Cope-type rearrangement. *Tetrahedron* **1992,** *48* (23), 4879-84.

64. Boymond, L.; Rottlander, M.; Cahiez, G.; Knochel, P., Preparation of highly functionalized Grignard reagents by an iodine-magnesium exchange reaction and its application in solid-phase synthesis. *Angew. Chem., Int. Ed.* **1998,** *37* (12), 1701-1703.

65. Arendt, K. M.; Doyle, A. G., Dialkyl Ether Formation by Nickel-Catalyzed Cross-Coupling of Acetals and Aryl Iodides. *Angew Chem Int Ed Engl* **2015,** *54* (34), 9876-80.

66. Jameson, D. L.; Goldsby, K. A., 2,6-bis(N-pyrazolyl)pyridines: the convenient synthesis of a family of planar tridentate N3 ligands that are terpyridine analogs. *The Journal of Organic Chemistry* **1990,** *55* (17), 4992-4994.

67. Arendt, K. M.; Doyle, A. G., Dialkyl Ether Formation by Nickel-Catalyzed Cross-Coupling of Acetals and Aryl Iodides. *Angew. Chem., Int. Ed.* **2015,** *54* (34), 9876-9880.

68. Gong, D.; Jia, X.; Wang, B.; Zhang, X.; Jiang, L., Synthesis, characterization, and butadiene polymerization of iron(III), iron(II) and cobalt(II) chlorides bearing 2,6-bis(2-benzimidazolyl)pyridyl or 2,6-bis(pyrazol)pyridine ligand. *J. Organomet. Chem.* **2012,** *702*, 10-18.

69. Halcrow, M. A.; Kilner, C. A.; Thornton-Pett, M., Bis{2,6-bis[3-(2,4,6-trimethylphenyl)pyrazol-1-yl-κN2]pyridine-κN}zinc(II) diperchlorate bis(nitromethane) solvate. *Acta Crystallogr., Sect. C: Cryst. Struct. Commun.* **2000,** *C56* (12), 1425-1426.

70. Halcrow, M. A., Iron(II) complexes of 2,6-di(pyrazol-1-yl)pyridines—A versatile system for spin-crossover research. *Coordination Chemistry Reviews* **2009,** *253* (21-22), 2493-2514.

71. Tenza, K.; Hanton, M. J.; Slawin, A. M. Z., Ethylene Oligomerization Using First-Row Transition Metal Complexes Featuring Heterocyclic Variants of Bis(imino)pyridine Ligands. *Organometallics* **2009,** *28* (16), 4852-4867.

72. Catalano, V. J.; Kurtaran, R.; Heck, R. A.; Ohman, A.; Hill, M. G., Bdmpp complexes of Ru(II) as structural analogs for Ru(II)-2,2%:6%,2%%-terpyridine species (where bdmpp is 2,6-bis(3,5-dimethyl-N- pyrazoyl)pyridine). *inorganica Chimica Acta* **1999,** *286*, 181-188.

73. Jo, D. H.; Yeo, H. J., Syntheses and reactivities with olefins of ruthenium(IV) oxo/ruthenium(II)-aqua complexes that contain 2,6-bis(N-pyrazolylpyridine). *Bull. Korean Chem. Soc.* **1993,** *14* (6), 682-6.

74. Fung, W.-H.; Yu, W.-Y.; Che, C.-M., Mechanistic Investigation of the Oxidation of Aromatic Alkenes by Monooxoruthenium(IV). Asymmetric Alkene Epoxidation by Chiral Monooxoruthenium(IV) Complexes. *J. Organomet. Chem.* **1998,** *63* (22), 7715-7726.

75. Bessel, C. A.; See, R. F.; Jameson, D. L.; Churchill, M. R.; Takeuchi, K. J., Synthesis, characterization and crystal structure of trans-[2,6-bis(3-phenylpyrazol-1-yl-κN2)pyridine-κN]chlorobis(trimethylphosphine)ruthenium(II) perchlorate: evidence for meridional steric crowding. *J. Chem. Soc., Dalton Trans.* **1991,** (11), 2801-5.

76. Bessel, C. A.; See, R. F.; Jameson, D. L.; Churchill, M. R.; Takeuchi, K. J., Synthesis and characterization of ruthenium complexes which utilize a new family of terdentate ligands based upon 2,6-bis(pyrazol-1-yl)pyridine. *J. Chem. Soc., Dalton Trans.* **1993,** (10), 1563-76.

77. Chakrabarty, S.; Sarkhel, P.; Poddar, R., Ruthenium(II) and palladium(II) complexes with 2,6-(bispyrazol-1-yl)pyridines. *J. Coord. Chem.* **2010,** *63* (9), 1563-1569.

78. Rülke, R. E.; Kaasjager, V. E.; Kliphuis, D.; Elsevier, C. J.; van Leeuwen, P. W. N. M.; Vrieze, K.; Goubitz, K., Insertion Reactions Involving Palladium Complexes with Nitrogen Ligands. 2. Carbon monoxide and Alkene Insertion Reactions with Novel Palladium Compounds Containing Terdentate Ligands. *Organometallics* **1996,** *15* (2), 668-677.

79. Pelascini, F.; Wesolek, M.; Peruch, F.; De Cian, A.; Kyritsakas, N.; Lutz, P. J.; Kress, J., Iron complexes of terdentate nitrogen ligands: formation and X-ray structure of three new dicationic complexes. *Polyhedron* **2004,** *23* (18), 3193-3199.

80. Rajnak, C.; Titis, J.; Fuhr, O.; Ruben, M.; Boca, R., Single-Molecule Magnetism in a Pentacoordinate Cobalt(II) Complex Supported by an Antenna Ligand. *Inorg. Chem.* **2014,** *53* (16), 8200-8202.

81. Hopa, C.; Kurtaran, R.; Azizoglu, A.; Alkan, M.; Arslan, N. B.; Kazak, C., Zinc(II) and Mercury(II) Complexes of Pyrazole-Based NNN-Type Ligands: Syntheses, X-ray Structures, Thermal Analyses and DFT Studies. *Z. Anorg. Allg. Chem.* **2011,** *637* (9), 1238-1245.

82. Turhan, O.; Kurtaran, R.; Namli, H., In situ IR monitoring of complexation reaction between 2,6-bis(3,5-dimethylpyrazoyl)pyridine and some metal ions. *Vib. Spectrosc.* **2011,** *56* (2), 111-115.

83. Yang, Z. N.; Sun, T. T., Dichlorido(2,6-dipyrazol-1-ylpyridine)zinc(II). *Acta Crystallogr., Sect. E: Struct. Rep. Online* **2008,** *64* (11), m1374, m1374/1-m1374/6.

84. Arici, C.; Ulku, D.; Kurturan, R.; Emregul, K. C.; Atakol, O., Synthesis, crystal structure and electrochemical behaviour of [2,6-bis(3,5-dimethylpyrazolyl)pyridine](dithiocyanato)cobalt(II). *Zeitschrift für Kristallographie* **2003,** *218*, 497-500.

85. Harris, C. M.; Lockyer, T. N.; Stephenson, N. C., Five-coordinated 2,2',2"-terpyridyl complexes of cobalt(II), manganese(II), and copper(II). *Aust. J. Chem.* **1966,** *19* (9), 1741-3.

86. Grirrane, A.; Pastor, A.; Alvarez, E.; Mealli, C.; Ienco, A.; Rosa, P.; Montilla, F.; Galindo, A., Manganese oxydiacetate complexes: Synthesis, structure and magnetic properties. *Eur. J. Inorg. Chem.* **2004,** (4), 707-717.

87. Mantel, C.; Baffert, C.; Romero, I.; Deronzier, A.; Pecaut, J.; Collomb, M.-N.; Duboc, C., Structural Characterization and Electronic Properties Determination by High-Field and High-Frequency EPR of a Series of Five-Coordinated Mn(II) Complexes. *Inorg. Chem.* **2004,** *43* (20), 6455-6463.

88. Holland, J. M.; Barrett, S. A.; Kilner, C. A.; Halcrow, M. A., Control of the spin state of Fe(II) 2,6-di(pyrazol-1-yl)pyridine complexes by distal ligand substitution. *Inorg. Chem. Commun.* **2002,** *5* (5), 328-332.

89. Zheng, A. X.; Si, J.; Tang, X. Y.; Miao, L. L.; Yu, M.; Hou, K. P.; Wang, F.; Li, H. X.; Lang, J. P., Reactions of the cationic zinc thiolate model complex [Zn(Tab)4](PF6)2 with N-donor ligands and cobalt dichloride. *Inorg Chem* **2012,** *51* (19), 10262-73.

90. Willison, S. A.; Jude, H.; Antonelli, R. M.; Rennekamp, J. M.; Eckert, N. A.; Bauer, J. A. K.; Connick, W. B., A Luminescent Platinum(II) 2,6-Bis(N-pyrazolyl)pyridine Complex. *Inorganic Chemistry* **2003,** *43*, 2548-2555.

91. Calderazzo, F.; Englert, U.; Hu, C.; Marchetti, F.; Pampaloni, G.; Passarelli, V.; Romano, A.; Santi, R., Synthesis and structural characterization of iron(II) derivatives of heterocyclic tridentate amines. *Inorganica Chimica Acta* **2002,** *344*, 197-206.

92. Rajnak, C.; Titis, J.; Salitros, I.; Boca, R.; Fuhr, O.; Ruben, M., Zero-field splitting in pentacoordinate Co(II) complexes. *Polyhedron* **2013,** *65*, 122-128.

93. Sofetis, A.; Fotopoulou, F.; Raptopoulou, C. P.; Zafiropoulos, T. F.; Perlepes, S. P.; Klouras, N., Reactions of titanocene dihalides with N,N′,N″-chelates: Preparation, X-ray structure and characterization of bis(chloro){2,6-bis[(3,5-dimethyl)pyrazol-1-yl]pyridine}(η2-peroxo)titanium(IV). *Polyhedron* **2009,** *28* (15), 3356-3360.

94. Hopa, Ç.; Alkan, M.; Kazak, C.; Burcu Arslan, N.; Kurtaran, R., Iron(III) complex of a tridentate NNN type ligand: synthesis, X-ray structure, thermal analysis and voltammetric studies. *Transition Metal Chemistry* **2009,** *34* (4), 403-407.

95. Tastekin, M.; Durmus, S.; Sahin, E.; Arici, C.; Emregul, K. C.; Atakol, O., Crystal structure and thermal analysis of new mononuclear nickel (II) complexes with NNN type pyrazolyl ligands and halides. *Z. Kristallogr.* **2008,** *223* (6), 424-429.

96. Intille, G. M.; Pfluger, C. E.; Baker, W. A., Crystal and molecular structure of chloro(2,2′,2″-terpyridine)palladium(II)chloride dihydrate, C15H15Cl2N3O2Pd. *Journal of Crystal and Molecular Structure* **1973,** *3* (1), 47-54.

97. Bruker, BRUKER APEX2 (Version 1.0-28) and SAINT-PLUS (Version 6.25). **2012**.

98. Sheldrick, G. M., SHELXS97 and SHELXL97. **1997**.

99. Sheldrick, G. M., SHELSTL, Version 6.14. **2000**.